MAPPING UNDERLYING DYNAMIC EFFECTIVE CONNECTIVITY IN NEURAL SYSTEMS USING THE DECONVOLVED NEURONAL ACTIVITY

by

Seo Hyon Baik

MS in Statistics, Texas A&M University, 2003

Submitted to the Graduate Faculty of

the Department of Statistics in partial fulfillment

of the requirements for the degree of

Doctor of Philosophy

University of Pittsburgh

2010

UNIVERSITY OF PITTSBURGH

STATISTICS DEPARTMENT

This dissertation was presented

by

Seo Hyon Baik

It was defended on

August 19, 2010

and approved by

Leon J. Gleser, Department of Statistics

Yu Cheng, Department of Statistics

Robert T. Krafty, Department of Statistics

Wesley K. Thompson, Department of Psychiatry, UC San Diego

Dissertation Director: Leon J. Gleser, Department of Statistics

ABSTRACT

MAPPING UNDERLYING DYNAMIC EFFECTIVE CONNECTIVITY IN NEURAL SYSTEMS USING THE DECONVOLVED NEURONAL ACTIVITY

Seo Hyon Baik, PhD

University of Pittsburgh, 2010

Event-related functional magnetic resonance imaging (**fMRI**) has emerged as a tool for studying the functioning of the human brain. The study on **fMRI** supplies information on the underlying mechanism of the human brain, such as how a brain in good shape functions, how a brain affected by different diseases works, how a brain struggles to recover after damage and how different stimuli can modulate this recovery process.

The variable of interest is the neuronal activities given a stimulus, however the signal being quantified by **MRI** scanner is the blood oxygenation level-dependent (**BOLD**) response which is the subordinate repercussion of the underlying neuronal activity such as local changes in blood flow, volume and oxygenation level that takes place within a few second of changes in neuronal activity. From this point of view, one may think that the neuronal-activity-based and **BOLD**-based studies would be dissimilar in yielding information on the underlying mechanism of the human brain. This dissertation is devoted primarily to estimating underlying neuronal activities given a stimuli. In particular, we develop a method of estimating intrinsic neuronal signals and haemodynamic responses under the fact that a BOLD response is expressed as a convolution of the underlying neuronal signal and the haemodynamic response function. We also present differences between the use of estimated neuronal signals and of observed **BOLD** responses in investigating causal relationships among heterogeneous brain regions using an ordinary vector autoregressive model.

TABLE OF CONTENTS

LIST OF TABLES

LIST OF FIGURES

PREFACE

I am indebted to many people for the successful completion of this document. I would like to acknowledge a group of individuals, the contributions from whom have been invaluable in many ways. First, I would like to express the deepest appreciation to my advisor, Dr. Leon J. Glesr, who has the attitude and the substance of a genius: he continually and convincingly conveyed a spirit of adventure in regard to research and scholarship. Without his guidance and persistent help this dissertation would not have been possible. I also extend special thanks to Dr. Wesley K. Thompson and Dr. Robert Krafty, whose contributions, influence, and support have had an immeasurable effect on my development over the past years. They have been an unending source of advice and encouragement and been with me throughout the years as mentor, colleague, editor, and friend. Their excellent guidance with endless patience always leads me to the right direction. I am honored to be their student.

There are many other people without whom I would never have made it to the end of a successful graduate career. I thank the other members of my committee, Dr. Yu Cheng and Dr. Taeyoung Park for their friendship and guidance. I also wish to offer a special thanks to the rest of faculty, staff and students of the statistics department at University of Pittsburgh for their encouragement, support and friendship throughout my graduate years.

Finally, I owe my greatest debts to my family. I would like to thank my parents and mother-in-law for their support, encouragement, and tolerance, both over the years and in the years to come. I also am grateful to my son, John, for growing up healthily and reminding me daily that miracles exist everywhere around us. Last but not least, I would like to thank my wife, Hyewook, for being always there for me. I would not have been able to complete it without her. This dissertation is equally her achievement. I'd like to dedicate this dissertation to my family.

1.0 INTRODUCTION

Event-related functional magnetic resonance imaging (**fMRI**) has emerged recently as a tool for studying the functioning of the human brain. **fMRI** can provide the location and temporal evolution of neuronal activity and the association among neuronal activities from several different brain regions resulting from sensory stimulation or cognitive function. It therefore supplies information on the underlying mechanism of the human brain, such as how a brain in good shape functions, how a brain affected by different diseases works, how a brain struggles to recover after damage and how different stimuli can modulate this recovery process.

The variable of interest in the study of **fMRI** is the intrinsic neuronal activity given a stimulus. Given a stimuli, the **fMRI** scanner records the signals from the human brain. It was found that there exists differences in the magnetic susceptibilities of oxygenated hemoglobin and deoxygenated hemoglobin that track the blood-flow-related phenomena of neuronal activations, which is referred to as **B**lood **O**xygenation **L**evel **D**ependent (**BOLD**) responses (Ogawa et al., 1990a) [48]. This enables a **fMRI** scanner to visualize the location of neuronal activation. However, **BOLD** responses are not precise measures of the underlying neuronal activities because they are measured at the level of haemodynamic response, not at a neuronal level. Moreover, one may think that **BOLD** response-based **fMRI** studies would not be precise enough to make inferences on the complex human brain network but the study based upon well approximated or estimated neuronal activities would render the study explicit. The possibility of approximating or estimating latent neuronal activity stems from the fact that a **BOLD** response is expressed as a convolution of the underlying neuronal signal and the haemodynamic response function (**HRF**). This approximation or estimation

technique is referred to as a *deconvolution* of latent neuronal activity.

Studies on **fMRI** can be divided into two categories, *functional segregation* and *functional integration*. The study of functional segregation is referred to as an *activation* study and the essential consideration of this type of study is to identify the region of activity. In contradiction to the study of functional segregation, the study of functional integration (which is referred as *connectivity* study) investigates the liaison among the intrinsic neuronal activities from several different regions in the human brain. Therefore, connectivity studies enable us to map out the complex human brain network. One possible application of mapping the complex human brain network is that it would benefit recovery processes in unhealthy brains, such as attention deficit hyperactivity disorder (**ADHD**), Alzheimer's disease (**AD**) and so on. Until now, most connectivity studies have been carried out using the observed **BOLD** responses. We expect that using the approximated neuronal activity instead of the observed **BOLD** responses would make **fMRI** studies concrete and the inferences on connectivity structure among several regions in the human brain would be more accurate.

In chapter 2, we provide the background of **fMRI** and in chapter 3, we summarize and review several studies which have been done both on effective connectivity (Section 3.1) and on deconvolution of underlying neuronal activity (Section 3.2). In chapters, 4 and 5, we describe the our proposed deconvolution method, referred to as **Blind Deconvolution** technique, and discuss how the approximated neuronal activity and the observed **BOLD** reponse differ and present differences between the use of estimated neuronal signals and of observed BOLD responses in investigating causal relationships among heterogeneous brain regions using an ordinary vector autoregressive model.

2.0 FMRI BACKGROUND

In the previous chapter, we presented the variable of interest in the **fMRI** study, **BOLD** response, and briefly described the possible risk to use **BOLD** response as a measure of underlying neuronal activity. Furthermore, we also provided the idea of approximating underlying neuronal activity based on **BOLD** responses. We now turn our attention to some basic concepts in the study of **fMRI**.

2.1 BLOOD OXYGENATION LEVEL DEPENDENT RESPONSE

Functional Magnetic Resonance Image (**fMRI**) is based on the change in blood flow or volume that goes together with neuronal activity in the human brain, resulting in a corresponding local reduction in deoxyhemoglobin (Fox and Raichle, 1985) [19]. Blood oxygenation level dependent (**BOLD**) response represents the changes in blood oxygenation level. Given a stimulus, some neurons in the human brain fire and their firing requires energy in the form of sugar and oxygen. Since neurons do not have reservoir of energy inside, the blood supplies energy in the form of oxygen to active neurons at a greater rate than to the inactive neurons. In other words, neuron firing results in a change in local blood volume and flow and consequently oxygen extraction. According to the fact that oxyhaemoglobin (or oxygenated blood) has no considerable magnetic characteristics, but deoxyhaemoglobin (or deoxygenated blood) is strongly paramagnetic, an active region has increased intensity of blood deoxygen level whereas an inactive region does not. The difference in magnetic susceptibility between oxygenated and deoxygenated blood leads to magnetic signal variation and it enables an **fMRI** scanner to visualize the active brain regions given a stimuli (Ogawa,

et al, 1990a [48] and b [47], 1992 [49]; Belliveau, et al, 1990 [6], 1991 [5]; Turner, et al., 1991 [64]; Tank, et al , 1992 [63]; Kwong 1992 [39]).

2.2 HAEMODYNAMIC RESPONSE FUNCTION

Haemodynamics, literally meaning *blood movement*, is the study of blood flow and is precisely referred to as a medical terminology for the dynamic regulation of the blood flow in the brain. In other words, the blood supply of the brain is dynamically modulated by haemodynamics to give active neurons more energy whilst inactive neurons receive less energy. Furthermore, the haemodynamic response function (**HRF**) is defined to be a function of blood oxygenation, flow, and volume and known to reach its peak 4 to 6 seconds, undershoot from approximately 10 to 30 seconds and return to baseline about 20 to 30 seconds after a stimuli is applied (Buxton et al., 1998) [11]. In addition, initial undershoot can be observed (Malonek and Grinvald, 1996) [42] and the haemodynamic response function (**HRF**) is found to be different across regions within individuals (Schacter et al., 1997) [57] and different across individuals (Aguirre et al., 1998) [2]. Haemodynamic response function (**HRF**) is usually modeled by a Poisson, Gaussian or Gamma distribution or by the mixture of two Gamma densities. It is also known that a linear convolution of underlying neuronal activity and haemodynamic response function (**HRF**) yields the **BOLD** response.

2.3 VOXEL VS REGIONS-OF-INTEREST BASED STUDY

The **fMRI** scanner measures signals from the area being scanned and the area being scanned is represented as **voxels**. Each voxel typically represents the area of activity of a particular coordinate in three dimensional space. The size of a voxel is typically a volume of $27mm^3$ (a cube with $3mm$ length sides). The regions of interest (**ROIs**) are defined to be a set of voxels and are also called volumes-of-interest (**VOIs**). The **fMRI** study is based on either voxel- or **ROIs**-based **BOLD** responses. An advantage of **ROIs**-based study over

voxel-based study is that one can control for Type I error by limiting the number of statistical tests to a few **ROIs** (Poldrack, 2007) [53]. The following is a list of **ROIs** and their functions in the human brain;

1. Anterior cingulate cortex (**ACC**)

   : The *anterior cingulate cortex* (**ACC**) is the frontal part of the cingulate cortex and can be split anatomically depending on its attributed functionalities into executive (anterior part), evaluative (posterior part), cognitive (dorsal part), and emotional (ventral part) components (Bush et al., 2000) [10].

2. Brodmann Area 24 (**BA24**)

   : *Brodmann area* 24 (**BA24**) is subsection of the anterior cingulate cortex (**ACC**) in the human brain and it occupies most of the anterior cingulate cortex. It plays major roles in in emotional and cognitive processing (Vogt et al., 1987) [67].

3. Brodmann Area 25 (**BA25**)

   : *Brodmann Area* 25 (**BA25**) is an associational cortical area in the medial prefrontal region of the frontal lobe and it is involved in governing personal and social behavior, emotion, and decision making (Mayberg et al., 2005) [43]. For the complete list of Brodmann areas, one may visit http://spot.colorado.edu/ dubin/talks/brodmann/neuronames.html.

4. Dorsolateral prefrontal cortex (**DLPFC**)

   : *Dorsolateral prefrontal cortex* (**DLPFC**) is the most anterior in the human brain and it is in charge of planning, organization, and regulation. It plays an important role in the integration of mnemonic information and the regulation of intellectual function and action. It is also involved in working memory. It has been suggested that in the early stages of Alzheimer's disease (**AD**), the brain is able to compensate by enhancing function via increased neural activity and metabolism in **DLPFC** (Robertson et al., 2001 [55]; Procyk et al., 2006 [54]).

5. Hippocampus (Left, Right)

   : The *hippocampus* is a part of the forebrain, located in the medial temporal lobe and it plays major roles in short term memory and spatial navigation. In Alzheimer's disease (**AD**), the hippocampus is one of the first regions of the brain to suffer damage (Gray et al., 2000 [30]; Scoville et al., 2000 [59]).

6. Posterior cingulate Cortex

   : The *posterior cingulate cortex* is the back most part of the cingulate cortex, lying behind the anterior cingulate cortex (**ACC**). It is associated with *Brodmann areas* 23 and 31 and participates in limbic and parietal associational integration (Hinton et al., 2004) [33].

7. Amygdala (Left, Right)

   : *Amygdala* is an almond-shaped group of neurons located deep within the medial temporal lobes of the brain in complex vertebrates, including humans. It is involved in emotion, cognition and the regulation of autonomic processes (Amunts et al., 2005) [4].

The **ROIs** listed above are a small portion of the regions-of-interest in the human brain; for the complete list of **ROIs**, one may refer to http://www.sylvius.com/index/. The **ROIs** enumerated above are the ones that are involved in the data analysis in chapter 5.

3.0 LITERATURE REVIEWS

3.1 THE STUDIES ON EFFECTIVE CONNECTIVITY

The study of functional magnetic resonance imaging(**fMRI**) supplies informations on the intrinsic neuronal activities, which are evoked by the external sensorimotor or cognitive stimuli, as a principle of organization in the human brain. The variable of interest is the underlying neuronal activities, however the signal being quantified is the blood oxygenation level-dependent (**BOLD**) response, since the neuronal activity is not directly observable. The **BOLD** response is the subordinate repercussion of haemodynamic changes (such as local changes in blood flow, volume and oxygenation level) that take place within a few second of changes in neuronal activity.

Based on **BOLD** responses, inferences on structure-functional relationship in the human brain are made. These inferences are made on functional segregation and functional integration in the human brain. The study of functional segregation yields an answer to the question, *"where are regional responses to experimental input(stimuli) located ?"*. In other words, the cardinal consideration of this study is to identify the region of activity. Due to the identification of sites of activation, the inference are made through the univariate analysis of regionally specific effect. This kind of study is referred to as an *activation study*. In contradistinction, the investigation of functional integration answers to the query, *"how does one region influence another* (*or coupling between regions*)?". The matter of primary concern in such a study is to demonstrate the liaison among disparate regions and the multivariate analysis of regional interactions produces the desired inference on functional integration. This type of study is referred to as a *connectivity study*. Con-

nectivity studies can be further divided into studies of *functional connectivity* and *effective connectivity*. A model-free approach to scrutinize functional integration by exploring the correlation of activity (or undirected path) between brain regions is referred to as *functional connectivity* (Friston 1993b [23]; Hampson(2002) [31]) and to say that two brain regions have a functional connectivity is equivalent to saying that activities from these regions are significantly correlated without considering how the correlation is arbitrated. Therefore, the fact that regions A and B are functionally connected reveals nothing about whether activity in A causes that in B or vice versa. Due to this, *functional connectivity* is skeptical about unveiling the causal relationship of activities from different brain areas. The study of *effective connectivity*, defined to be the influence or effect one neuronal system exerts upon others (Friston 1993a [22], 1994 [20]), deals with this handicap by exhibiting statistical models of directed neuronal interactions.

To date, **fMRI** has mostly been utilized to corroborate functional segregation through the detection of *hot spots*. However, there is increasing concern in studying the potential interactions between heterogeneous brain regions to explain the functional integration of the brain. The model of effective connectivity is intended to place an appropriate metric of influence among interrelated regions in the human brain. There are assorted approaches to modeling the effective connectivity; however, the inspiration of each approach is on common ground: to investigate the causal relationships among the underlying neuronal connectivities.

The modeling of effective connectivity dates back to McIntosh and Gonzalez-Lima(1994) [46] and Buechel and Friston(1997) [8] who suggested the use of structural equation modeling, and Buechel and Friston(1998) [9] who proposed variable parameter regression to investigate the effective connectivity.

McIntosh and Gonzalez-Lima (1994) made use of structural equation modeling of **fMRI** data to map the underlying effective connectivity in the human brain in the sense that a measure of covariance of the evoked neural activities corresponds to the degree to which activities of two sites are related to one another [46]. In other words, the association

between neural activities should be quantified in terms of covariance because one neural activity can instigate the change of, therefore the variance of, another. For their application of structural equation modeling, they also introduced the terms *anatomical* and *functional* model (McIntosh and Gonzalez-Lima, 1993 [44]; McIntosh et al., 1994 [45]). The anatomical model simply portrays the neuroanatomical couplings between brain regions. The numerical weights (or path coefficients) to these couplings, using the interregional correlations of activities over the anatomical model, leads to the functional model. Therefore, the functional model displays the influences of regions on each other through the anatomical couplings. In some aspects, the functional model can be recognized as the effective connectivity in that both depict the influence of one on another. Based on the anatomical and functional model, the association among brain areas is depicted by a simple linear equation of the variance of a region influenced by the variance of another;

$$\eta = \beta \eta + \Psi \tag{3.1}$$

For example,

$$\begin{bmatrix} A \\ B \\ C \\ D \end{bmatrix} = \begin{bmatrix} 0 & 0 & 0 & 0 \\ w & 0 & 0 & 0 \\ v & y & 0 & 0 \\ x & z & 0 & 0 \end{bmatrix} \begin{bmatrix} A \\ B \\ C \\ D \end{bmatrix} + \begin{bmatrix} \Psi_A \\ \Psi_B \\ \Psi_C \\ \Psi_D \end{bmatrix}$$

In (3.1), η, β and Ψ denote the vectors of variances of regional activities from the selected regions being studied, the matrix of the path coefficients in the functional model and a vector of residual effects, respectively. The path coefficients in the functional model are estimated via iterative maximum likelihood estimation and subsequently the estimated covariance matrix is computed and compared with the observed covariance matrix. On the basis of the difference between these matrices, estimated parameters are updated iteratively and iterations stop when the difference between the observed and estimated covariance matrices is in a reasonable range. The performance is likely to be poor only when singularity exits in the dataset. However, this approach has several shortcomings: First, it ignores the temporal correlation in the data and accordingly may lead to erroneous estimates and standard errors. Second, they assume that connectivity among activated brain regions is invariant over

time, yet the recent studies has shown that the connectivity between brain regions may be time-varying.

Buechel and Friston (1998) recommended the use of variable parameter regression to investigate the effective connectivity in the human brain [9]. This method addresses one of the limitations described in the structural equation modeling by permitting time-varying (or dynamic) connectivity in the model. In this study, Buechel and Friston focused their attention on the effect of attention on the connection between two regions of interest (**ROI**), namely the motion-sensitive area V5 and the posterior parietal cortex (**PP**) in the right hemisphere. Regressing PP ($x(t)$) on V5 ($y(t)$) with time-varying connectivity coefficients allows us to evaluate the effective connectivity between the two brain areas over time. Formally, the variable parameter regression model consists of two hierarchies,

$$\begin{aligned} y(t) &= x(t)\beta(t) + u(t), \quad t = 1, \cdots, T \\ & \quad u(t) \sim N(0, \sigma^2) \\ \\ \beta(t) &= \beta(t-1) + p(t), \quad t = 2, \cdots, T \\ & \quad p_t \sim N(0, \sigma^2 P) \end{aligned} \tag{3.2}$$

In (3.2), the first equation constitutes the ordinary regression model and the second represents the time-varying model of the effective connectivity coefficients (β) which is assumed to follow a random walk with mean zero over time. Furthermore, $\sigma^2 P$ is the stationary covariance matrix of $p(t)$ and if $P = 0$, then variable parameter regression reduces to the ordinary stationary coefficient linear regression. Kalman filtering (Kalman, 1960) [38] permits estimation of the trajectory of the $\beta(t)$, and P and σ^2 are estimated by maximum likelihood estimation. Moreover, this approach enables us to test the null hypothesis $H_0 : P = P_0$, especially $H_0 : P = 0$, i.e., no dynamic change of $\beta(t)$ over time, by comparing a chi-square distribution with the test statistic of the form;

$$-2ln(\lambda) = -2\left[L^*(P_0) - L^*(\hat{P})\right]$$

Using the variable parameter regression, it is shown that the changes in activity from PP could explain the changes in activity from V5 over time. That is, the activities from V5 could be demonstrated as a function of time and activity from PP. However, since this approach is restricted to probe into the rapport between only two brain regions, it should be further generalized to create a model which can handle multiple brain regions.

There have been several attempts to relax the weaknesses described in the structural equation model and the variable parameter regression model. These may be divided into two categories: (i) the first approach models dynamic connectivity by simply measuring relationships within the measured data (e.g., multivariate autoregressive modeling), whereas (ii) the second approach includes equations of dynamic connectivity in the model (e.g., state-space modeling).

Harrison et al. (2003) recommended a multivariate autoregressive (**MAR**) model to model **fMRI** time series to explore the intrinsic effective connectivity in the human brain [32]. The application of a **MAR** model differs from that of a state-space model in that it models time-varying effects across **ROI** *without* making use of the state equation. In other words, the use of **MAR** modeling characterizes dependencies among regions in terms of the historical influence one region has on another. Thus, the vector of present time series is expressed as a linear function of previous time series. For **MAR(P)** model, the present time series can be expressed by

$$\begin{aligned} y(t) &= \sum_{i=1}^{p} y(t-i)A(i) + e(t) \\ \iff \underbrace{y(t)}_{1\times d} &= \underbrace{x(t)}_{1\times(pd)} \underbrace{W}_{(pd)\times d} + \underbrace{e(t)}_{1\times d} \end{aligned} \tag{3.3}$$

where $y(t) = [y_1(t), \cdots, y_d(t)]$, $x(t) = [y(t-1), \cdots, y(t-p)]$ and d is the number of **ROIs**. In addition, W represents the matrix of **MAR** coefficients containing a total of pd^2 non-zero **MAR** coefficients and $e(t)$ is Gaussian noise with mean zero and covariance R. Here, the off-diagonal elements of W demonstrate the amplitude of the influence one region exerts

on another, whereas the diagonal elements of W manifest the intensity of self-connection. The special feature of this approach is in the utilization of nonlinear coupling in the model. According to (3.3), the response $y(t)$ is affected by the linear combination of inputs $x(t)$. However, this expression is not true if the interaction of inputs yields the response. That is, the response $y(t)$ cannot be expressed by the sum of inputs $x(t)$ anymore and it would yield more precise expression to introduce interaction terms in the model. Such interactions are demonstrated by employing bilinear terms. The bilinear expression of the interaction (3.4) between $y_j(t)$ and $y_k(t)$ is expressed by

$$I_{jk}(t) \;=\; y_j(t)y_k(t), \tag{3.4}$$

that is, $I_{jk}(t)$ denotes the interaction between responses from two different **ROIs**, j and k. In addition, its corresponding augmented **MAR** model has the form as below,

$$\begin{aligned} [y(t), I_{jk}(t)] \;&=\; \sum_{i=1}^{p} [y(t-i), I_{jk}(t-i)]\, \tilde{A}(i) + e(t), \\ \Longleftrightarrow Y \;&=\; XW + E, \end{aligned} \tag{3.5}$$

where $X = [\{y(t-1), I_{jk}(t-i)\}, \cdots, \{y(t-p), I_{jk}(t-p)\}]$ and $W = \tilde{A}(i)$. Based on the above augmented **MAR** model in (3.5), the inferences can be made in two different ways: by maximum likelihood estimation and by Bayesian estimation. The *MLE* for **MAR** coefficients and its associated covariance matrix are

$$\begin{aligned} \hat{W}_{ML} \;&=\; (X^T X)^{-1} X^T Y, \\ \hat{\Sigma}_{ML} \;&=\; S_{ML} \otimes (X^T X)^{-1}. \end{aligned} \tag{3.6}$$

where

$$S_{ML} \;=\; \frac{1}{N - pd^2} (Y - X\hat{W}_{ML})^T (Y - X\hat{W}_{ML})$$

It is also feasible to draw inferences on **MAR** coefficients within a Bayesian framework (Penny and Roberts, 2002) [52]. Using the following prior distribution,

$$\begin{aligned} P(W|p) &\sim N(0, \alpha I), \\ P(\alpha|p) &\sim Gamma(b, c), \\ P(\Lambda|p) &= |\Lambda|^{-(d+1)/2}, \end{aligned} \tag{3.7}$$

the posterior distributions of **MAR** coefficients, the precision of the Normal prior distribution (α) and the noise precision (Λ) are given by

$$\begin{aligned} P(W|Y, p) &= N\left(\hat{W}_B, \hat{\Sigma}_B\right) \\ P(\alpha|Y, p) &= Gamma\left(\hat{b}, \hat{c}\right) \\ P(\Lambda|Y, p) &= Wishart(s, B) \end{aligned} \tag{3.8}$$

This posterior distribution enables one to make inferences about the intensity of effective connectivities. However, it is worth noting that the **MAR** modeling with bilinear terms only considers the interaction between two different brain regions. It might perform better if two or higher way interactions were considered in the model, because an activity from a region could be influenced by coupling activities from several other brain regions.

Goebel et al. (2003) and Roebroeck et al. (2005) put forward a framework which is designed to unveil the effective connectivity (or "directed influences" in their terminology) in the human brain using vector-autoregressive (**VAR**) modeling in the context of Granger causality. [27] [56]. They advocate this approach for several reasons. First, the **VAR** model can model the temporal structure in the variations of individual components and in the interdependence between such components. Second, the autoregressive coefficients representing the the degree of dependence between components can be easily estimated. Third, several complex random processes can be approximated by the **VAR** model with large p where p is the number of autoregressive coefficients. Lastly, a measure of effective connectivity based on the concept of Granger causality can be defined. The notion of Granger causality introduced by Granger(1969, 1980) is based on the perception that causes always

go ahead of effects, so that something in the future cannot lead to something in the past or present [28] [29]. Conceptually, if a series y generates a series x, then awareness of y should assist in predicting future values of x. Furthermore, we say y Granger causes x if the current value of x, x_t, can be better forecast based on the past values of x and y together (information set D) than based on the past value of x alone (information set $D - y$). Here, the information sets D and $D - y$ are defined by

$$D = \{y; x\} = \{y(n-1), y(n-2), \cdots; x(n-1), x(n-2), \cdots\},$$

$$D - y = \{x\} = \{x(n-1), x(n-2), \cdots\}.$$

Therefore if x_t is better predicted by the previous value of x and y together, the temporal dependency between x and y can be used to determine the direction of potential influence of one over another. Goebel and Roebroeck also noted that if there are other series which have possible causal influences on both x and y, then these should be included in the information set D. Otherwise, it would lead to *spurious* causality between x and y. Here, the *spurious* causality is defined to be a mathematical association in which two occurrences have no causal connection, yet it may be inferred that they do, due to confounding factors. Since the **VAR** model,

$$q_t = -\sum_{i=1}^{p} A_{q,i} q_{t-i} + w_t, \quad var(w_t) = \begin{bmatrix} \Sigma_2 & C \\ C^T & T_2 \end{bmatrix}$$

where

$$\begin{aligned} q_t &= \begin{bmatrix} x_t \\ y_t \end{bmatrix}, \\ x_t &= -\sum_{i=1}^{p} A_{x,i} x_{t-i} + u_t, \quad var(u_t) = \Sigma_1, \\ y_t &= -\sum_{i=1}^{p} A_{y,i} y_{t-i} + v_t, \quad var(v_t) = T_1, \end{aligned}$$

can be understood as a linear prediction model, the **VAR** coefficients, $A_{q,i}$, can be thought of as quantifying Granger causality between x and y. Based on the model above, Geweke's

method (1982) is employed to calculate a measure of linear influence, $F_{x,y}$, between series x and y defined as follows [24];

$$F_{x,y} \quad = \quad F_{x\to y} + F_{y\to x} + F_{x\cdot y}$$

where

$$\begin{aligned} F_{x,y} &= ln\left(|\Sigma_1| \cdot |T_1|/|Y|\right), \\ F_{x\to y} &= ln\left(|T_1|/|T_2|\right), \\ F_{y\to x} &= ln\left(|\Sigma_1|/|\Sigma_2|\right), \\ F_{x\cdot y} &= ln\left(|\Sigma_2| \cdot |T_2|/|Y|\right), \end{aligned} \tag{3.9}$$

where $|A|$ is the determinant of A. Here, each component in (3.9) represents a measure of the total linear dependence between x and y, of linear directed influence from x to y, of linear directed influence from y to x and of the instantaneous influence between x and y. Thus, $F_{x,y} = 0$ implies no linear dependence between x and y, $F_{x\to y} = 0$ (or $F_{y\to x} = 0$) implies no linear direct influence from x to y (or y to x). This approach is different from Harrison's approach described in the previous paragraph in that it investigates the association of activities from the two different brain regions using variance components whereas Harrison explores the relationship using estimating **AR** coefficients. Furthermore, since it only considers two different brain regions, it would be expected to better if several other regions are considered all together at once.

Eichler (2005) suggested a graphical approach to investigate the underlying relationship in the human brain to supplement the use of **VAR** model in the context of Granger causality [15]. The potential dependencies among the observed **fMRI** time series are sketched in a graph, either bivariate or multivariate path diagram. *Spurious causality* is a falsely detected causal relationship in the presence of confounding factors and either a bivariate or a multivariate path diagram is utilized to avoid the *spurious causality*. It is found that multivariate path diagrams best describe the relationship of activities from different brain regions only when they are not confounded by the same latent variables. In contradiction

to multivariate path diagrams, the bivariate path diagrams are suitable for describing the relationship of observed activities only when they are influenced by a same confounder. They found that if this instruction is violated, one can face the spurious causality. Furthermore, the spurious causality is divided into two categories (Hsiao, 1982) [36], spurious causality of type I and II. The former,the spurious causality of type I, is characterized by the phenomenon that a Granger causal relationship fades away once one or more variables are removed from the information set, whereas the latter, the spurious causality of type II is defined to be the phenomenon that a Granger-causal relationship vanishes once additional variables are added. However, in practice, some Granger-causalities are best described by a multivariate path diagram and some of them by a bivariate path diagram. So the choice of one against another may cause one of the spurious causalities described above. To this end, Eichler proposed a new graphical representation, *general path diagram*, which is a mixture of multivariate and bivariate path diagrams and demonstrated that the general path diagram is suitable for visualizing the effective connectivity of the complex brain network.

Valdes-Sosa et al. (2005) noted several pitfalls of previously described methods of estimating effective connectivity in the voxel-based study [66]. First, even though an ordinary **MAR** (or **VAR**) model is ideally expected to give rise to the detection of the effective connectivities in the context of Granger causality, the **MAR** modeling works only well for the situation in which the number of time points, N_t, at which the **BOLD** response is being measured is sufficiently larger than the number of activation spots, p. Such a situation is rare in the analysis of voxel-based neuroimaging data. The general **MAR** model is;

$$y_t = \sum_{i=1}^{N_t} A_k y_{t-k} + e_t, \qquad t = N_k + 1, \cdots, N_t \tag{3.10}$$

where $A_k = \{a_{i,j}^k\}_{1 \le i,j \le p}$ is the matrix of autoregressive coefficients defined at time lag k, $y_t = \{y_{t,i}\}_{1 \le i \le p; 1 \le t \le N_t}$ is the vector of observations at time t, and e_t is the Gaussian noise with mean vector zero and covariance matrix R. In (3.10), the total number of **MAR** coefficients to be estimated, $N_k p^2 + (p^2 + p)/2$, is too large for good estimation to be possible. For

example, the first order ordinary **MAR** model $y_t = A_1 y_{t-1} + e_t, \quad t = 2, \cdots, N_t$ can be written as a multivariate regression such that

$$Z \;=\; XB + E, \quad E_i \sim N(0, \Sigma) \quad i = 1, \cdots, m$$

where

$$\begin{aligned}
&m = N_t - 1, \\
&Z_{(m\times p)} = [y_2, \cdots, y_t, \cdots, y_{N_t}]^T = [z_1, \cdots, z_i, \cdots, z_p], \\
&B_{(p\times p)} = A_1^T = [\beta_1, \cdots, \beta_p], \\
&X_{(m\times p)} = [y_1, \cdots, y_m]^T, \\
&E_{(m\times p)} = [e_2, \cdots, e_t, \cdots, e_{N_t}],
\end{aligned}$$

and obtaining the usual **MLE** of B is equivalent to finding (or estimating) B which minimizes the squared distance from Z to XB with respect to B;

$$\hat{B} \;=\; \arg\min_B ||(Z - XB)||^2_\Sigma \tag{3.11}$$

so that

$$\hat{B} \;=\; (X^T X)^{-1} X^T Z.$$

However, it is worthwhile to note that this **MLE** functions only if m is greater than p; that is, the number of time points at which data are being measured are larger than the number of the activation spots. Such a situation is rare in the analysis of **fMRI** data. Secondly, the **MAR** approach requires the specification of a small number of nodes (or voxels) and pre-determined sparsity structure. Here, the predetermined sparsity structure is made through elimination of edges (or effective connectivities) based on prior knowledge, but it may cause spurious causality at the cost of dumping relevant but latent informations from other nodes. To overcome the pitfalls described above, Valdes-Sosa et al. recommended employing a *sparse* **MAR** (**SMAR**) model in which the sparsity structures of the effective connectivity are obtained via variable selection instead of predetermination. They recognized

that penalized regression techniques turned out to be very useful for variable selection (Fan and Peng, 2001, 2004) [17] [18]. By iteratively employing a penalized regression method such as *ridge regression* (Hoerl and Kennard, 1970 [35]) for variable selection, the number of edges in the brain network representing the effective connectivities can be reduced, leading to a **SMAR** model. Ridge regression replaces (3.11) with

$$\hat{B} \quad = \quad \arg\min_{B} ||(Z - XB)||^2_{\Sigma} + \lambda^2 ||(PB)||^2, \tag{3.12}$$

so that

$$\hat{B} \quad = \quad (X^T X + \lambda^2 P^T P)^{-1} X^T Z,$$

where P in (3.12) is a penalty function, the spatial Laplacian operator (Valdes-Sosa, 2004) [65]. The estimation of the effective connectivity can be performed by means of iterative application of ridge regression:

$$\hat{\beta}_i^{k+1} = (X^T X + \lambda^2 D(\hat{\beta}_i^k)) X^T z_i, \quad i = 1, \cdots, p,$$

where $D(\hat{\beta}_i^k)$ is a diagonal matrix with the diagonal components $p'_\lambda(\hat{\beta}_i^k)/|\hat{\beta}_i^k|$, $k = 1, \cdots, p$ and $p'_\lambda(\hat{\beta}_i^k) = 2\lambda\hat{\beta}_i^k$ is the derivative of the penalty function. The **SMAR** modeling seems to be successful in the case of the voxel-based study but questionable for the region-of-interest (**ROI**)-based study because each **ROI** is composed of several hundred thousand voxels, the number of time points is usually larger than the number of **ROIs** and one may prefer to using the usual **MAR** model rather than the **SMAR** model.

Moon-Ho Ringo Ho et al.(2005) proposed a state space approach to modeling brain dynamics [34]. The state space approach differs from the **MAR** (or **VAR**) approach in that it estimates the connectivity by utilizing equations of connectivity rather than by simply measuring relationship in the observed data. Their model consists of two equations, namely the activation and the connectivity equation corresponding to the observation and

the state equation in the state-space modeling terminology. For example, activations from two vitalized brain areas are expressed by

$$\begin{aligned}\begin{pmatrix} y_1(t) \\ y_2(t) \end{pmatrix} &= \begin{pmatrix} \alpha_1 \\ \alpha_2 \end{pmatrix} + \begin{pmatrix} x_1(t) & 0 \\ 0 & x_2(t) \end{pmatrix} \begin{pmatrix} \beta_1(t) \\ \beta_2(t) \end{pmatrix} + \begin{pmatrix} e_1(t) \\ e_2(t) \end{pmatrix} \\ \iff y_t &= \alpha + A_t\beta_t + e_t, \quad e_t \sim N_2\left(\underset{\sim}{0}, \Sigma_e\right),\end{aligned} \tag{3.13}$$

where

$$\Sigma_e = \begin{pmatrix} \sigma^2_{e_1} & 0 \\ 0 & \sigma^2_{e_2} \end{pmatrix}.$$

Here, y_t, x_t, e_t, β_t and α in (3.13) denote the *observed* **BOLD** response, the *delay* of the **BOLD** response which is obtained from convolving a haemodynamic response function(**HRF**, $h(t)$) with the past stimulus($s(t-u), u \leq t$) value, measurement noise, intensity of the delay of **BOLD** response and baseline respectively. (3.13) is referred to as the activation equations. Here, the magnitudes of activation, β_t, is time-varying and the activation from one area can be displayed as a function of past records of itself and another region, that is,

$$\begin{aligned}\begin{pmatrix} \beta_1(t) \\ \beta_2(t) \end{pmatrix} &= \begin{pmatrix} \gamma_{11}x_1(t-1) & \gamma_{12}x_2(t-1) \\ \gamma_{21}x_1(t-1) & \gamma_{22}x_2(t-1) \end{pmatrix} \begin{pmatrix} \beta_1(t-1) \\ \beta_2(t-1) \end{pmatrix} + \begin{pmatrix} \omega_1(t) \\ \omega_2(t) \end{pmatrix} \\ \iff \beta_t &= \Gamma_t A_{t-1}\beta_{t-1} + \omega_t, \quad \omega_t \sim N_2\left(\underset{\sim}{0}, \Sigma_\omega\right),\end{aligned} \tag{3.14}$$

where

$$\Sigma_\omega = \begin{pmatrix} \sigma^2_{\omega_1} & 0 \\ 0 & \sigma^2_{\omega_2} \end{pmatrix}.$$

Here γ_{12} and γ_{21} represent the *coupling* relationship between two different brain regions, γ_{11} and γ_{22} stand for self-feedback, and ω_t are the Gaussian random errors. (3.14) is referred as the connectivity equations. Based on these coefficients, one can test hypotheses such as

1. No coupling relationship between the two brain regions, $H_0 : \gamma_{12} = \gamma_{21} = 0$
2. region 1 is not a *leading indicator* of region 2, $H_0 : \gamma_{12} = 0$

3. region 2 is not a *leading indicator* of region 1, $H_0 : \gamma_{21} = 0$

According to (3.13) and (3.14), the parameters of interests are

$$\Omega = \{\alpha, \Gamma, \Sigma_e, \Sigma_\omega\}. \tag{3.15}$$

The maximum likelihood estimator of parameters in (3.15) are obtained by utilizing the EM-algorithm (Dempster, Laird and Rubin, 1977; Shumway and Stoffer, 1982) [14] [60]. Shumway and Stoffer (1982) showed that the log-likelihood function can be maximized by applying EM-algorithm so that **ML** estimators can be obtained [60]. However, in this state space approach, the effective connectivity between areas (γ_{ij}) is postulated not to be time-varying and this assumption has been proved to be unrealistic in general (Aertsen et al., 1991; Friston, 1994; McIntosh et al., 1994; Buechel et al., 1998) [1] [20] [46] [9]. The alternative state space approach was developed by Moon-Ho Ringo Ho.

Bhattacharya and Moon-Ho Ringo Ho(2006) developed an alternative state-space approach to model the time-varying connectivity within a Bayesian framework [7]. In short, this approach has three components of interest which constitute a model with three levels of hierarchy.

1. The first component is the intensity of activation which is denoted by $\beta_i(t)$.
2. The second component is the magnitude of influence of the j th region on the i th region at time point t which is denoted by γ_{ij}.
3. The third component models time varying effective connectivity parameter $\gamma_{ij}(t)$.

Based on these components, one can construct the model as below;

$$\begin{aligned} y_t &= \alpha + A_t\beta_t + e_t, \quad e_t \sim N_2\left(\underset{\sim}{0}, \Sigma_e\right), && (3.16)\\ \beta_t &= \Gamma_t A_{t-1}\beta_{t-1} + \omega_t, \quad \omega_t \sim N_2\left(\underset{\sim}{0}, \Sigma_\omega\right), && (3.17)\\ \Gamma_t &= \Gamma_{t-1} + \delta_t, && (3.18) \end{aligned}$$

where $i = 1, \cdots, n$ and $t = 1, \cdots, T$ denote the region-of-interest(**ROI**) and time index respectively. The underlying assumptions behind this approach are

1. $e_i(t)$ follows AR(autoregressive) process of order p with an unknown parameter ρ_i, $|\rho_i| < 1$,
2. $\omega_i(t) \sim i.i.d\, N(0, \sigma_\omega^2)$,
3. $\delta_{i,j}(t) \sim i.i.d\, N(0, \sigma_\delta^2)$,
4. $\omega_i(t)$ and $\delta_{i,j}(t)$ are independent given the condition 1.

The inferences on three components are made through Bayesian parameter estimation via Gibbs sampling and it was shown that the state space approach described here works well for modeling the time varying effective connectivity.

3.2 DECONVOLUTION OF NEURAL ACTIVATION

The study of **fMRI** time-series data analysis can supply information about the intrinsic neuronal response to a given stimuli using the observed blood oxygenation level-dependent (**BOLD**) responses which are measured by a **fMRI** scanner. However, it might be problematic to use the **BOLD** response as a proxy for the underlying neuronal activity because it is measured at the level of haemodynamic response, not at a neuronal level. In other words, **BOLD** is not a direct measure of neuronal activity, but rather a secondary consequence of neuronal activity.

Until now, most activation and connectivity studies on analyzing fMRI time series data have utilized **BOLD** response to investigate functional integration and functional segregation. However, the study might be more precise if the well approximated or estimated underlying neuronal activity is utilized instead of the **BOLD** response, because, as described above, the **BOLD** response measures the change in haemodynamic response rather than that in neuronal activity.

The possibility of approximating or estimating latent neuronal activity comes from the fact that a **BOLD** response is expressed as a convolution of the neuronal signal and the haemodynamic (or impulse) response function (**HRF** or **IRF**). Therefore, the estimating procedures described below will be understood by deconvolving the neuronal signal from the observed **BOLD** response using assumed **HRF** (or **IRF**). Due to the assumed **HRF**, it is referred to as a **Semi-Blind** deconvolution method.

Glover (1999) suggested a deconvolution method in which the *Wiener* filter is utilized to restore the inherent neuronal signal by removing the haemodynamic response function (**HRF**) from the **BOLD** response [26]. If the observed response, $y(t)$ is expressed as the linear convolution of the underlying neuronal signal, $f(t)$ and the assumed haemodynamic response $h(t)$ with additive noise $e(t)$;

$$y(t) \quad = \quad h(t) * f(t) + e(t), \tag{3.19}$$

then an approximation of the underlying neuronal activity, $\hat{f}(t)$ can be obtained using the *Wiener* filter $w(t)$ (Papoulis, 1977) [51],

$$\hat{f}(t) \quad = \quad w(t) * y(t).$$

Using the *Fourier* transformations of $y(t)$, $h(t)$, $e(t)$ and $w(t)$, the *Wiener* deconvolved neuronal signal, $\hat{f}(t)$ is expressed as,

$$\hat{f}(t) \quad = \quad \mathcal{F}^{-1}\left\{W(\omega)Y(\omega)\right\}, \tag{3.20}$$

where

$$W(\omega) \quad = \quad \frac{H^*(\omega)}{|H(\omega)|^2 + |E(\omega)|^2}. \tag{3.21}$$

Here in (3.20) and (3.21), $H(\omega)$, $Y(\omega)$, $E(\omega)$ and $W(\omega)$ represent the *Fourier* transformation of $h(t)$, $y(t)$, $n(t)$ and $w(t)$, respectively, and $*$ and $\mathcal{F}^{-1}$ denote complex conjugate and the inverse *Fourier* transform operator. Glover notes that deconvolution using the *Wiener* filter is efficient in diminishing the blurring and distortion factor (or the haemodynamic response function) from the observed **BOLD** response and consequently obtaining the well approximated intrinsic neuronal response to the applied stimuli. However, he also noted that the achievement of deconvolution depends on the validity of the haemodynamic response function. Therefore, the choice of a reasonable haemodynamic response function should be made at the beginning of the study.

Zarahn(2000) [70] proposed a deconvolution method in which a linear time invariant (**LTI**) model is employed to model the transform from the latent neuronal signal to the observed **BOLD** response. **LTI** model is defined to be a model whose output is the convolution of the input with an impulse response function (**IRF**) (Oppenheim et al., 1983) [50]. Therefore, in the study of **fMRI** time series data, linear time invariant transform of the underlying neuronal signal to the observed **BOLD** response is expressed as

$$y(t) \quad = \quad h(t) * f(t) + e(t), \tag{3.22}$$

or

$$Y \quad = \quad HF + E, \tag{3.23}$$

where Y, H, F and E are a matrix of the observed **BOLD** response, a matrix of the haemodynamic response, a matrix of the unknown neuronal signal and a matrix of the additive noise, respectively. To estimate the implicit neural signal, Zarahn recommended the utilization of the ordinary least squares deconvolution method. However, Zarahn also noted that the use of the ordinary least squares deconvolution method is problematic when the mapping from **fMRI** signals to the neuronal signal is not unique,-that is, an inverse transform does not exist. To overcome the non-existence of an inverse transform, Zarahn recommended the use of a product of a spanning matrix (or neuronal basis matrix) G and a vector of unknown weights β instead of a matrix of the unknown neuronal signal F in (3.23). The use of G and β guarantees a unique mapping from the **fMRI** signal to the neuronal signal. Moreover, due to the fact that the **fMRI** signals are measured at a rate determined by repetition time (**TR**) of stimuli, **fMRI** signals are down-sampled to the **TR**. On this account, a down-sampling matrix M is multiplied, that is, (3.23) is replaced by

$$Y \quad = \quad MHG\beta + E. \tag{3.24}$$

Therefore, the ordinary least-square deconvolved neuronal signal is given by

$$G\hat{\beta} = G\left((MHG)^T(MHG)\right)^{-1}(MHG)^T Y. \tag{3.25}$$

Here, $G\hat{\beta}$ can be regarded as a deblurred (or deconvolved) neuronal signal via the *Wiener* deconvolution in (3.20). However, despite having a unique mapping from **fMRI** signal to underlying neuronal signal, Zarahn noted that increasing the number of spanning (or neuronal basis) vectors in G may result in collinearity and consequently inefficient estimation. Thus, the choice of a reasonable number of neuronal basis vectors should be made at the beginning of the study.

Gitelman et al. (2003) proposed a deconvolution method in which the empirical Bayes formulation is employed to restore underlying neuronal signals from observed **BOLD** responses distorted by a haemodynamic response function (**HRF**) [25]. In this approach, the observed **BOLD** response from region A, $y_A(t)$, is expressed as the linear convolution of the underlying neuronal signal, $f_A(t)$, and the assumed haemodynamic response, $h(t)$, with additive noise, $e(t)$ as in (3.19). Next, the underlying neuronal signal $f_A(t)$ is expanded in terms of a *Fourier* series or a set of cosine functions X,

$$f_A(t) \quad = \quad X\beta,$$

where β are unknown parameters which control the expression of different frequency components of $f(t)$. Then, using matrix notation, (3.19) can be replaced by

$$y_A \quad = \quad HX\beta + e. \tag{3.26}$$

Therefore, we can obtain the deconvolved neuronal signal by first estimating unknown parameter β and then post multiplying it by X. To estimate β, a Gaussian prior assumption is made on the unknown parameter β in (3.26) (Friston, 2002) [21] and the Bayesian estimate of β is obtained,

$$\hat{\beta}_{MAP} = \left(X^T H^T \Sigma^{-1} HX + \sigma^2 C_\beta^{-1}\right)^{-1} X^T H^T \Sigma^{-1} y_A, \tag{3.27}$$

where $\hat{\beta}_{MAP}$ is the Bayesian estimate of β, C_β^{-1} is the prior precision of β, and Σ is the covariance matrix of additive noise, e. Therefore, the deconvolved neuronal signal is given by

$$X\hat{\beta}_{MAP} = X\left(X^T H^T \Sigma^{-1} HX + \sigma^2 C_\beta^{-1}\right)^{-1} X^T H^T \Sigma^{-1} y_A. \tag{3.28}$$

Gitelman investigated the performance of the proposed method by juxtaposing the product of two **BOLD** responses, $y_A(t)y_B(t)$ and the post-convolved product of two estimated neural signal with **HRF**, $H(f_A(t)f_B(t))$. Based on Gitelman's simulation, it is found that the **BOLD**-based study is insensitive to the corresponding inception of the neural activation. It it worthwhile to note that the idea of expanding $f(t)$ in terms of a *Fourier* series or a set of cosine functions is the special case of Zarahn's method in which the type of neuronal basis

vector is unspecified and also the way of estimating β is different from Zarahn's method in that Bayes method is utilized rather than the ordinary least square method. In addition, one can also notice that setting the leading diagonal elements of C_β to infinity would make (3.28) equivalent to (3.25).

4.0 THE PROPOSED DECONVOLUTION METHOD

4.1 BLIND DECONVOLUTION METHOD

As discussed in the previous section, the goal of deconvolution in **fMRI** study is to estimate the true neuronal activity from the observed **BOLD** response. The previously studied deconvolution methods restore the true neuronal activity assuming a known haemodynamic response function (**HRF** or blurring factor), which is referred to as **Semi-Blind Deconvolution**. That is, an observed **BOLD** response is represented by the following linear model:

$$\begin{aligned} y(t) &= f(t) * h(t) + \eta(t) \\ &= \sum_{\substack{u=1 \\ t,u \in T}}^{t} h(u) f(t-u) + \eta(t), \end{aligned} \tag{4.1}$$

in which $*$ denotes the linear convolution operator, T is the set of time points and $y(t)$, $f(t)$, $h(t)$ and $\eta(t)$ represent the observed **BOLD** response, the true neuronal activity, the haemodynamic response function and the additive noise respectively. In (4.1), the observed **BOLD** response can be estimated to be the convolution of the true neuronal activity with the haemodynamic response function (**HRF**). The problem of restoring the true $f(t)$ in the Semi-Blind deconvolution requires the separation of assumed $h(t)$ and the underlying $f(t)$ based on the measured $y(t)$. In this approach, the haemodynamic response function, $h(t)$, is usually modeled by a Poisson, Gaussian or Gamma distribution or by the difference of two Gamma densities. The method we are going to propose here differs from the semi-blind deconvolution method in that both the true neuronal activity function $f(t)$ and the blurring factor function $h(t)$ are assumed to be unknown or partially known and it requires

estimation of both $f(t)$ and $h(t)$. This type of deconvolution method is referred to as **Blind Deconvolution**.

4.2 BLIND DECONVOLUTION VIA MAXIMUM LIKELIHOOD ESTIMATION

Blind deconvolution via a maximum likelihood parameter estimation method involves modeling the true neuronal activity $f(t)$ as a autoregressive (**AR**) process and considering the **HRF** $h(t)$ as an unknown constant. Consequently, estimating AR parameters and unknown $h(t)$s allow us to identify the true neuronal activity function, $f(t)$ and the unknown haemodynamic response function, $h(t)$ from the observed **BOLD** response, $y(t)$.

4.2.1 AR model of the Underlying Neuronal Activity

The underlying neuronal activity function, $f(t)$ is modeled as a autoregressive (**AR**) process:

$$\begin{aligned} f(t) &= \sum_{l=1}^{p} a(l) f(t-l) + \nu(t), \\ & t \in T = \{1, 2, \cdots, T\}, \end{aligned} \tag{4.2}$$

where $\nu(t)$ is a zero mean multivariate Gaussian noise with covariance matrix $\sigma_\nu^2 I$ which is statistically independent of the underlying neuronal activity function, $f(t)$. Using matrix notation, (4.2) is equivalent to

$$\begin{bmatrix} f(1) \\ f(2) \\ f(3) \\ \vdots \\ \vdots \\ f(T) \end{bmatrix} = \begin{bmatrix} 0 & 0 & 0 & \cdots & \cdots & 0 \\ a(1) & 0 & 0 & \cdots & \cdots & 0 \\ a(2) & a(1) & 0 & \cdots & \cdots & 0 \\ \vdots & \vdots & \ddots & \ddots & \vdots & \vdots \\ 0 & a(p) & \cdots & a(1) & 0 & 0 \\ 0 & 0 & a(p) & \cdots & a(1) & 0 \end{bmatrix} \begin{bmatrix} f(1) \\ f(2) \\ f(3) \\ \vdots \\ \vdots \\ f(T) \end{bmatrix} + \begin{bmatrix} \nu(1) \\ \nu(2) \\ \nu(3) \\ \vdots \\ \vdots \\ \nu(T) \end{bmatrix}$$

or

$$\mathbf{f} \;=\; \mathbf{A}\mathbf{f} + \nu, \tag{4.3}$$

where the matrix A is a *Toeplitz* matrix (diagonal-constant matrix), which is defined to be a matrix in which each descending diagonal from left to right is constant. Here, p denotes the number of **AR** parameters and in order to determine p, model order selection should be made at the beginning of the study. The autocorrelation function (**ACF**) and partial autocorrelation function (**PACF**) are expected to give several candidates for p and each candidate should be investigated via a measures of the goodness of fit of a statistical model such as **Akaike Information Criterion** (**AIC**) (Akaike, 1971) [3] or **Bayesian Information Criterion** (**BIC**) (Schwarz, 1978) [58].

4.2.2 Multivariate Gaussian model of the Observed BOLD response

As discussed at the beginning of this chapter, Blind Deconvolution via a **ML** estimation method involves considering $h(t)$ as an unknown constant and the effect of **HRF** $h(t)$ on the observed **BOLD** response $y(t)$ can be modeled as a finite impulse response (**FIR**) filter. Consequently, the observed **BOLD** response, $y(t)$ is expressed as,

$$y(t) \;=\; \sum_{u=1}^{t-1} h(u) f(t-u) + \eta(t),$$

where η is a zero mean multivariate Gaussian noise with covariance matrix $\sigma_\eta^2 I$ which is statistically independent of f in (4.3). Again, using the matrix notation, (4.1) can be expressed as:

$$\begin{bmatrix} y(1) \\ y(2) \\ y(3) \\ \vdots \\ \vdots \\ y(T) \end{bmatrix} = \begin{bmatrix} 0 & 0 & 0 & \cdots & \cdots & 0 \\ h(1) & 0 & 0 & \cdots & \cdots & 0 \\ h(2) & h(1) & 0 & \cdots & \cdots & 0 \\ \vdots & \vdots & \ddots & \ddots & \vdots & \vdots \\ h(T-2) & h(T-3) & \cdots & h(1) & 0 & 0 \\ h(T-1) & h(T-2) & \cdots & \cdots & h(1) & 0 \end{bmatrix} \begin{bmatrix} f(1) \\ f(2) \\ f(3) \\ \vdots \\ \vdots \\ f(T) \end{bmatrix} + \begin{bmatrix} \eta(1) \\ \eta(2) \\ \eta(3) \\ \vdots \\ \vdots \\ \eta(T) \end{bmatrix}$$

or

$$\mathbf{y} \;=\; \mathbf{Hf} + \eta, \tag{4.4}$$

where $\mathbf{H}$ is again a *Toeplitz* matrix. Solving for f in (4.3), we obtain

$$\mathbf{f} = (\mathbf{I} - \mathbf{A})^{-1}\nu. \tag{4.5}$$

Thus, by replacing f in (4.4) with (4.5), (4.4) can be expressed as

$$\mathbf{y} \;=\; \mathbf{H}(\mathbf{I} - \mathbf{A})^{-1}\nu + \eta, \tag{4.6}$$

where $\mathbf{I}$ is the identity matrix whose diagonal elements are 1 and off-diagonal elements are all zero. From (4.6), one can see that our proposed method, the blind deconvolution technique, consists of estimating $a(l)$, $h(u)$ for $l, u \in T = \{1, 2, \cdots, T\}$, σ_ν^2 and σ_η^2. Once these parameters are estimated, the intrinsic neural activity, $f(t)$, can be approximated or estimated by the fact that,

$$\begin{bmatrix} f \\ y \end{bmatrix} \;=\; \mathbf{MVN}\left[\begin{pmatrix} \underset{\sim}{0} \\ \underset{\sim}{0} \end{pmatrix}, \begin{pmatrix} \Sigma_{ff} & \Sigma_{fy} \\ \Sigma_{yf} & \Sigma_{yy} \end{pmatrix}\right], \tag{4.7}$$

and

$$\mathbf{E}(f|y) \;=\; \underset{\sim}{\mu_f} + \Sigma_{fy}\Sigma_{yy}^{-1}(\mathbf{Y} - \underset{\sim}{\mu_y}),$$

where $\underset{\sim}{\mu_f}$, $\underset{\sim}{\mu_f}$, Σ_{fy} and Σ_{yy} are the mean vectors of f, the mean vector of y, the covariance matrix of f and y, and the variance-covariance matrix of y, respectively. Therefore, the approximated underlying neuronal signal f can be expressed as

$$\hat{f} \;=\; \hat{\Sigma}_{fy}\hat{\Sigma}_{yy}^{-1}\mathbf{Y}, \tag{4.8}$$

4.2.3 Maximum Likelihood Estimation

The maximum likelihood (**ML**) methods enable us to estimate the unknown parameters -name by the **AR** coefficients, the **HRF** $h(t)$, and the variances σ_η^2, σ_ν^2 of the two additive noises, $\eta(t)$ and $\nu(t)$. That is, the parameter set of interest is

$$\Theta = \left\{ \{a(l)\}_{l=1}^{p}, \{h(u)\}_{u=1}^{T-1}, \sigma_\eta^2, \sigma_\nu^2 \right\}. \tag{4.9}$$

An estimate of these parameters is obtained by maximizing the likelihood function of Θ obtained from the observed **BOLD** response. Since (4.6) is a linear combination of two Gaussian vectors with zero means and covariance matrices $\sigma_\eta^2 I$ and $\sigma_\nu^2 I$, and since these two vectors are assumed to be independent, the resulting y is also normally distributed with mean zero and covariance matrix Ω; that is,

$$y = H(I-A)^{-1}\nu + \eta \;\; \sim \;\; MVN\left(\underset{\sim}{0}, \Omega\right), \tag{4.10}$$

where

$$\begin{aligned} \Omega &= \sigma_\nu^2 H(I-A)^{-1}(I-A)^{-T}H^T + \sigma_\eta^2 I \\ &\equiv \sigma_\nu^2 \Lambda\Lambda^T + \sigma_\eta^2 I, \end{aligned} \tag{4.11}$$

and $\Lambda = H(I-A)^{-1}$. The likelihood function is given by

$$\begin{aligned} L(\Theta|y) &= \prod_{i=1}^{T} f(y_i|\Theta) \\ &= \left(\frac{1}{\sqrt{2\pi|\Omega|}}\right)^T \exp\left\{-\frac{1}{2}\sum_{i=1}^{T} y_i^T \Omega^{-1} y_i\right\}. \end{aligned} \tag{4.12}$$

Therfore, the negative log-likelihood function is proportional to

$$\begin{aligned} l(\Theta) &= -2\log L(\Theta) \\ &\approx T\log|\Omega| + \sum_{i=1}^{T}(y_i^T\Omega^{-1}y_i) \\ &= T\log|\Omega| + tr\left(\Omega^{-1}\sum_{i=1}^{T} y_i y_i^T\right) \\ &= T\log|\Omega| + tr\left(\Omega^{-1}\right)\left(\sum_{i=1}^{T}(y_i-\bar{y})(y_i-\bar{y})^T + T\;\bar{y}\;\bar{y}^T\right). \end{aligned} \tag{4.13}$$

The **MLE** of Θ is obtained by minimizing (4.13) and is given by

$$\hat{\Theta}_{ML} \quad = \quad \arg\min_{\Theta} \left\{ T \log |\Omega| + tr\left(\Omega^{-1}\right) \left(\sum_{i=1}^{T} (y_i - \bar{y})(y_i - \bar{y})^T + T\ \bar{y}\ \bar{y}^T \right) \right\}. \quad (4.14)$$

4.2.4 Some Assumptions on the HRF

In practice, the haemodynamic response function coefficients encountered in the blind deconvolution method have a noticeably large support. Without supplementary information on the links among the haemodynamic response function coefficients, estimating $\{h(u)\}_{u=1}^{T-1}$ strikes snags such as high computational complexity for the haemodynamic response function, instability of estimating algorithms and non-unique solutions (Lagendijk, 1990) [40]. Consequently, the blind deconvolution method delineated in the previous section would be less suitable for handling a large number of haemodynamic response function coefficients for the following reason: The negative log-likelihood function $l(\Theta)$ in (4.13) becomes unresponsive to variation in Θ if the haemodynamic response function and the underlying neuronal signal model incorporate a large number of free coefficients, in other words, the extrema in (4.13) would become doubtful. Since the ML estimate of the parameters (4.9) is obtained numerically using an optimization algorithm, inaccuracies in solving (4.13) would hinder convergence to the correct ML estimator. Furthermore, the convergence speed plunges drastically because of this behavior of $l(\Theta)$.

Inspired by the foregoing discussion, we suggest decreasing the number of unknown parameters by assuming that we have some information on the structure of the haemodynamic response function. It is in general not realistic to model a haemodynamic response function as a set of free coefficients $h(t)$ becaise only a limited subset of all plausible $h(t)$ combinations would represent physically realistic haemodynamic response functions.

For this reason, we impose the following additional restrictions on the haemodynamic response function, $h(t)$.

1. $\sum_{u=1}^{T} h(u) = 1$. This assumption restricts the number of possible ambiguous solutions to the problem.

2. the **HRF** reaches its peak at about 6 seconds and **HRF**s at 5 seconds and 7 seconds are very close or approximately the same. This restriction implies the uniqueness, and also stability of the solution of the estimation algorithm.

The restrictions enumerated above are expected to guarantee the identifiability of the parameters. In section 4.2.5, we showed that all parameters in (4.9) are identifiable under these restrictions. In general (4.14) must be solved by numerical method and we employ an active set algorithm. Convergence to the ML estimator is normally achieved within 100 iteration steps.

4.2.5 Identifiability of Parameters

The general purpose of studying identifiability is to determine whether the unknown parameters in a model can be estimated uniquely from the observed data. If a model is overparameterized, then one may expect increased uncertainty in the parameter values. As seen in (4.9), the proposed approach requires $p + (T - 1) + 2$ parameters to be estimated and it would be problematic if some of the parameters are not identifiable. In this section, we are going to show the identifiability of each parameter in the model under the conditions on $h(t)$ listed in Section 4.2.4.

We begin with the following definitions and propositions developed by Kenneth R. Drissel in 2006.

Definition 4.2.1. (Kenneth R. Driessel, 2006) Let $\mathbf{l} = (l_0, l_1, ..., l_{n-1})$. Then **LToep(l)** denotes the *lower triangular Toeplitz* matrix which has l_0 as its diagonal elements, l_1 as its first lower sub-diagonal elements and so on. In other words, **LToep(l)**(i, j) := l_{i-j} if $j \leq i$ and 0 otherwise. Furthermore, a lower triangular Toeplitz matrix is **strict** if its diagonal elements are all zeros.

Definition 4.2.2. (Kenneth R. Driessel, 2006) Z_n denotes the $n \times n$ lower **shift** matrix which is defined by Z_n = **LToep**$(0, 1, 0, \cdots, 0)$. In other words, Z_n is the lower triangular Toeplitz matrix which is zero except for ones on the first sub-diagonal.

For example, when $n = 3$, Z_3 is defined to be;

$$Z_3 = \begin{bmatrix} 0 & 0 & 0 \\ 1 & 0 & 0 \\ 0 & 1 & 0 \end{bmatrix}.$$

The word **shift** implies that multiplication by Z_n on the left shifts the rows of an $n \times n$ matrix down and multiplication by Z_n on the right shifts the columns to the left.

Proposition 4.2.3. *(Kenneth R. Driessel, 2006) The lower shift matrix is* ***nilpotent****. In fact, Z_n^k is the lower triangular Toeplitz matrix which is 0 except for ones on the (k + 1)st subdiagonal. In particular, $Z_n^n = 0$.*

For instance, when $n = 3$,

$$Z_3^2 = \begin{bmatrix} 0 & 0 & 0 \\ 0 & 0 & 0 \\ 1 & 0 & 0 \end{bmatrix},$$

and $Z_3^3 = 0$.

Proposition 4.2.4. *(Kenneth R. Driessel, 2006) Every lower triangular Toeplits matrix can be represented as a linear combination of powers of the lower shift matrix Z_n:*

$$LToep(l_0, l_1, \cdots, l_{n-1}) = l_0 I + l_1 Zn + l_2 Z_n^2 + \cdots + l_{n-1} Z_n^{n-1}.$$

Proposition 4.2.5. *(Kenneth R. Driessel, 2006) The product of two $n \times n$ lower triangular Toeplitz matrices is also a lower triangular Toeplitz matrix.*

For example, when n=3, we have

$$\begin{aligned} & LToep(l_0, l_1, l_2) LToep(m_0, m_1, m_2) \\ = \; & (l_0 I + l_1 Z_3 + l_2 Z_3^2)(m_0 I + m_1 Z_3 + m_2 Z_3^2) \\ = \; & l_0 m_0 I + (l_0 m_1 + m_0 l_1) Z_3 + (l_0 m_2 + m_0 l_2 + l_1 m_1) Z_3^2 \\ = \; & LToep\left(I_0 m_0, (l_0 m_1 + m_0 l_1), (l_0 m_2 + m_0 l_2 + l_1 m_1)\right). \end{aligned}$$

Proposition 4.2.6. *(Kenneth R. Driessel, 2006) If the diagonal entry of a lower triangular Toeplitz matrix is non-zero, then it is non-singular. Its inverse is a lower triangular Toeplitz matrix. Furthermore, if a matrix Z_n is a strictly lower triangular Toeplitz matrix,*

$$Z_n = LToep(0, l_1, \cdots, l_{n-1}),$$

then we have

$$(I - Z_n)^{-1} = I + Z_n + Z_n^2 + \cdots + Z_n^{n-1},$$

where I is an $n \times n$ identity matrix.

We can see that Matrices A in (4.3) and H in (4.4) are strict lower triangular Toeplitz matrices and matrix $(I-A)$ in (4.11) is non-singular and its inverse is a lower triangular matrix by Proposition (4.2.6). Furthermore, since matrices H and $(I-A)^{-1}$ can be represented as a linear combination of powers of the lower shift matrix Z_n by Proposition (4.2.4), the product of two matrices H and $(I-A)^{-1}$ can be obtained and consequently it is also a lower triangular Toeplitz matrix by Proposition (4.2.5). Therefore, the matrix $\Lambda = H(I-A)^{-1}$ in (4.11) is expressed as;

$$\Lambda = LToep\left(\lambda_1, \lambda_2, \lambda_3, \cdots, \lambda_T\right), \tag{4.15}$$

where $\lambda_1 = 0$ and T is the number of time points. Thus, the variance covariance matrix Ω in (4.11) has the following components;

$$\begin{aligned}
\Omega_{1,1} &= \sigma_\eta^2, \\
\Omega_{1,j} &= \Omega_{i,1} = 0, \quad i, j \neq 1, \\
\Omega_{i,i} &= \sigma_\nu^2 \sum_{k=1}^{i} \lambda_k^2 + \sigma_\eta^2, \quad i \neq 1, \qquad (4.16) \\
\Omega_{i,j} &= \Omega_{j,i,} = \sigma_\nu^2 \sum_{k=0}^{min(i-1,j-1)} \lambda_{i-k}\lambda_{j-k}, \qquad (4.17)
\end{aligned}$$

where $i \neq j \in \{2, 3, \cdots, T\}$ and has the form below,

$$\Omega = \begin{bmatrix} \sigma_\eta^2 & 0 & 0 & \cdots & \cdots & 0 \\ 0 & \Omega_{2,2} & \Omega_{2,3} & \cdots & \cdots & \Omega_{2,T} \\ 0 & \Omega_{3,2} & \Omega_{3,3} & \cdots & \cdots & \Omega_{3,T} \\ \vdots & \vdots & \ddots & \ddots & \vdots & \vdots \\ 0 & \Omega_{T-1,2} & \Omega_{T-1,3} & \cdots & \cdots & \Omega_{T-1,T} \\ 0 & \Omega_{T,2} & \Omega_{T,3} & \cdots & \cdots & \Omega_{T,T} \end{bmatrix}. \tag{4.18}$$

From (4.17), one can see that Ω in (4.18) is symmetric and for $i, j \neq 1$, each component of Ω can be further expressed as

$$\Omega_{i,j} = \sigma_\nu^2 \lambda_i \lambda_j + \Omega_{i-1,j-1}. \tag{4.19}$$

It is clear that the variance covariance matrix $\Omega = E(y^T y)$ is identifiable but that without any constraints, only $\sigma_\eta^2 = E(y_1^2)$ is identifiable among the parameters listed in (4.9). In other words, other parameters enumerated in (4.9) except for σ_η^2 are not identifiable but functions of them are identifiable. In particular, the following functions of parameters listed in (4.9) are identifiable

$$E(y_i^2) = \sigma_\nu^2 \sum_{k=1}^{i} \lambda_k^2 + \sigma_\eta^2, \tag{4.20}$$

$$E(y_i y_j) = \sigma_\nu^2 \sum_{k=0}^{min(i-1,j-1)} \lambda_{i-k} \lambda_{j-k}. \tag{4.21}$$

For example, for a model with one **AR** coefficient and eight time points (i.e., a model with $1 + (8-1) + 2 = 10$ parameters), Λ in (4.15) is defined to be;

$$\Lambda = LToep\left(\lambda_1, \lambda_2, \lambda_3, \lambda_4, \lambda_5, \lambda_6, \lambda_7, \lambda_8\right), \tag{4.22}$$

where

$$\begin{aligned} \lambda_1 &= 0, \\ \lambda_2 &= h(1), \\ \lambda_3 &= h(1)a(1) + h(2), \\ \lambda_4 &= h(1)a(1)^2 + h(2)a(1) + h(3), \\ \lambda_5 &= h(1)a(1)^3 + h(2)a(1)^2 + h(3)a(1) + h(4), \\ \lambda_6 &= h(1)a(1)^4 + h(2)a(1)^3 + h(3)a(1)^2 + h(4)a(1) + h(5), \\ \lambda_7 &= h(1)a(1)^5 + h(2)a(1)^4 + h(3)a(1)^3 + h(4)a(1)^2 + h(5)a(1) + h(6), \\ \lambda_8 &= h(1)a(1)^6 + h(2)a(1)^5 + h(3)a(1)^4 + h(4)a(1)^3 + h(5)a(1)^2 + h(6)a(1) + h(7), \end{aligned} \tag{4.23}$$

and λ_t can be written as

$$\lambda_t = a(1)\lambda_{t-1} + h(t-1). \tag{4.24}$$

From (4.20) - (4.24), one can see that for $t \geq 3$,

$$\begin{aligned} \frac{E(y_t y_2)}{E(y_2^2) - E(y_1^2)} &= \frac{\lambda_t}{\lambda_2} \\ &= a(1)\frac{\lambda_{t-1}}{\lambda_2} + \frac{h(t-1)}{\lambda_2} \\ &= a(1)\frac{E(y_{t-1}y_2)}{E(y_2^2) - E(y_1^2)} + \frac{h(t-1)}{h(1)}. \end{aligned} \tag{4.25}$$

Accordingly, the parameters in (4.9) would be identifiable if they can be expressed as functions of expected values. In other words, the identifiability issue becomes whether or not the linear equations in (4.25) can be solved for $a(1)$ and $\{h(u)\}_{u=1}^{7}$. Since there are six linear equations available with eight different parameters, these linear equations are not solvable for the parameters, $a(1)$ and $\{h(u)\}_{u=1}^{7}$. However, if one places the second restriction enumerated in (4.2.4), that is, the **HRF** reaches its peak at about 6 seconds and the **HRF**s at 5 seconds and 7 seconds are very close or approximately same, the linear equations in (4.25) can be solved with respect to $a(1)$. In other words, if $h(5)$ and $h(7)$ are assumed to be very close or approximately same, then the linear equations for $t = 6, 8$ in (4.25) become

$$\begin{aligned} \frac{E(y_6 y_2)}{E(y_2^2) - E(y_1^2)} &= a(1)\frac{E(y_5 y_2)}{E(y_2^2) - E(y_1^2)} + \frac{h(5)}{h(1)}, \\ \frac{E(y_8 y_2)}{E(y_2^2) - E(y_1^2)} &= a(1)\frac{E(y_7 y_2)}{E(y_2^2) - E(y_1^2)} + \frac{h(5)}{h(1)}, \end{aligned} \tag{4.26}$$

and $a(1)$ can be expressed by a function of expected values

$$a(1) = \frac{E(y_8 y_2) - E(y_6 y_2)}{E(y_7 y_2) - E(y_5 y_2)}. \tag{4.27}$$

That is, $a(1)$ becomes identifiable. Since $a(1)$ turns out to be identifiable, the ratios of $h(t-1)$ to $h(1)$ in (4.25)

$$\frac{E(y_t y_2)}{E(y_2^2) - E(y_1^2)} - \hat{a}(1)\frac{E(y_{t-1}y_2)}{E(y_2^2) - E(y_1^2)} = \frac{h(t-1)}{h(1)}, \quad t \geq 3, \tag{4.28}$$

are also identifiable where $\hat{a}(1)$ is a function of sample moments, an estimate of $a(1)$. Furthermore, if one adopts the first restriction enumerated in (4.2.4), $\sum_{u=1}^{T} h(u) = 1$, and sums up (4.28) over time points,

$$\begin{aligned}\sum_{t=3}^{8}\left(\frac{E(y_t y_2)}{E(y_2^2)-E(y_1^2)} - \hat{a}(1)\frac{E(y_{t-1}y_2)}{E(y_2^2)-E(y_1^2)}\right) &= \sum_{t=3}^{8}\frac{h(t-1)}{h(1)} \\ &= \frac{1-h(1)}{h(1)},\end{aligned}$$

then we see that

$$h(1) = \frac{1}{\sum_{t=3}^{8}\left(\frac{E(y_t y_2)}{E(y_2^2)-E(y_1^2)} - \hat{a}(1)\frac{E(y_{t-1}y_2)}{E(y_2^2)-E(y_1^2)}\right)+1} \tag{4.29}$$

becomes identifiable. Due to the identifiability of $a(1)$ and $h(1)$, by (4.28) and (4.29), one can show that $h(t)$'s are also identifiable and have the form below;

$$h(t-1) = \hat{h}(1)\left(\frac{E(y_t y_2)}{E(y_2^2)-E(y_1^2)} - \hat{a}(1)\frac{E(y_{t-1}y_2)}{E(y_2^2)-E(y_1^2)}\right), \tag{4.30}$$

where $\hat{a}(1)$ and $\hat{h}(1)$ are estimates of $a(1)$ and $h(1)$ in (4.27) and (4.29) respectively. Finally, since $a(1)$, $\{h(u)\}_{u=1}^{7}$ and σ_η^2 are identifiable, from (4.20), one can show that σ_ν^2 is also identifiable and has the following form,

$$\sigma_\nu^2 = \frac{E(y_t^2)-E(y_1^2)}{\sum_{k=1}^{t}\lambda_k^2}. \tag{4.31}$$

Therefore, all parameters listed in (4.9) are identifiable.

5.0 DATA ANALYSIS

5.1 DATA ACQUISITION

The data that is utilized for the analysis in this chapter was obtained by Greg J. Siegle in the department of Psychiatry at University of Pittsburgh. In his study, forty two patients with major depressive disorder and twenty four healthy control subjects participated in 60 slow-event related trials. Each participant was asked to view a fixation cue for 1 second followed by a positive(stimulus type 1), negative(stimulus type 2), or neutral(stimulus type 4) word for 200 milliseconds, followed by a mask for 10.8 seconds. Each stimulus type was repeated 20 times in random order. Participants were instructed to push a button for whether the word was relevant, somewhat relevant, or not relevant to them or their lives, as quickly and accurately as they could. Right immediately after each stimulus type was applied to participants, a **MRI** scanner started measuring **BOLD** responses from each participant for 8 seconds (Siegle et al., 2007) [62]. Therefore, the **BOLD** response $y_{ijklm}(t)$ that he measured in his experiment is indexed by $i = 1, 2$, $j = 1, 2, 3$, $k = 1, \cdots, 20$,$l = 1, \cdots, 5$, $m = 1 \cdots n_i$ and $t = 1, \cdots, 8$ which denote subject type, stimulus type, repetition, regions of interest, individual in each type of subject group and scanned time, respectively. In the dataset we are utilizing for the data analysis, for each individual, there are three different kinds of stimuli, each stimulus is repeated twenty times and for each stimulus, an **fMRI** signal is measured for eight seconds from each of the five different brain regions.

5.2 MODEL ORDER SELECTION

As described in chapter 4, the preliminary step in the blind deconvolution method is to determine the number of **AR** coefficients. To determine the number of **AR** coefficients, the autocorrelation function and partial autocorrelation function, abbreviated as **ACF** and **PACF**, are plotted to investigate possible candidate models with p **AR** coefficients. Table 1 below provides a way to identify possible candidates for the **ARMA** model from the observed **ACF** and **PACF** (Shumway and Stoffer, 2000) [61].

Table 1: Behavior of the ACF and PACF

	$AR(p)$	$MA(q)$	$ARMA(p,q)$
ACF	Tails off to zero	Cuts off after lag q	Tails off to zero
$PACF$	Cuts off after lag p	Tails off to zero	Tails off to zero

Each candidate model with different number of **AR** coefficients is examined by calculating *Akaike* Information Criterion (**AIC**) (Akaike, 1974) [3] and *Bayesian* Information Criterion (**BIC**) (Schwarz, 1978) [58]. Here, since we assume that the underlying neuronal activity and the unknown haemodynamic response function are different over the regions-of-interest (**ROIs**), **ACF** and **PACF** are plotted separately for the mean of observed **BOLD** responses from each of the **ROIs**.

Figures 1 - 5 plot the arithmetic mean of observed **BOLD** responses from five regions-of-interest against time and its corresponding **ACF** and **PACF**. Based on **ACF** and **PACF** in Figures 1 - 5, one may say that **ACF** tails off to zero and **PACF** cuts off after lag 1. Therefore, according to Table 1, the possible candidate order of **AR** coefficients is $p = 1$. However, determining order of **AR** coefficients depending solely on **ACF** and **PACF** would be risky because it is too subjective. Accordingly, we also provide both **AIC** and **BIC** for models with **AR** orders $p = 1, 2$, to measure the goodness of fit of each candidate model.

According to Tables 2 and 3, both **AIC** and **BIC** model selection procedures agree to identify the model with the order $p = 1$ for the best fit for the **BOLD** responses from all five regions-of-interest. On this account, the underlying neuronal activities from five regions-of-

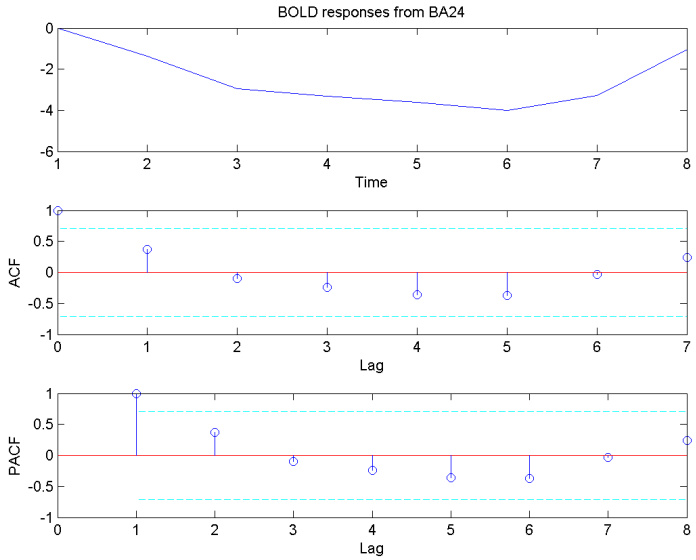

Figure 1: Mean BOLD signal from Brodmann Area 24 and its ACF and PACF

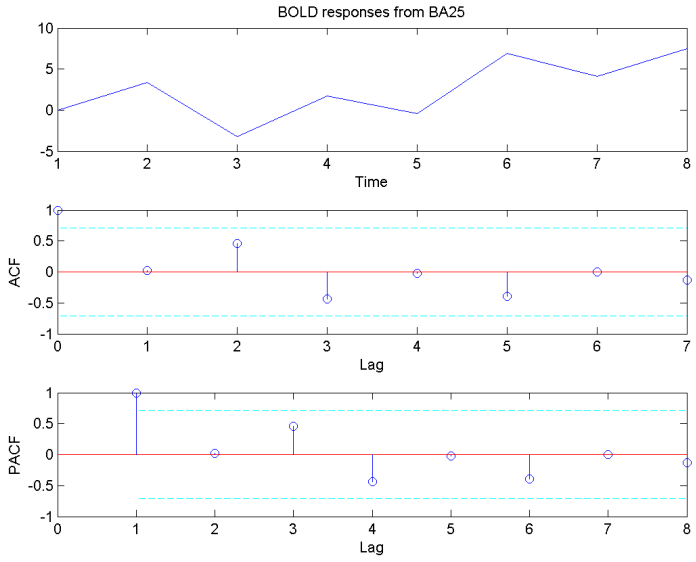

Figure 2: Mean BOLD signal from Brodmann Area 25 and its ACF and PACF

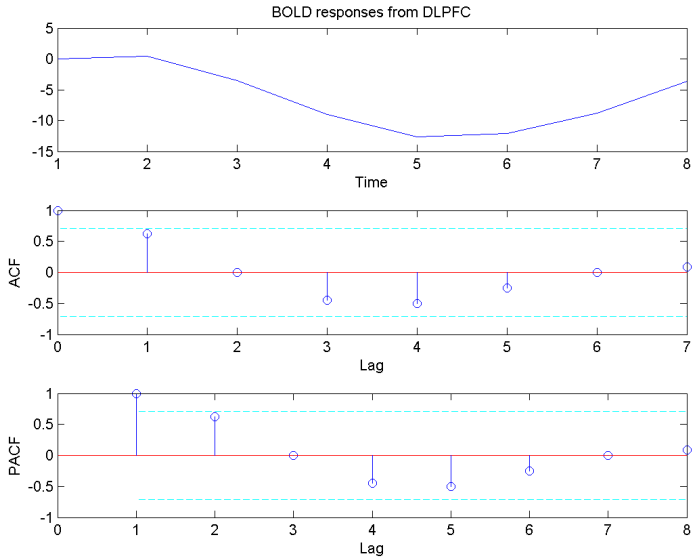

Figure 3: Mean BOLD signal from Dorsolateral prefrontal cortex and its ACF and PACF

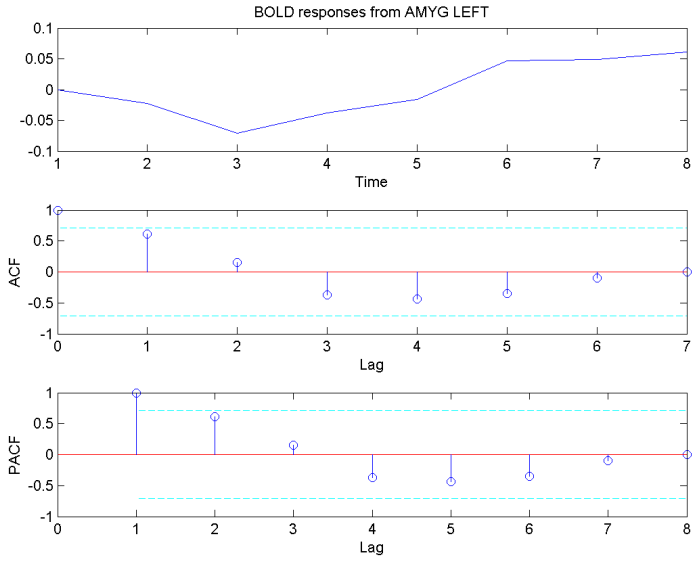

Figure 4: Mean BOLD signal from Amygdala Left and its ACF and PACF

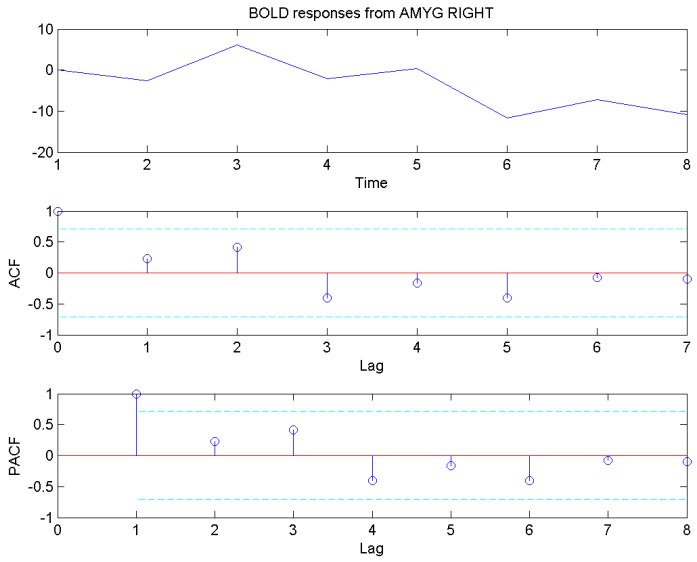

Figure 5: Mean BOLD signal from Amygdala Right and its ACF and PACF

Table 2: AIC Model Selection for mean BOLD response from 5 ROIs

ROI	$AR(1)$	$AR(2)$
BA24	-235.27	-233.27
BA25	-27.27	-25.27
DLPFC	-82.47	-80.82
AMYG Left	-90.86	-88.86
AMYG Right	-123.18	-121.18

Table 3: BIC Model Selection for mean BOLD response from 5 ROIs

ROI	$AR(1)$	$AR(2)$
BA24	-227.31	-224.31
BA25	-19.30	-16.31
DLPFC	-74.51	-71.85
AMYG Left	-82.90	-79.90
AMYG Right	-115.22	-112.22

interest are modeled by the **AR** process with order 1 and the corresponding matrix A in (4.3) is the following **Toeplitz** matrix;

$$A = \begin{bmatrix} 0 & 0 & 0 & 0 & 0 & 0 & 0 & 0 \\ a(1) & 0 & 0 & 0 & 0 & 0 & 0 & 0 \\ 0 & a(1) & 0 & 0 & 0 & 0 & 0 & 0 \\ 0 & 0 & a(1) & 0 & 0 & 0 & 0 & 0 \\ 0 & 0 & 0 & a(1) & 0 & 0 & 0 & 0 \\ 0 & 0 & 0 & 0 & a(1) & 0 & 0 & 0 \\ 0 & 0 & 0 & 0 & 0 & a(1) & 0 & 0 \\ 0 & 0 & 0 & 0 & 0 & 0 & a(1) & 0 \end{bmatrix} \tag{5.1}$$

Similar analyses are made for the rest of participants in the study and corresponding tables of **AIC** and **BIC** are enumerated in Appendix A. It turns out that all observed **BOLD** responses from sixty six participants are best described by the model with one **AR** coefficients and their associated underlying neuronal activities seems to be best explained by **AR** models with $p = 1$. Accordingly, the **AR** coefficient $p = 1$ is utilized to construct a **Toeplitz** matrix A in (4.3) and consequently underlying neuronal activities $f(t)$ in (4.5) will be approximated or estimated by (4.8).

5.3 ESTIMATION OF PARAMETERS: BLIND DECONVOLUTION

Once the order of the **ARMA** model is determined, the parameters listed in (4.9) are estimated by minimizing the negative log-likelihood function in (4.13) and their estimates have the form of (4.14). The log-likelihood function in (4.13) is a function of ten variables (or parameters) and it is very complicated to find values which minimize the negative log-likelihood function. In order to minimize the negative log-likelihood function in (4.13), we employed a built-in **MATLAB** function, *fmincon*, which attempts to find a constrained minimum of a function of several variables (or parameters) starting at a vector of initial guesses of parameters. This is generally referred to as a constrained nonlinear optimization problem. In section 4.2.4, some constraints on **HRF**, $h(t)$, were discussed. Under these constraints, *fmincon* minimizes the negative log-likelihood function and consequently yields the estimates of the parameters listed in (4.9).

5.3.1 Estimation of Haemodynamic Response Function

Haemodynamics, literally meaning *blood movement*, is the study of blood flow and precisely referred to as a medical terminology for the dynamic regulation of the blood flow in the brain. In other words, the blood supply of the brain is dynamically modulated by haemodynamics to give active neurons more energy whilst inactive neurons receive less energy. Furthermore, haemodynamic response function (**HRF**) is defined to be a function of blood oxygenation, flow, and volume and known to reach its peak after 4 to 6 seconds, undershoot from approximately 10 to 30 seconds and return to baseline about 20 to 30 seconds after a stimuli is applied (Buxton et al., 1998) [11]. In addition, initial undershoot can be observed (Malonek and Grinvald, 1996) [42] and the hamodynamic response function (**HRF**) is found to be different across regions within an individual (Schacter et al., 1997) [57] and different across individuals (Aguirre et al., 1998) [2]. Figure 6 displays plots of estimated haemodynamic response functions for two subjects, a healthy control subject (top) and a patient with major depressive disorder (bottom) in accordance to the type of stimulus (column1 = positive, column2 = negative, column3 = neutral). Moreover, in each plot in Figure 6, the

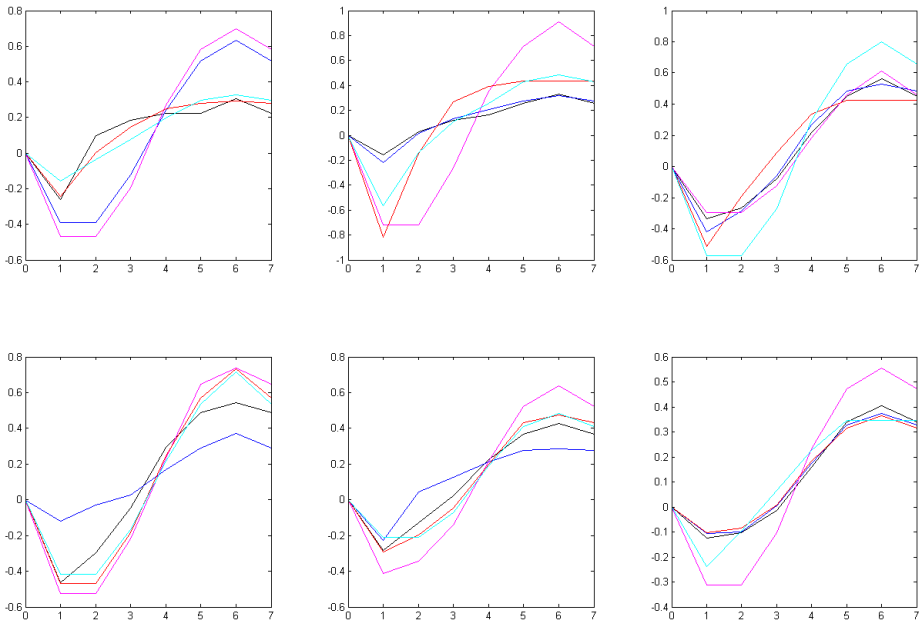

Figure 6: Control vs Case Estimated Haemodynamic Response functions for five different brain regions

estimated hamodynamic response functions of five **ROI**s, *Brodmann Area* 24 [2], *Brodmann Area* 25 [3], *Dorsolateral prefrontal cortex* [4], *Amygdala Left* [7], and *Amygdala Right* [7] are displayed by black, blue, red, purple and cyan solid lines respectively. From Figure 6, one can see that irrespective of type of subject and stimulus, the estimated haemodynamic response functions are similar in overall shape, such as initial undershoots and peak at six seconds. Figure 7 is a subplot of Figure 6, the middle of the bottom row, representing the estimated haemodynamic response functions of five **ROI**s for a subject with major depressive disorder after stimulus type = 2 (negative) was applied. According to Figure 7, one can see that the estimated haemodynamic response functions within a subject vary across **ROI**s. For instance, all estimated haemodynamic response functions reach their bottom at one seconds but **DLPFC** has the largest intensity (about -0.4) and the slowest baseline return (about 3.5 seconds) whereas **BA 25** has the smallest intensity (about -0.2) but the fastest baseline

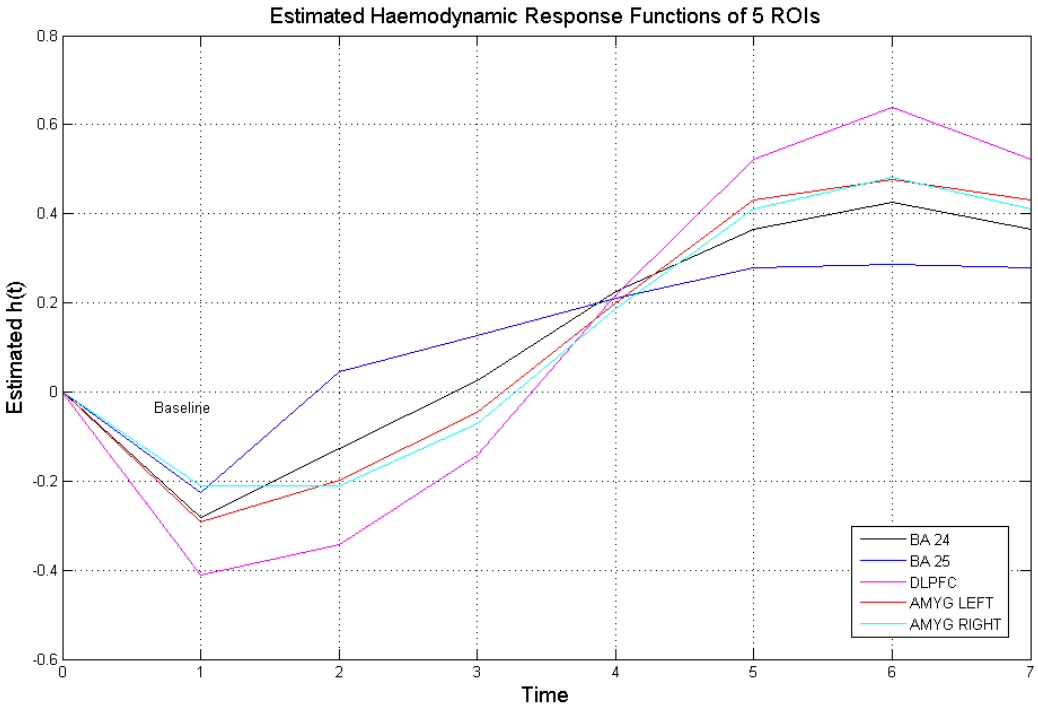

Figure 7: Estimated Haemodynamic Response functions for five different brain regions

return (about 1.8 seconds). Figure 6 indicates that the estimated haemodynamic response functions differ in intensities and times to baseline return with respect to stimulus within a region, regions within individual and individual. Similar analyses are made for the rest of the subjects and corresponding plots of the estimated haemodynamic response functions are listed in Appendix B.

5.3.2 Estimation of Underlying Neuronal Activity

A study of fMRI time-series data analysis can supply information about the intrinsic neuronal activity to a given stimulus using the observed blood oxygenation level-dependent (**BOLD**) responses that come out after intrinsic neuronal activity in the human brain. However, it might be problematic to use the **BOLD** response as a proxy for the underlying neuronal activity, because it is measured at the level of haemodynamic response, not at a

neuronal level. Furthermore, changes in **BOLD** responses for the first several time periods would not be due to a given stimulus but a previous stimulus. In other words, **BOLD** response for the first several times would not represent intrinsic neuronal signals right after a stimulus is applied because **BOLD** responses show up sometimes after intrinsic neuronal activity presents. Therefore, the utilization of well estimated intrinsic neuronal signals instead of **BOLD** responses is expected to make a **fMRI** study precise.

The possibility of estimating latent neuronal activity comes from the fact that a BOLD response is expressed as a convolution of latent neuronal signals and the haemodynamic responses. Therefore, the estimating procedures can be understood by deconvolving latent neuronal signals and haemodynamic responses from the observed **BOLD** response. The proposed estimating algorithm (Blind Deconvolution) is discussed in Chapter 4. To be brief, after the parameters listed in (4.9) are obtained, the latent neuronal signals can be approximated or estimated by the fact that,

$$\begin{bmatrix} f \\ y \end{bmatrix} \sim \mathbf{MVN}\left[\begin{pmatrix} \underset{\sim}{0} \\ \underset{\sim}{0} \end{pmatrix}, \begin{pmatrix} \Sigma_{ff} & \Sigma_{fy} \\ \Sigma_{yf} & \Sigma_{yy} \end{pmatrix}\right].$$

and

$$\mathbf{E}(f|y) = \underset{\sim}{\mu_f} + \Sigma_{fy}\Sigma_{yy}^{-1}(\mathbf{Y} - \underset{\sim}{\mu_y}).$$

Therefore, the approximated underlying neuronal signal f can be expressed as

$$\hat{f} = \hat{\Sigma}_{fy}\hat{\Sigma}_{yy}^{-1}\mathbf{Y},$$

where

$$\hat{\Sigma}_{fy} = \hat{\sigma}_\nu^2(I - \hat{A})^{-1}(I - \hat{A})^{-T}\hat{H}^T, \tag{5.2}$$

$$\hat{\Sigma}_{yy} = \hat{\sigma}_\nu^2\hat{H}(I - \hat{A})^{-1}(I - \hat{A})^{-T}\hat{H}^T + \hat{\sigma}_\eta^2 I. \tag{5.3}$$

Figure 8 displays average patterns of behavior of **BOLD** response and estimated intrinsic neuronal signal from *Dorsolateral prefrontal cortex* for a subject with major depressive disorder after stimulus type = 2 (negative word) was applied. Similar analyses are made

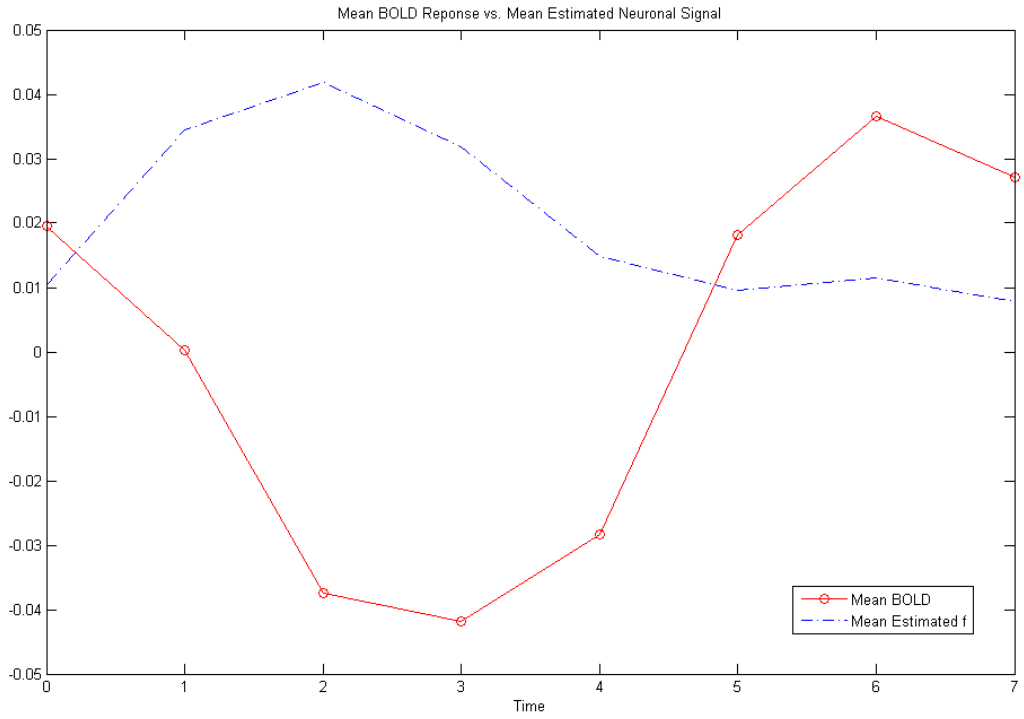

Figure 8: Average Behaviors of BOLD Response vs. Estimated Neuronal Signal

over different stimuli, **ROI**s and subjects, and corresponding plots are listed in Appendix C. Since neuron firing results in change in local blood volume and flow, and consequently oxygen extraction, a change in latent neuronal signal is always followed by change in **BOLD** response. In other words, **BOLD** responses come out sometimes after neuronal activities present. From Figure 8, one can see that immediately after the stimulus is applied, estimated neuronal activity (blue dashed line) increases for the first one second period, changes its increasing rate for the second one second period, reaches its peak at two seconds and decreases after two seconds. The same patterns of behavior are found in the **BOLD** response, but these present after four seconds. That is, a change in underlying neuronal activity is realized in the form of **BOLD** response four seconds after a stimulus presents. From this point of view, one may think that **BOLD** responses for the first four seconds would not represent neuronal response to a current stimulus, but rather to a prior stimulus. Furthermore, we

suspect that a **BOLD** response based **fMRI** study would provide erroneous information on underlying neuronal responses to a stimulus. In section 5.4, we will investigate how **BOLD** responses and estimated neuronal activities differ in unveiling the effective connectivity in the human brain.

5.4 MAPPING EFFECTIVE CONNECTIVITY

5.4.1 BOLD vs Estimated Neuronal Signal

The study of functional magnetic resonance imaging(**fMRI**) supplies informations on the intrinsic neuronal activities, which are evoked by the external cognitive stimuli, as a principle of organization in the human brain. The variable of interest is generated by the underlying neuronal activities, however the signal being quantified is the blood oxygenation level-dependent (**BOLD**) response, since the neuronal activity is not directly observable. The **BOLD** response is the subordinate repercussion of haemodynamic changes such as local changes in blood flow, volume and oxygenation level that takes place within a few second of changes in neuronal activity. As explained in section 5.3.2, we suspect that the utilization of the **BOLD** response in the study of **fMRI** would lead one to an inaccurate information on the human brain network. In this section, we are going to probe into the difference between **BOLD** and neuronal signal based **fMRI** studies.

5.4.2 Effective Connectivity and Granger Causality

The *effective connectivity* is defined to be the influence or effect one neuronal system exerts upon others (Friston 1993a [22], 1994 [20]). Accordingly, models of effective connectivity aim to place an appropriate metric of influence among interrelated regions in the human brain. The notion of Granger causality introduced by Granger(1969, 1980) is based on the perception that causes always go ahead of effects, so that something in the future cannot lead to something in the past or present [28] [29]. Conceptually, if a series y generates a series x, then awareness of y should assist in predicting future values of x. The vector-

autoregressive (**VAR**) model proposed by Harrison et al. (2003) enables us to estimate the effective connectivity in the context of Granger causality and has the form below:

$$y_t = \sum_{i=1}^{p} y_{t-i} A_i + e_t \tag{5.4}$$

where $y_t = [y_t(1), \cdots, y_t(d)]$ and d is the number of **ROIs**. In addition, A_i represents the $d \times d$ matrix of the ith order **VAR** coefficients and e_t is the Gaussian noise. Here, the off diagonal elements of A_i demonstrate the amplitude of the influence one region exerts on another whereas the diagonal elements manifest the intensity of self-connection. First, based on the observed **BOLD** response from an individual with a stimulus, the underlying neuronal signal is estimated. The dissimilarity between the observed **BOLD** response and the estimated neuronal signal was discussed in section 5.3.2. Then, both observed **BOLD** response and estimated neuronal signal are modeled by a **VAR** model. For both cases, it turns out that the **VAR** model with the order 1 is the best **VAR** model in terms of *Bayesian information criterion*. Table 4 and 5 display the estimates of 1st order **VAR** coefficients based on the observed **BOLD** and the estimated neuronal signal respectively. The elements in both Table 4 and 5 present the intensity of the influence one region's past activity exerts on another region's (or its own) current activity.

Table 4: BOLD based Estimates of VAR coefficients

	BA 24	BA 25	DLPFC	L AMYG	R AMYG
BA 24	0.1630	-0.1902	-0.1452	-0.0240	0.0669
BA 25	-3.0196	0.0808	2.9171	-0.8889	1.9469
DLPFC	-0.6952	-0.0233	1.8238	-0.0984	0.9719
L AMYG	-0.1659	-0.6227	2.5970	-0.2523	1.9296
R AMYG	1.4843	-0.1978	-2.7248	0.2680	-1.0568

For example, both Table 4 and 5 show that *Broadman Area* 24 (**BA 24**) [2]'s activity is negatively influenced by *Broadman Area* 25 (**BA 25**) [3]'s previous activity and *vice versa*. If this relation is statistically significant, one may say that two regions *Granger* cause each

Table 5: Estimated Neuronal Signal based Estimates of VAR coefficients

	BA 24	BA 25	DLPFC	L AMYG	R AMYG
BA 24	-0.5096	-0.1933	-1.4275	0.3312	-0.4561
BA 25	-1.3160	0.2492	4.8074	-1.4734	2.7552
DLPFC	0.3151	-0.1543	0.8471	-0.1009	0.3410
L AMYG	-1.4194	-0.2562	4.3027	-0.8405	3.2698
R AMYG	-0.4597	0.0062	-1.4989	0.2337	-0.3678

other. The red numbers in Table 4 and 5 represent statistically significant connections among five different regions of interest based on simultaneous 95 % confidence interval for **VAR** coefficients in Table 6 and 7.

Table 6: 95 % Confidence interval for BOLD Based VAR coefficients

	BA 24	BA 25	DLPFC	L AMYG	R AMYG
BA 24	(-0.3192, 0.6452)	(-0.3500, -0.0305)	(-1.1578, 0.8674)	(-0.2845, 0.2365)	(-0.5291, 0.6629)
BA 25	(-4.1793, -1.8599)	(-0.3033, 0.4650)	(0.4817, 5.3524)	(-1.5156, -0.2623)	(0.5135, 3.3803)
DLPFC	(-5.2439, 3.8535)	(-1.5301, 1.4835)	(-7.7286, 11.3762)	(-2.5563, 2.3594)	(-4.6503, 6.5941)
L AMYG	(-11.8751, 11.5432)	(-4.5013, 3.2560)	(-21.9924, 27.1864)	(-6.5793, 6.0746)	(-12.5428, 16.4020)
R AMYG	(-5.1980, 8.1666)	(-2.4114, 2.0157)	(-16.7578, 11.3082)	(-3.3428, 3.8787)	(-9.3161, 7.2025)

Table 7: 95 % Confidence interval for Estimated Neuronal Signal Based VAR coefficients

	BA 24	BA 25	DLPFC	L AMYG	R AMYG
BA 24	(-0.9917, -0.0274)	(-0.3530, -0.0335)	(-2.4401, -0.4150)	(0.0707, 0.5917)	(-1.0520, 0.1399)
BA 25	(-2.4757, -0.1563)	(-0.1349, 0.6334)	(2.3720, 7.2428)	(-2.1000, -0.8467)	(1.3219, 4.1886)
DLPFC	(-4.2336, 4.8638)	(-1.6610, 1.3525)	(-8.7053, 10.3995)	(-2.5587, 2.3570)	(-5.2812, 5.9632)
L AMYG	(-13.1285, 10.2898)	(-4.1349, 3.6225)	(-20.2867, 28.8921)	(-7.1674, 5.4864)	(-11.2026, 17.7422)
R AMYG	(-7.1420, 6.2226)	(-2.2073, 2.2198)	(-15.5319, 12.5341)	(-3.3770, 3.8444)	(-8.6271, 7.8915)

From Table 4 - 7, one can see the difference between the observed **BOLD** and the estimated neuronal signal in disclosing the *Granger causality* or *effective connectivity*. Figure 9 displays statistically significant *Granger Causality* (or effective connectivity). The blue

solid lines represent the significant effective connectivity based on the observed **BOLD** response. It reveals that regions *Broadman* 24 (**BA 24**) [2]), *Dorsolateral prefrontal cortex* (**DLPFC**) [4]), *Amygdala* (**L AMYG** and **R AMYG**) [7]) *Granger* cause *Broadman* 25 (**BA 25**) [3]).

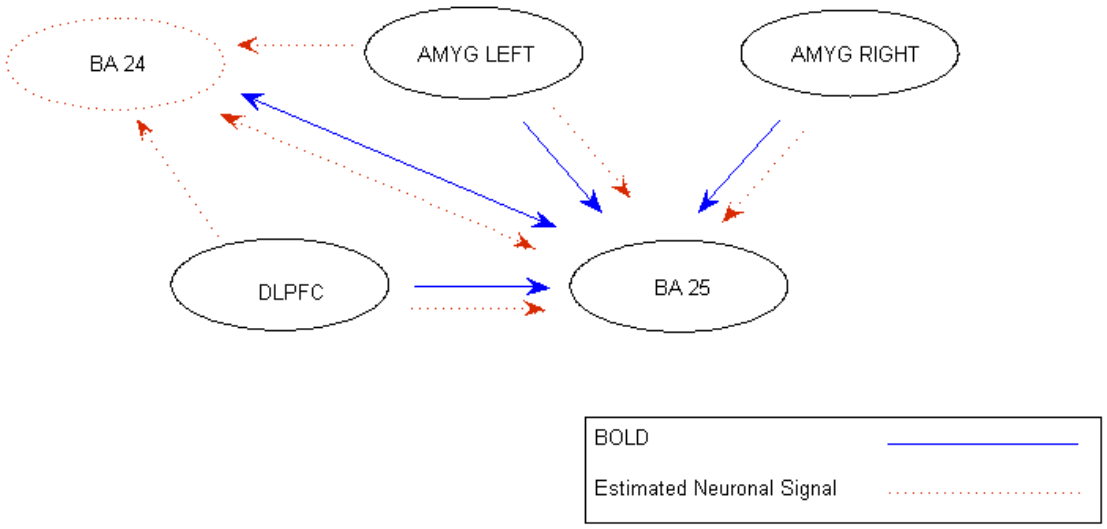

Figure 9: Significant Granger causal relationship among five different regions of interest

The red dotted lines in Figure 9 display the critical effective connectivity based on the estimated neuronal signal. In addition to the *effective connectivity* based on the observed **BOLD** response, the estimated neuronal signal based study additionally identifies that **BA 24** *Granger* causes itself, and that **DLPFC** and **L AMYG** *Granger* cause **BA** 24.

6.0 SUMMARY AND CONCLUSION

Much of this dissertation has focused on developing a method to estimate the underlying neuronal signals. The **Blind Deconvolution** via **ARMA** parameter estimation, our proposed estimating scheme, enables one to estimate the haemodynamic response function (**HRF**) $h(t)$ given a stimulus in addition to the underlying neuronal activity, $f(t)$. A **BOLD** response $y(t)$ usually occurs within a few seconds after the underlying neuronal activity $f(t)$ is present. The delay of the BOLD response is usually modeled by a convolution of haemodynamic response function (**HRF**) $h(t)$ and the intrinsic neuronal activities $f(t)$ in the past time points. In section 5.3, we presented that the approximated underlying neuronal activity, $f(t)$ at current time point t predict the changes in **BOLD** response at future time point, that is, change in underlying neuronal activity is realized in the form of BOLD response four seconds after a stimuli presents. Furthermore, in section 5.4, we also provided that the delay of **BOLD** response causes dissimilar result in causal relationships among heterogeneous brain regions and the estimated neuronal signal based study identifies more connections among brain regions than the observed **BOLD** response based study does.

We presented blind deconvolution (or separation) of underlying neuronal activity and its corresponding haemodynamic response function via **ARMA** parameter estimation. The limitation of blind deconvolution via **ARMA** parameter estimation is threefold: 1) it has the risk of ill-convergence local minima, and 2) the total number of parameters cannot be very large for practical computations, and 3) usually, the restoration by these methods is not uniquely decided unless additional assumptions are made on haemodynamic response function (**HRF**). We notice that there are several different alternative ways that blind deconvolution or separation can be achieved, such as *Zero sheet separation* (Lane et al., 1987)

[41], *Priori blur identification methods* (Cannon et al., 1976; Chang et al., 1991; Fabian et al., 1991) [12] [13] [16], *Nonparametric methods based on higher order statistics* (Wiggins, 1978; Wu, 1990; Jacovitti, 1990) [68] [69] [37] and so on. We shall employ those blind deconvolution techniques on our data to compare the approximated neuronal activities obtained by techniques enumerated above with the the one obtained by our proposed method.

APPENDIX A

MODEL DIAGNOSTICS AND SELECTION

Table 8: AIC of Model with p=1 for Control Group with Stimulus Type=1

ID	BA24	BA25	DLPFC	L AMYG	R AMYG
1	−235.28	−27.27	−82.48	−90.87	−123.19
2	232.30	533.71	168.44	271.14	420.94
3	−251.12	−250.72	−131.69	−275.23	−231.51
4	34.41	154.79	−35.31	−26.25	90.91
5	−162.46	23.63	−110.68	−31.60	−60.91
6	−91.81	−154.34	−38.98	−93.40	−39.91
7	−218.55	−51.69	−71.97	−53.23	−52.08
8	−138.31	93.31	−199.54	−113.37	−15.52
9	12.77	133.45	89.90	96.34	244.21
10	−255.21	−109.91	−246.65	−173.63	−179.10
11	−253.36	−19.96	−83.06	−11.69	−126.78
12	−8.16	−173.19	69.81	35.70	−0.43
13	−301.42	236.18	−55.76	−150.72	17.25
14	−43.50	34.59	−35.74	13.91	34.43
15	−140.12	182.54	−169.07	−131.93	−35.38
16	−32.30	−0.50	−26.61	117.44	43.69
17	−187.67	98.02	−104.26	67.17	41.92
18	−83.71	−68.68	−23.99	−150.83	−125.71
19	−175.88	−32.58	−141.18	−146.85	−123.97
20	−153.65	−23.97	7.77	−110.13	−112.89
21	−284.30	−35.27	−112.26	−365.62	−62.35
22	−249.16	−287.06	−319.87	−158.68	−95.63
23	−164.98	135.98	−166.35	−51.47	−30.79
24	95.25	215.11	131.87	98.29	175.16

Table 9: AIC of Model with p=2 for Control Group with Stimulus Type=1

ID	BA24	BA25	DLPFC	L AMYG	R AMYG
1	−233.28	−25.27	−80.82	−88.87	−121.19
2	233.91	547.52	169.92	273.13	422.95
3	−249.50	−248.74	−129.72	−275.05	−231.81
4	36.41	156.73	−33.31	−24.46	92.11
5	−160.46	25.63	−108.68	−29.60	−58.91
6	−118.35	−152.34	−38.27	−91.87	−38.37
7	−216.56	−49.69	−69.97	−51.25	−50.38
8	−136.31	95.31	−197.54	−111.38	−13.56
9	14.77	135.45	91.90	98.34	246.21
10	−253.44	−107.91	−244.65	−171.64	−177.19
11	−251.36	−17.96	−81.06	−9.69	−124.86
12	−6.16	−171.19	71.81	37.70	1.57
13	−301.50	238.18	−53.92	−148.72	19.25
14	−41.80	36.59	−33.89	15.65	36.40
15	−138.89	184.54	−167.07	−129.93	−33.41
16	−30.30	1.50	−24.61	119.44	45.56
17	−186.41	100.02	−102.26	68.97	43.51
18	−81.71	−66.68	−21.99	−148.83	−123.71
19	−174.72	−30.59	−139.35	−145.15	−122.07
20	−151.65	−23.93	9.75	−108.13	−110.89
21	−282.30	−33.27	−110.26	−364.08	−60.35
22	−247.17	−285.44	−317.87	−157.91	−95.42
23	−162.98	137.98	−164.36	−49.47	−28.79
24	95.21	694.26	130.47	100.29	177.16

Table 10: BIC of Model with p=1 for Control Group with Stimulus Type=1

ID	BA24	BA25	DLPFC	L AMYG	R AMYG
1	−227.31	−19.31	−74.51	−82.90	−115.22
2	240.26	541.67	176.41	279.10	428.91
3	−243.16	−242.76	−123.73	−267.26	−223.55
4	42.38	162.75	−27.34	−18.28	98.87
5	−154.49	31.60	−102.71	−23.64	−52.95
6	−83.84	−146.38	−31.01	−85.43	−31.95
7	−210.58	−43.72	−64.00	−45.27	−44.11
8	−130.34	101.28	−191.58	−105.40	−7.56
9	20.74	141.41	97.86	104.30	252.18
10	−247.24	−101.95	−238.68	−165.67	−171.13
11	−245.39	−12.00	−75.09	−3.73	−118.81
12	−0.19	−165.22	77.78	43.66	7.53
13	−293.46	244.15	−47.79	−142.75	25.22
14	−35.53	42.56	−27.77	21.87	42.40
15	−132.15	190.50	−161.10	−123.96	−27.41
16	−24.34	7.47	−18.65	125.40	51.65
17	−179.71	105.99	−96.30	75.13	49.89
18	−75.75	−60.72	−16.03	−142.86	−117.75
19	−167.91	−24.61	−133.22	−138.88	−116.00
20	−145.68	−16.01	15.73	−102.16	−104.92
21	−276.33	−27.30	−104.30	−357.65	−54.39
22	−241.20	−279.10	−311.90	−150.71	−87.66
23	−157.02	143.94	−158.39	−43.50	−22.82
24	103.21	223.08	139.84	106.25	183.13

Table 11: BIC of Model with p=2 for Control Group with Stimulus Type=1

ID	BA24	BA25	DLPFC	L AMYG	R AMYG
1	−224.32	−16.31	−71.86	−79.91	−112.22
2	242.87	556.48	178.89	282.10	431.91
3	−240.54	−239.78	−120.75	−266.09	−222.85
4	45.37	165.69	−24.35	−15.50	101.07
5	−151.50	34.59	−99.72	−20.64	−49.95
6	−109.39	−143.38	−29.30	−82.91	−29.41
7	−207.60	−40.73	−61.00	−42.29	−41.42
8	−127.35	104.27	−188.58	−102.42	−4.60
9	23.73	144.41	100.86	107.30	255.17
10	−244.48	−98.95	−235.69	−162.67	−168.23
11	−242.40	−9.00	−72.10	−0.73	−115.89
12	2.80	−162.23	80.77	46.66	10.53
13	−292.54	247.14	−44.95	−139.76	28.21
14	−32.84	45.56	−24.92	24.61	45.36
15	−129.93	193.50	−158.11	−120.96	−24.45
16	−21.34	10.47	−15.65	128.40	54.53
17	−177.44	108.98	−93.30	77.93	52.48
18	−72.75	−57.72	−13.03	−139.87	−114.75
19	−165.76	−21.62	−130.39	−136.19	−113.11
20	−142.69	−14.97	18.71	−99.16	−101.93
21	−273.33	−24.31	−101.30	−355.12	−51.39
22	−238.21	−276.48	−308.91	−148.95	−86.46
23	−154.02	146.94	−155.40	−40.51	−19.83
24	104.17	703.22	139.43	109.25	186.13

Table 12: AIC of Model with p=1 for Control Group with Stimulus Type=2

ID	BA24	BA25	DLPFC	L AMYG	R AMYG
1	−109.15	34.72	10.33	6.05	49.23
2	95.56	277.63	240.16	93.04	237.29
3	−218.83	−269.25	−149.59	−169.20	−279.67
4	−101.66	118.25	−189.45	−25.90	97.71
5	−227.65	−89.20	−168.29	−8.21	−93.19
6	−37.81	−108.54	−21.09	−97.56	−35.34
7	−287.70	−67.54	−200.52	−172.96	−48.60
8	−209.29	128.21	−130.89	−106.56	81.76
9	−57.11	22.50	−109.24	110.68	260.02
10	−206.07	−193.90	−206.33	−127.72	−112.40
11	−222.16	27.13	−137.20	−71.99	−57.25
12	−21.68	−149.44	42.22	−57.41	−80.16
13	−279.05	108.68	−190.68	−149.82	−100.31
14	−129.83	−20.00	−52.83	28.68	53.54
15	−133.32	−33.89	−55.50	−135.03	−70.97
16	211.28	24.29	116.65	355.08	74.21
17	8.47	237.71	−16.32	169.54	199.98
18	−104.55	−140.69	−80.37	−129.56	−150.18
19	−294.63	−83.49	−90.50	−214.30	−151.04
20	−218.70	−19.83	−30.54	27.48	−37.80
21	−226.14	22.76	−163.88	−138.71	−75.78
22	−358.60	−217.41	−235.42	−164.53	−100.30
23	−215.39	101.38	−151.63	−74.05	−63.68
24	30.70	333.82	116.52	106.04	216.49

Table 13: AIC of Model with p=2 for Control Group with Stimulus Type=2

ID	BA24	BA25	DLPFC	L AMYG	R AMYG
1	−107.15	36.72	11.50	8.05	36.97
2	97.56	279.63	168.23	95.04	145.10
3	−216.83	−267.25	−147.59	−167.20	−277.89
4	−99.66	117.52	−187.46	−24.09	98.96
5	−225.65	−87.20	−166.29	−6.21	−64.40
6	−38.23	−106.54	−22.14	−95.61	−33.34
7	−285.70	−65.54	−200.19	−173.35	−46.60
8	−209.02	128.75	−129.01	−104.65	83.47
9	−55.47	24.50	−109.00	111.58	409.80
10	−204.07	−191.92	−204.33	−125.72	−110.40
11	−220.16	29.13	−135.20	−69.99	−55.25
12	−19.68	−147.44	44.22	−55.41	−78.16
13	−277.10	110.68	−188.73	−147.82	−98.31
14	−127.83	−18.58	−50.83	28.74	55.53
15	−131.32	−31.90	−53.50	−133.03	−69.48
16	213.28	26.29	118.65	261.51	75.88
17	10.42	239.71	−15.44	171.53	201.98
18	−102.55	−139.07	−78.43	−127.56	−148.18
19	−250.49	−81.49	−90.10	−212.31	−149.04
20	−216.70	−17.93	−28.54	27.67	−36.92
21	−200.52	23.90	−162.54	−136.71	−74.12
22	−356.60	−215.41	−233.42	−162.65	−101.04
23	−213.39	103.38	−149.63	−72.05	−61.68
24	31.46	335.22	117.01	106.99	218.24

Table 14: BIC of Model with p=1 for Control Group with Stimulus Type=2

ID	BA24	BA25	DLPFC	L AMYG	R AMYG
1	−101.18	42.69	18.29	14.02	57.19
2	103.53	285.60	248.13	101.00	245.26
3	−210.87	−261.28	−141.62	−161.24	−271.70
4	−93.69	126.21	−181.48	−17.93	105.68
5	−219.68	−81.24	−160.33	−0.24	−85.23
6	−29.84	−100.57	−13.12	−89.59	−27.38
7	−279.73	−59.57	−192.55	−165.00	−40.63
8	−201.32	136.18	−122.92	−98.59	89.72
9	−49.15	30.46	−101.27	118.65	267.99
10	−198.10	−185.93	−198.36	−119.75	−104.43
11	−214.19	35.10	−129.23	−64.02	−49.28
12	−13.72	−141.48	50.19	−49.44	−72.20
13	−271.08	116.65	−182.72	−141.85	−92.34
14	−121.87	−12.03	−44.87	36.64	61.50
15	−125.35	−25.92	−47.53	−127.06	−63.01
16	219.25	32.26	124.61	363.05	82.17
17	16.44	245.68	−8.36	177.51	207.94
18	−96.58	−132.72	−72.41	−121.60	−142.21
19	−286.66	−75.52	−82.53	−206.34	−143.08
20	−210.73	−11.87	−22.58	35.45	−29.84
21	−218.18	30.73	−155.91	−130.75	−67.81
22	−350.63	−209.44	−227.45	−156.56	−92.33
23	−207.42	109.35	−143.67	−66.08	−55.71
24	38.67	341.79	124.48	114.00	224.46

Table 15: BIC of Model with p=2 for Control Group with Stimulus Type=2

ID	BA24	BA25	DLPFC	L AMYG	R AMYG
1	−98.18	45.69	20.46	17.02	45.93
2	106.53	288.59	177.19	104.00	154.06
3	−207.87	−258.29	−138.63	−158.24	−268.92
4	−90.69	126.48	−178.50	−15.13	107.92
5	−216.68	−78.24	−157.33	2.75	−55.43
6	−29.27	−97.58	−13.18	−86.65	−24.38
7	−276.74	−56.58	−191.23	−164.39	−37.64
8	−200.05	137.71	−120.05	−95.69	92.44
9	−46.50	33.46	−100.04	120.54	418.76
10	−195.11	−182.96	−195.36	−116.76	−101.44
11	−211.19	38.09	−126.24	−61.03	−46.29
12	−10.72	−138.48	53.18	−46.44	−69.20
13	−268.14	119.64	−179.77	−138.85	−89.35
14	−118.87	−9.62	−41.87	37.70	64.50
15	−122.36	−22.93	−44.53	−124.07	−60.51
16	222.24	35.25	127.61	270.48	84.84
17	19.38	248.67	−6.48	180.49	210.94
18	−93.59	−130.11	−69.46	−118.60	−139.22
19	−241.53	−72.53	−81.14	−203.35	−140.08
20	−207.74	−8.97	−19.58	36.63	−27.96
21	−191.56	32.86	−153.57	−127.75	−65.16
22	−347.63	−206.45	−224.45	−153.69	−92.08
23	−204.43	112.34	−140.67	−63.09	−52.72
24	40.42	344.19	125.97	115.95	227.21

Table 16: AIC of Model with p=1 for Control Group with Stimulus Type=4

ID	BA24	BA25	DLPFC	L AMYG	R AMYG
1	−302.90	−19.03	−58.27	−149.85	−115.54
2	105.83	548.50	303.96	151.49	171.67
3	−354.15	−227.27	−133.95	−255.79	−228.87
4	−118.75	34.22	−159.30	−88.42	−64.77
5	−292.46	−91.05	−250.79	−130.73	−134.65
6	−198.48	−174.07	−80.88	−188.63	−47.85
7	−303.87	−77.28	−119.86	−187.96	−39.04
8	−186.66	21.34	−226.09	−160.07	44.08
9	−276.63	−6.25	−109.99	−15.02	199.14
10	−163.47	−192.62	−178.73	−229.40	−233.90
11	−266.61	104.36	−105.73	−9.62	−2.91
12	−37.78	−256.61	−51.65	−264.28	−169.36
13	−253.29	321.43	−85.83	−82.80	36.64
14	−156.36	23.73	−78.93	−60.38	−24.52
15	−225.20	69.31	−127.15	−134.25	−18.65
16	62.81	83.32	15.99	254.13	−2.23
17	−248.03	120.92	−51.36	45.87	70.00
18	−21.78	214.55	31.95	−25.32	11.72
19	−54.02	23.46	−68.88	−132.54	−136.85
20	−130.76	−161.06	−11.62	−198.63	−164.17
21	−238.75	13.95	−127.83	−209.83	−6.87
22	−174.31	−318.78	−171.08	−222.18	−169.45
23	1.27	186.36	−101.07	27.64	45.79
24	123.27	566.33	101.99	255.94	73.85

Table 17: AIC of Model with p=2 for Control Group with Stimulus Type=4

ID	BA24	BA25	DLPFC	L AMYG	R AMYG
1	−286.17	−17.03	−56.30	−147.87	−113.54
2	107.83	442.86	395.51	172.82	173.67
3	−352.15	−225.27	−131.95	−253.79	−226.87
4	−117.12	36.15	−157.39	−86.43	−64.08
5	−290.46	−89.05	−248.79	−128.73	−131.41
6	−196.76	−172.07	−78.88	−187.10	−46.07
7	−301.87	−75.28	−120.82	−187.15	−37.14
8	−184.66	23.29	−224.09	−158.36	45.70
9	−274.63	−4.25	−107.99	−13.02	201.14
10	−161.47	−190.62	−176.73	−227.40	−231.90
11	−264.61	106.36	−103.73	−9.45	−1.30
12	−141.99	−254.61	−49.65	−246.25	−167.36
13	−253.89	323.39	−84.62	−80.80	38.64
14	−144.45	25.73	−78.06	−58.38	−22.52
15	−223.20	71.31	−125.18	−132.27	−16.65
16	64.28	85.32	17.40	256.03	−0.76
17	−246.03	122.92	−50.87	47.58	71.57
18	−19.78	216.55	33.95	−23.32	13.72
19	−265.56	25.34	−66.98	−130.96	−134.85
20	−128.76	−159.11	−9.79	−196.71	−162.91
21	−261.36	15.95	−126.34	−207.85	−5.20
22	−172.31	−317.08	−169.08	−220.42	−167.45
23	3.27	188.36	−99.07	29.64	47.79
24	125.43	569.30	104.95	258.43	76.6503

Table 18: BIC of Model with p=1 for Control Group with Stimulus Type=4

ID	BA24	BA25	DLPFC	L AMYG	R AMYG
1	−294.94	−11.06	−50.30	−141.88	−107.58
2	113.80	556.46	311.93	159.45	179.64
3	−346.18	−219.30	−125.99	−247.82	−220.90
4	−110.79	42.18	−151.33	−80.45	−56.81
5	−284.49	−83.08	−242.83	−122.77	−126.69
6	−190.51	−166.10	−72.92	−180.67	−39.88
7	−295.91	−69.32	−111.90	−179.99	−31.07
8	−178.69	29.30	−218.12	−152.11	52.05
9	−268.67	1.72	−102.03	−7.06	207.10
10	−155.51	−184.66	−170.77	−221.44	−225.94
11	−258.65	112.32	−97.76	−1.66	5.05
12	−29.81	−248.64	−43.69	−256.31	−161.39
13	−245.33	329.40	−77.86	−74.84	44.61
14	−148.39	31.70	−70.97	−52.42	−16.56
15	−217.23	77.27	−119.19	−126.28	−10.69
16	70.77	91.29	23.96	262.09	5.74
17	−240.06	128.89	−43.40	53.84	77.97
18	−13.82	222.52	39.92	−17.36	19.68
19	−46.05	31.43	−60.91	−124.57	−128.89
20	−122.80	−153.10	−3.65	−190.67	−156.20
21	−230.79	21.92	−119.86	−201.86	1.09
22	−166.35	−310.81	−163.11	−214.22	−161.48
23	9.24	194.32	−93.11	35.61	53.76
24	131.24	574.30	109.96	263.91	81.81

Table 19: BIC of Model with p=2 for Control Group with Stimulus Type=4

ID	BA24	BA25	DLPFC	L AMYG	R AMYG
1	−277.20	−8.07	−47.34	−138.91	−104.58
2	116.79	451.83	404.47	181.78	182.63
3	−343.19	−216.30	−122.99	−244.83	−217.90
4	−108.15	45.11	−148.43	−77.47	−55.12
5	−281.50	−80.09	−239.83	−119.77	−122.45
6	−187.80	−163.11	−69.92	−178.14	−37.11
7	−292.91	−66.32	−111.85	−178.19	−28.18
8	−175.70	32.25	−215.12	−149.40	54.66
9	−265.67	4.71	−99.03	−4.06	210.10
10	−152.51	−181.66	−167.77	−218.44	−222.94
11	−255.65	115.32	−94.76	−0.48	7.67
12	−133.03	−245.65	−40.69	−237.29	−158.40
13	−244.93	332.35	−75.66	−71.84	47.60
14	−135.48	34.69	−69.10	−49.42	−13.56
15	−214.24	80.27	−116.22	−123.31	−7.69
16	73.24	94.28	26.36	265.00	8.20
17	−237.07	131.88	−41.90	56.55	80.53
18	−10.82	225.51	42.92	−14.36	22.68
19	−256.60	34.30	−58.01	−122.00	−125.89
20	−119.80	−150.15	−0.83	−187.75	−153.95
21	−252.40	24.91	−117.38	−198.89	3.77
22	−163.35	−308.12	−160.12	−211.46	−158.48
23	12.23	197.32	−90.11	38.60	56.75
24	133.34	576.58	112.51	266.87	84.77

Table 20: AIC of Model with p=1 for Case Group with Stimulus Type=1

ID	BA24	BA25	DLPFC	L AMYG	R AMYG
1	−170.54	197.25	−198.74	2.88	178.45
2	−163.02	29.63	−59.86	−65.71	28.93
3	−264.04	−109.32	−143.14	−180.03	26.16
4	−147.34	−83.78	−209.69	−75.75	−56.86
5	−321.25	−134.31	−202.89	−149.73	−79.32
6	−128.71	49.55	−100.72	−132.74	10.48
7	250.58	580.63	326.14	259.41	255.59
8	−134.85	−8.72	−121.14	−19.61	156.53
9	−238.66	−36.54	−204.17	−38.87	84.12
10	−183.38	29.25	−207.91	1.25	−9.41
11	−154.70	−31.95	−3.88	−5.19	−13.74
12	−188.03	78.94	−216.16	80.98	75.54
13	−228.99	64.62	−116.73	−153.09	23.53
14	−87.37	−46.73	−6.30	141.39	221.62
15	−96.97	78.42	−73.63	103.40	4.83
16	−185.37	−210.96	−200.51	−170.29	−141.41
17	−199.88	50.46	−117.27	−223.04	−18.71
18	−83.90	407.05	28.98	135.26	226.29
19	−282.15	103.41	−233.87	9.14	104.97
20	−196.52	−258.65	−106.28	−308.00	−212.09
21	−120.83	99.01	5.54	26.91	141.60
22	−53.79	188.20	−37.32	47.61	71.58
23	−52.94	35.17	55.86	−26.60	−14.16
24	−92.27	175.23	6.75	42.23	118.41
25	−66.50	−130.89	−46.19	−4.10	−45.55

Continued on next page

Table 20 – continued from previous page

ID	BA24	BA25	DLPFC	L AMYG	R AMYG
26	−167.10	110.08	−24.47	−189.64	−60.41
27	−262.34	−4.87	−208.27	12.10	−97.67
28	90.21	136.71	55.88	234.49	131.31
29	−201.93	403.07	33.25	−53.79	46.50
30	−333.20	−248.05	−332.21	−278.24	−217.09
31	−82.77	90.85	−75.80	−37.66	20.38
32	−116.34	213.79	−53.33	95.26	6.32
33	−188.15	−65.22	−88.78	−125.25	−0.48
34	−279.37	243.69	−260.00	−83.98	189.77
35	−95.10	179.23	−56.89	10.94	1.22
36	27.79	360.25	251.08	200.55	267.31
37	−52.38	174.43	74.19	179.82	101.85
38	−345.86	−305.21	−417.57	−197.72	−180.59
39	−118.14	141.87	−13.66	60.87	114.66
40	−52.39	124.97	134.61	112.27	27.37
41	−282.94	−125.24	−312.36	−256.78	−276.94
42	−167.17	256.76	30.67	−57.99	137.77

Table 21: AIC of Model with p=2 for Case Group with Stimulus Type=1

ID	BA24	BA25	DLPFC	L AMYG	R AMYG
1	−167.56	199.93	−196.59	5.58	180.71
2	−160.58	31.76	−57.20	−63.04	31.52
3	−261.92	−106.60	−140.62	−177.49	28.18
4	−145.08	−81.68	−206.72	−73.05	−54.43
5	−318.84	−131.66	−200.24	−147.06	−77.00
6	−126.11	52.05	−97.92	−130.56	12.64
7	252.84	583.40	328.59	261.53	257.77
8	−132.25	−6.00	−118.71	−16.61	158.95
9	−235.95	−33.63	−201.34	−36.70	86.21
10	−181.16	32.14	−205.83	3.28	−6.81
11	−152.58	−29.62	−1.74	−2.63	−11.27
12	−185.74	81.64	−213.99	83.86	78.23
13	−226.67	66.82	−114.34	−150.42	26.23
14	−84.94	−44.70	−3.47	143.58	224.26
15	−94.46	81.16	−70.83	105.77	6.86
16	−183.29	−208.46	−198.45	−167.83	−139.34
17	−197.62	52.94	−114.87	−220.06	−16.39
18	−81.10	409.95	31.51	137.42	228.82
19	−280.12	106.02	−231.45	12.00	107.62
20	−193.59	−256.03	−103.62	−305.35	−209.68
21	−118.10	101.87	8.17	29.29	144.42
22	−51.31	191.01	−35.03	49.80	74.30
23	−50.36	37.74	58.29	−24.17	−11.20
24	−90.03	177.42	8.76	44.72	120.94
25	−64.04	−128.65	−43.21	−1.98	−43.23

Continued on next page

Table 21 – continued from previous page

ID	BA24	BA25	DLPFC	L AMYG	R AMYG
26	−164.14	112.97	−22.30	−187.05	−58.30
27	−259.79	−2.84	−206.16	14.33	−95.06
28	92.73	139.20	58.25	236.87	134.08
29	−199.69	405.24	35.45	−51.21	48.92
30	−330.72	−245.07	−329.72	−275.98	−215.00
31	−80.15	93.56	−73.46	−35.37	22.64
32	−113.66	216.29	−50.38	97.88	8.47
33	−185.76	−62.75	−85.86	−122.98	1.81
34	−277.00	245.75	−257.95	−81.15	192.21
35	−92.12	181.91	−54.15	13.92	3.74
36	29.83	362.29	253.35	203.28	269.76
37	−49.49	176.50	76.61	182.17	104.73
38	−342.95	−302.69	−415.03	−195.13	−178.07
39	−115.35	143.97	−10.72	62.98	117.60
40	−50.29	127.79	137.03	115.17	30.01
41	−280.68	−122.43	−309.38	−253.90	−273.98
42	−164.84	259.48	32.97	−55.18	140.01

Table 22: BIC of Model with p=1 for Case Group with Stimulus Type=1

ID	BA24	BA25	DLPFC	L AMYG	R AMYG
1	−162.57	205.21	−190.78	10.85	186.42
2	−155.06	37.59	−51.90	−57.74	36.89
3	−256.07	−101.36	−135.17	−172.06	34.13
4	−139.37	−75.82	−201.73	−67.78	−48.89
5	−313.29	−126.34	−194.92	−141.76	−71.35
6	−120.74	57.52	−92.75	−124.77	18.44
7	258.55	588.59	334.10	267.37	263.55
8	−126.88	−0.75	−113.18	−11.64	164.49
9	−230.69	−28.57	−196.20	−30.90	92.09
10	−175.41	37.21	−199.95	9.22	−1.45
11	−146.73	−23.99	4.09	2.78	−5.77
12	−180.07	86.91	−208.20	88.94	83.50
13	−221.02	72.59	−108.76	−145.12	31.50
14	−79.40	−38.77	1.67	149.35	229.59
15	−89.00	86.38	−65.67	111.36	12.79
16	−177.41	−202.99	−192.54	−162.33	−133.44
17	−191.91	58.43	−109.31	−215.07	−10.74
18	−75.93	415.02	36.94	143.23	234.26
19	−274.19	111.37	−225.90	17.11	112.94
20	−188.55	−250.69	−98.31	−300.03	−204.12
21	−112.86	106.97	13.51	34.88	149.56
22	−45.83	196.17	−29.35	55.58	79.55
23	−44.98	43.13	63.83	−18.63	−6.20
24	−84.31	183.20	14.71	50.20	126.38
25	−58.54	−122.92	−38.23	3.87	−37.59

Continued on next page

Table 22 – continued from previous page

ID	BA24	BA25	DLPFC	L AMYG	R AMYG
26	−159.14	118.05	−16.50	−181.67	−52.44
27	−254.38	3.09	−200.30	20.07	−89.71
28	98.17	144.68	63.85	242.45	139.27
29	−193.96	411.04	41.22	−45.82	54.46
30	−325.24	−240.08	−324.24	−270.27	−209.12
31	−74.80	98.81	−67.84	−29.69	28.34
32	−108.37	221.76	−45.36	103.23	14.29
33	−180.19	−57.26	−80.82	−117.28	7.49
34	−271.40	251.66	−252.03	−76.01	197.73
35	−87.14	187.19	−48.92	18.91	9.18
36	35.76	368.21	259.04	208.52	275.27
37	−44.41	182.40	82.16	187.79	109.82
38	−337.90	−297.24	−409.61	−189.75	−172.62
39	−110.18	149.83	−5.70	68.84	122.62
40	−44.42	132.94	142.58	120.23	35.34
41	−274.97	−117.28	−304.39	−248.82	−268.97
42	−159.21	264.72	38.63	−50.03	145.73

Table 23: BIC of Model with p=2 for Case Group with Stimulus Type=1

ID	BA24	BA25	DLPFC	L AMYG	R AMYG
1	−159.89	207.76	−188.71	13.28	189.11
2	−152.77	40.02	−49.49	−54.85	39.48
3	−253.40	−98.71	−132.73	−169.67	36.94
4	−136.67	−73.17	−199.36	−65.01	−46.01
5	−311.22	−123.66	−192.16	−139.36	−68.36
6	−118.49	60.15	−90.13	−121.96	20.44
7	260.77	591.54	336.88	270.13	266.42
8	−124.22	1.46	−110.24	−9.27	167.10
9	−227.85	−25.86	−193.23	−28.69	95.08
10	−173.07	39.45	−197.75	12.01	1.08
11	−143.95	−21.87	6.23	5.73	−3.29
12	−177.39	89.51	−205.50	91.27	86.30
13	−219.01	75.04	−106.67	−142.45	33.73
14	−76.80	−36.31	4.19	151.79	232.09
15	−86.61	89.04	−63.14	114.20	15.69
16	−174.49	−200.22	−189.68	−159.56	−130.86
17	−189.91	60.78	−106.82	−212.91	−7.90
18	−73.47	417.68	39.34	146.09	236.99
19	−271.76	113.79	−223.23	20.10	115.52
20	−186.09	−247.84	−95.57	−297.52	−201.87
21	−110.09	109.80	16.03	37.76	152.23
22	−43.51	198.43	−27.01	58.16	81.63
23	−42.19	45.75	65.98	−16.48	−3.57
24	−81.83	185.78	17.30	52.40	129.04
25	−56.50	−120.38	−35.96	6.28	−34.86

Continued on next page

Table 23 – continued from previous page

ID	BA24	BA25	DLPFC	L AMYG	R AMYG
26	−156.96	120.92	−14.46	−178.92	−49.55
27	−251.65	5.36	−197.54	22.90	−86.73
28	100.65	147.00	66.09	245.24	142.04
29	−191.81	413.16	43.66	−43.50	57.05
30	−322.90	−237.14	−321.55	−267.74	−206.19
31	−72.20	101.46	−65.48	−27.60	30.92
32	−106.18	224.24	−42.63	105.34	16.30
33	−177.45	−54.62	−78.42	−115.14	9.61
34	−269.16	254.20	−249.35	−73.33	200.60
35	−84.22	189.84	−46.22	21.40	11.67
36	38.03	370.75	261.49	210.71	278.12
37	−41.65	185.12	84.18	190.28	112.03
38	−335.71	−294.72	−407.28	−187.60	−170.07
39	−107.89	152.83	−3.27	70.89	125.25
40	−42.33	135.16	144.85	123.08	37.37
41	−272.40	−115.17	−302.20	−246.26	−266.36
42	−156.52	266.83	41.46	−47.10	148.09

Table 24: AIC of Model with p=1 for Case Group with Stimulus Type=2

ID	BA24	BA25	DLPFC	L AMYG	R AMYG
1	−249.13	230.54	−189.22	−94.57	89.99
2	−190.68	16.90	−119.81	−46.54	7.25
3	−253.59	−148.57	−215.32	−171.89	−62.56
4	−127.41	186.00	−186.59	−145.39	−46.36
5	−308.55	−114.77	−244.86	−208.07	−129.47
6	−13.17	21.43	−213.47	−163.65	50.12
7	−75.64	376.69	32.31	39.61	194.15
8	−108.68	−93.55	−137.05	23.31	111.19
9	−244.86	186.24	−78.18	−181.41	238.72
10	−105.63	−24.26	−185.83	11.71	33.97
11	−151.99	−62.74	−33.26	25.47	6.71
12	−96.77	−34.76	4.21	128.15	32.44
13	−217.22	115.79	−132.65	−156.77	16.95
14	11.09	−27.04	39.46	154.45	250.14
15	−120.95	76.35	−75.02	45.53	15.93
16	−193.73	−314.22	−202.60	−167.98	−155.03
17	−276.69	36.01	−163.15	−301.23	7.59
18	18.20	297.65	5.34	112.87	61.72
19	−252.08	23.26	−122.63	40.21	10.57
20	−106.99	−200.73	−21.36	−105.60	−205.00
21	−59.13	117.06	−24.65	16.50	192.65
22	−194.82	113.54	−161.12	188.29	85.97
23	13.58	2.29	−14.92	8.72	−5.31
24	−76.62	116.57	−175.90	−1.33	41.97
25	−124.36	−113.77	−39.88	−63.36	−40.44

Continued on next page

Table 24 – continued from previous page

ID	BA24	BA25	DLPFC	L AMYG	R AMYG
26	−120.08	85.27	−22.77	−138.09	−72.24
27	−293.49	77.41	−216.98	−53.11	−41.17
28	156.52	115.47	111.27	335.11	239.01
29	−126.68	522.68	43.93	−245.42	171.34
30	−362.47	−414.15	−494.44	−291.33	−249.13
31	18.43	272.11	52.68	67.66	194.34
32	−170.09	12.86	−94.05	−37.20	−44.14
33	−242.54	−206.51	−110.78	−97.56	−24.87
34	−274.75	260.83	−232.40	−98.70	227.85
35	−114.27	119.72	−32.68	−5.14	47.16
36	−17.64	285.58	246.67	219.31	240.14
37	−91.46	124.34	12.73	121.70	73.59
38	−269.69	−260.06	−298.64	−253.81	−130.43
39	−167.10	128.52	−47.06	46.84	78.48
40	−137.65	104.15	−22.53	−5.31	−73.74
41	−387.68	−221.61	−337.63	−317.81	−256.07
42	−59.44	277.35	43.73	53.17	183.71

Table 25: AIC of Model with p=2 for Case Group with Stimulus Type=2

ID	BA24	BA25	DLPFC	L AMYG	R AMYG
1	−247.13	232.54	−187.22	−92.57	91.99
2	−188.93	17.77	−117.81	−52.30	8.78
3	−251.59	−146.57	−213.32	−169.89	−60.56
4	−125.41	190.21	−184.66	−143.73	−44.36
5	−306.56	−112.82	−242.87	−206.43	−127.54
6	−176.54	23.43	−211.47	−161.65	52.12
7	−73.64	323.38	34.31	40.19	194.76
8	−106.68	−91.55	−135.05	24.92	109.59
9	−242.86	188.24	−76.18	−179.66	305.10
10	−103.75	−22.27	−183.83	11.47	35.15
11	−149.99	−60.74	−31.26	26.84	8.65
12	−94.83	−32.76	−115.22	130.14	33.74
13	−215.22	117.79	−130.65	−155.37	18.69
14	13.09	−25.04	41.46	156.45	252.12
15	−118.95	78.35	−73.02	47.53	17.63
16	−199.13	−313.66	−200.78	−166.57	−153.94
17	−274.96	38.01	−161.15	−299.38	9.59
18	20.19	297.39	7.33	114.18	62.09
19	−251.00	25.26	−120.63	42.21	9.91
20	−104.99	−198.73	−19.36	−103.60	−203.00
21	−64.02	114.54	−25.82	18.48	186.92
22	−193.01	115.54	−159.54	190.29	87.97
23	15.23	4.27	−12.93	10.72	−3.31
24	−74.62	118.55	−173.90	0.67	43.97
25	−122.36	−78.92	−37.88	−61.36	−38.44

Continued on next page

Table 25 – continued from previous page

ID	BA24	BA25	DLPFC	L AMYG	R AMYG
26	−118.14	86.51	−22.30	−136.84	−71.39
27	−291.70	75.04	−215.16	−51.66	−39.89
28	158.52	117.47	113.27	375.25	241.01
29	−125.10	491.91	45.93	−243.66	201.48
30	−360.47	−412.19	−493.33	−289.38	−247.16
31	18.12	274.11	49.63	68.28	196.32
32	−168.09	11.39	−92.05	−35.20	−42.14
33	−240.90	−204.51	−108.78	−95.56	−22.87
34	−277.68	262.45	−225.47	−97.21	229.18
35	−112.27	121.72	−30.68	−3.14	49.16
36	−15.64	287.58	248.67	246.87	242.17
37	−89.46	126.34	14.73	123.70	75.59
38	−267.69	−258.06	−296.64	−251.86	−128.43
39	−165.10	130.52	−45.06	48.80	79.95
40	−135.65	106.15	−20.78	−3.31	23.40
41	−385.68	−219.64	−335.63	−285.94	−254.07
42	−57.44	279.35	45.73	55.17	185.71

Table 26: BIC of Model with p=1 for Case Group with Stimulus Type=2

ID	BA24	BA25	DLPFC	L AMYG	R AMYG
1	−241.16	238.51	−181.26	−86.61	97.96
2	−182.72	24.87	−111.85	−38.57	15.21
3	−245.62	−140.61	−207.35	−163.93	−54.59
4	−119.44	193.97	−178.63	−137.43	−38.39
5	−300.59	−106.80	−236.90	−200.10	−121.50
6	−5.21	29.39	−205.50	−155.69	58.09
7	−67.67	384.65	40.27	47.57	202.12
8	−100.72	−85.59	−129.09	31.28	119.15
9	−236.89	194.20	−70.21	−173.45	246.69
10	−97.66	−16.29	−177.86	19.67	41.94
11	−144.02	−54.78	−25.30	33.44	14.67
12	−88.80	−26.79	12.18	136.12	40.41
13	−209.25	123.76	−124.68	−148.81	24.91
14	19.06	−19.07	47.42	162.41	258.11
15	−112.98	84.31	−67.06	53.50	23.89
16	−185.76	−306.25	−194.63	−160.02	−147.06
17	−268.73	43.98	−155.19	−293.26	15.56
18	26.17	305.61	13.31	120.84	69.69
19	−244.12	31.23	−114.66	48.18	18.53
20	−99.02	−192.77	−13.40	−97.64	−197.03
21	−51.16	125.03	−16.68	24.47	200.62
22	−186.85	121.51	−153.16	196.26	93.93
23	21.55	10.25	−6.95	16.69	2.66
24	−68.65	124.53	−167.94	6.63	49.94
25	−116.40	−105.80	−31.91	−55.39	−32.47

Continued on next page

Table 26 – continued from previous page

ID	BA24	BA25	DLPFC	L AMYG	R AMYG
26	−112.12	93.23	−14.80	−130.13	−64.28
27	−285.52	85.37	−209.01	−45.14	−33.20
28	164.49	123.44	119.24	343.07	246.98
29	−118.72	530.64	51.90	−237.45	179.31
30	−354.50	−406.18	−486.47	−283.36	−241.17
31	26.40	280.08	60.65	75.62	202.30
32	−162.12	20.83	−86.09	−29.24	−36.17
33	−234.57	−198.55	−102.82	−89.60	−16.90
34	−266.78	268.79	−224.44	−90.73	235.82
35	−106.31	127.68	−24.71	2.83	55.13
36	−9.67	293.55	254.63	227.28	248.11
37	−83.49	132.30	20.70	129.67	81.56
38	−261.72	−252.09	−290.67	−245.85	−122.46
39	−159.13	136.49	−39.10	54.80	86.44
40	−129.69	112.11	−14.56	2.66	−65.78
41	−379.72	−213.64	−329.66	−309.84	−248.10
42	−51.48	285.31	51.69	61.14	191.68

Table 27: BIC of Model with p=2 for Case Group with Stimulus Type=2

ID	BA24	BA25	DLPFC	L AMYG	R AMYG
1	−238.17	241.50	−178.26	−83.61	100.95
2	−179.97	26.74	−108.85	−43.34	17.74
3	−242.63	−137.61	−204.35	−160.93	−51.59
4	−116.45	199.17	−175.70	−134.76	−35.40
5	−297.59	−103.86	−233.90	−197.47	−118.57
6	−167.58	32.39	−202.50	−152.69	61.08
7	−64.68	332.34	43.27	49.15	203.73
8	−97.72	−82.59	−126.09	33.88	118.55
9	−233.89	197.20	−67.21	−170.70	314.07
10	−94.79	−13.31	−174.87	20.43	44.12
11	−141.03	−51.78	−22.30	35.80	17.62
12	−85.86	−23.80	−106.26	139.11	42.71
13	−206.26	126.75	−121.69	−146.41	27.65
14	22.05	−16.08	50.42	165.41	261.08
15	−109.99	87.31	−64.06	56.50	26.59
16	−190.17	−304.69	−191.81	−157.61	−144.98
17	−266.00	46.97	−152.19	−290.42	18.55
18	29.15	306.35	16.29	123.14	71.05
19	−242.04	34.22	−111.67	51.18	18.88
20	−96.03	−189.77	−10.40	−94.64	−194.04
21	−55.05	123.50	−16.86	27.45	195.89
22	−184.05	124.50	−150.58	199.25	96.93
23	24.19	13.23	−3.97	19.68	5.65
24	−65.66	127.51	−164.94	9.63	52.93
25	−113.40	−69.96	−28.92	−52.40	−29.48

Continued on next page

Table 27 – continued from previous page

ID	BA24	BA25	DLPFC	L AMYG	R AMYG
26	−109.18	95.48	−13.34	−127.88	−62.43
27	−282.73	84.00	−206.20	−42.70	−30.93
28	167.48	126.43	122.24	384.21	249.97
29	−116.14	500.88	54.89	−234.70	210.44
30	−351.50	−403.23	−484.37	−280.42	−238.20
31	27.09	283.07	58.59	77.24	205.28
32	−159.13	20.35	−83.09	−26.24	−33.18
33	−231.94	−195.55	−99.82	−86.60	−13.91
34	−268.71	271.41	−216.51	−88.25	238.14
35	−103.31	130.68	−21.72	5.83	58.13
36	−6.68	296.54	257.63	255.83	251.13
37	−80.49	135.30	23.70	132.67	84.55
38	−258.73	−249.09	−287.68	−242.89	−119.46
39	−156.14	139.48	−36.10	57.76	88.91
40	−126.69	115.11	−11.82	5.65	32.37
41	−376.72	−210.68	−326.66	−276.98	−245.10
42	−48.48	288.31	54.69	64.13	194.68

Table 28: AIC of Model with p=1 for Case Group with Stimulus Type=4

ID	BA24	BA25	DLPFC	L AMYG	R AMYG
1	−111.23	251.44	−168.68	−96.95	124.78
2	−115.28	−65.30	−91.33	−75.96	−0.21
3	−232.91	−96.89	−175.94	−252.02	17.43
4	−11.10	238.74	−166.06	−1.34	52.10
5	−473.00	−198.65	−289.11	−258.48	−119.17
6	−53.93	95.21	−134.26	−187.01	21.75
7	32.05	568.36	158.31	325.07	244.43
8	−201.62	−25.89	−236.91	−18.11	58.67
9	−278.68	−137.91	−214.17	−122.13	−61.65
10	−128.42	−58.24	−142.13	86.44	110.34
11	−150.42	45.24	56.84	32.38	10.71
12	−181.66	9.05	−205.37	137.71	26.19
13	−290.19	100.91	−108.09	−144.17	80.78
14	−54.82	117.54	9.55	188.71	251.54
15	−15.66	276.11	−112.74	−46.22	−33.10
16	−229.38	−207.03	−229.33	−157.41	−108.90
17	−330.59	−146.42	−179.36	−250.77	−97.20
18	−138.53	97.66	−57.47	57.67	−3.95
19	−392.04	71.71	−126.15	43.58	72.70
20	−205.58	−252.08	−115.20	−173.21	−182.71
21	−191.40	161.26	−20.60	−0.48	177.05
22	−139.08	235.60	−34.76	13.86	133.17
23	−55.01	16.91	−0.93	−31.96	23.98
24	23.57	371.62	−17.87	−2.17	52.60
25	−131.52	−244.50	−45.64	−39.10	−34.33

Continued on next page

Table 28 – continued from previous page

ID	BA24	BA25	DLPFC	L AMYG	R AMYG
26	−111.50	44.15	23.62	−203.78	−102.12
27	−381.86	0.24	−225.97	−151.48	−119.21
28	292.62	187.61	262.52	458.87	231.03
29	−229.18	440.79	73.77	−101.53	133.41
30	−416.48	−342.24	−347.94	−284.47	−207.94
31	−19.46	241.82	60.13	110.00	70.70
32	−138.12	133.51	−53.07	57.26	−20.62
33	−321.54	−70.30	−10.87	−193.33	−57.62
34	−242.44	456.22	−160.87	−35.47	289.41
35	−92.36	246.37	135.22	46.85	77.61
36	−107.92	409.72	225.93	−0.34	165.74
37	−13.83	169.43	107.79	107.17	116.82
38	−155.47	−250.98	−46.10	−129.26	−120.73
39	−93.24	140.41	23.43	147.24	71.31
40	−35.50	266.63	150.20	395.44	5.49
41	−329.21	−199.84	−336.12	−252.06	−277.60
42	−62.82	388.73	−56.88	−20.23	357.53

Table 29: AIC of Model with p=2 for Case Group with Stimulus Type=4

ID	BA24	BA25	DLPFC	L AMYG	R AMYG
1	−109.23	210.71	−168.08	−94.95	126.77
2	−113.29	−64.73	−89.35	−74.04	1.32
3	−230.91	−94.89	−173.94	−250.02	19.43
4	−10.89	238.76	−164.75	0.31	286.33
5	−471.00	−196.66	−287.29	−256.48	−117.85
6	−51.93	97.21	−132.26	−185.01	23.75
7	34.05	2928.38	160.27	306.24	246.43
8	−199.76	−23.89	−234.91	−16.25	59.35
9	−276.68	−135.92	−212.17	−120.13	−61.14
10	−128.81	−56.42	−140.13	87.23	111.39
11	−148.42	47.24	58.84	34.23	12.67
12	−179.66	10.85	−203.37	138.38	27.91
13	−288.19	102.90	−106.09	−142.17	82.78
14	−52.82	119.54	11.55	161.50	253.53
15	−13.66	304.69	−110.74	−44.47	−31.11
16	−228.16	−205.03	−227.45	−155.41	−107.05
17	−328.59	−144.42	−177.36	−248.78	−96.11
18	−136.53	99.61	−55.47	59.67	−2.33
19	−390.04	73.29	−124.23	45.40	74.70
20	−203.58	−250.09	−113.20	−171.21	−180.71
21	−190.09	161.83	−18.64	0.93	179.04
22	−137.08	237.42	−32.77	14.94	234.01
23	−53.01	18.91	1.07	−29.96	25.72
24	25.57	346.73	−16.03	−0.45	54.60
25	−129.52	−242.53	−43.64	−37.10	−32.33

Continued on next page

Table 29 – continued from previous page

ID	BA24	BA25	DLPFC	L AMYG	R AMYG
26	−109.50	46.15	25.62	−203.05	−100.12
27	−380.55	2.23	−224.21	−151.28	−29.13
28	294.62	189.44	264.52	470.44	233.03
29	−227.18	484.85	75.77	−99.53	135.38
30	−414.50	−340.25	−345.97	−282.47	−205.94
31	−17.98	243.82	61.97	112.00	72.70
32	−136.12	135.51	−51.07	59.26	−18.62
33	−319.77	−68.30	−200.28	−191.33	−55.72
34	−240.80	276.76	−158.89	−33.87	291.41
35	−90.36	248.37	137.10	48.85	79.61
36	−105.92	316.89	227.75	1.66	167.74
37	−11.83	171.43	109.79	109.17	118.81
38	−148.13	−252.31	−189.25	−127.26	−118.74
39	−111.76	142.41	25.43	149.24	72.99
40	−33.71	268.63	152.20	260.51	7.49
41	−327.28	−197.88	−334.66	−250.24	−277.13
42	−60.82	389.86	−54.88	−18.23	359.53

Table 30: BIC of Model with p=1 for Case Group with Stimulus Type=4

ID	BA24	BA25	DLPFC	L AMYG	R AMYG
1	−103.27	259.41	−160.71	−88.99	132.75
2	−107.32	−57.33	−83.36	−68.00	7.75
3	−224.94	−88.92	−167.98	−244.05	25.39
4	−3.13	246.70	−158.10	6.63	60.07
5	−465.04	−190.69	−281.14	−250.51	−111.20
6	−45.96	103.18	−126.30	−179.05	29.72
7	40.01	576.33	166.28	333.03	252.39
8	−193.65	−17.93	−228.94	−10.14	66.64
9	−270.71	−129.94	−206.20	−114.16	−53.69
10	−120.46	−50.27	−134.16	94.41	118.31
11	−142.46	53.21	64.81	40.35	18.68
12	−173.69	17.02	−197.41	145.68	34.16
13	−282.22	108.87	−100.13	−136.20	88.75
14	−46.85	125.51	17.52	196.68	259.50
15	−7.70	284.07	−104.78	−38.25	−25.13
16	−221.41	−199.07	−221.36	−149.44	−100.93
17	−322.62	−138.45	−171.39	−242.80	−89.23
18	−130.57	105.63	−49.51	65.64	4.02
19	−384.07	79.68	−118.19	51.55	80.66
20	−197.61	−244.11	−107.24	−165.25	−174.74
21	−183.43	169.22	−12.63	7.49	185.01
22	−131.12	243.56	−26.79	21.83	141.14
23	−47.04	24.87	7.04	−23.99	31.95
24	31.54	379.58	−9.90	5.80	60.56
25	−123.55	−236.54	−37.68	−31.14	−26.36

Continued on next page

Table 30 – continued from previous page

ID	BA24	BA25	DLPFC	L AMYG	R AMYG
26	−103.53	52.12	31.59	−195.81	−94.16
27	−373.89	8.20	−218.00	−143.51	−111.24
28	300.58	195.58	270.49	466.83	238.99
29	−221.21	448.76	81.73	−93.56	141.38
30	−408.51	−334.28	−339.97	−276.50	−199.97
31	−11.49	249.79	68.10	117.97	78.66
32	−130.15	141.48	−45.10	65.23	−12.65
33	−313.57	−62.33	−2.90	−185.37	−49.66
34	−234.47	464.19	−152.90	−27.51	297.38
35	−84.40	254.33	143.18	54.81	85.58
36	−99.95	417.68	233.90	7.63	173.70
37	−5.86	177.39	115.75	115.14	124.79
38	−147.50	−243.01	−38.14	−121.30	−112.76
39	−85.27	148.38	31.39	155.21	79.27
40	−27.54	274.60	158.16	403.40	13.46
41	−321.25	−191.87	−328.15	−244.09	−269.63
42	−54.85	396.70	−48.92	−12.27	365.50

Table 31: BIC of Model with p=2 for Case Group with Stimulus Type=4

ID	BA24	BA25	DLPFC	L AMYG	R AMYG
1	−100.27	219.67	−159.12	−85.99	135.73
2	−104.33	−55.77	−80.39	−65.08	10.28
3	−221.95	−85.93	−164.98	−241.06	28.39
4	−1.93	247.72	−155.79	9.27	295.30
5	−462.04	−187.70	−278.33	−247.52	−108.89
6	−42.96	106.18	−123.30	−176.05	32.71
7	43.01	2937.34	169.23	315.20	255.39
8	−190.80	−14.93	−225.94	−7.29	68.31
9	−267.71	−126.96	−203.20	−111.16	−52.18
10	−119.85	−47.46	−131.16	96.20	120.35
11	−139.46	56.20	67.80	43.19	21.64
12	−170.70	19.82	−194.41	147.34	36.87
13	−279.23	111.86	−97.13	−133.20	91.75
14	−43.86	128.50	20.51	170.46	262.49
15	−4.70	313.65	−101.78	−35.51	−22.15
16	−219.20	−196.07	−218.49	−146.45	−98.09
17	−319.63	−135.46	−168.40	−239.82	−87.14
18	−127.57	108.57	−46.51	68.64	6.63
19	−381.08	82.25	−115.27	54.36	83.66
20	−194.62	−241.13	−104.24	−162.25	−171.75
21	−181.13	170.80	−9.68	9.89	188.00
22	−128.12	246.38	−23.81	23.90	242.97
23	−44.05	27.87	10.04	−21.00	34.68
24	34.53	355.69	−7.07	8.51	63.56
25	−120.56	−233.57	−34.68	−28.14	−23.36

Continued on next page

Table 31 – continued from previous page

ID	BA24	BA25	DLPFC	L AMYG	R AMYG
26	−100.54	55.12	34.58	−194.09	−91.16
27	−371.59	11.20	−215.25	−142.32	−20.17
28	303.58	198.41	273.49	479.40	241.99
29	−218.22	493.81	84.73	−90.57	144.35
30	−405.53	−331.28	−337.01	−273.51	−196.98
31	−9.02	252.78	70.93	120.96	81.66
32	−127.16	144.47	−42.11	68.22	−9.65
33	−310.81	−59.34	−191.32	−182.37	−46.76
34	−231.84	285.72	−149.93	−24.91	300.37
35	−81.40	257.33	146.06	57.81	88.57
36	−96.96	325.85	236.71	10.62	176.70
37	−2.86	180.39	118.75	118.13	127.77
38	−139.17	−243.34	−180.29	−118.30	−109.78
39	−102.80	151.37	34.39	158.20	81.95
40	−24.74	277.59	161.16	269.47	16.45
41	−318.31	−188.92	−325.70	−241.28	−268.17
42	−51.86	398.83	−45.92	−9.27	368.49

APPENDIX B

ESTIMATED HAEMODYNAMIC RESPONSE FUNCTION

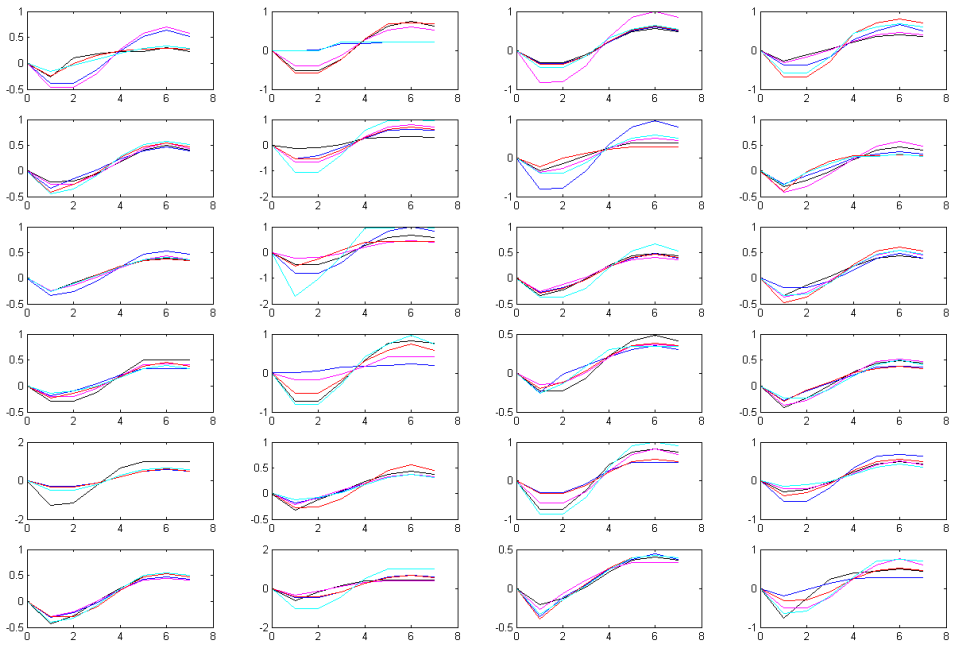

Figure 10: The plots of estimated HRFs for 24 control subjects with stimulus type = 1

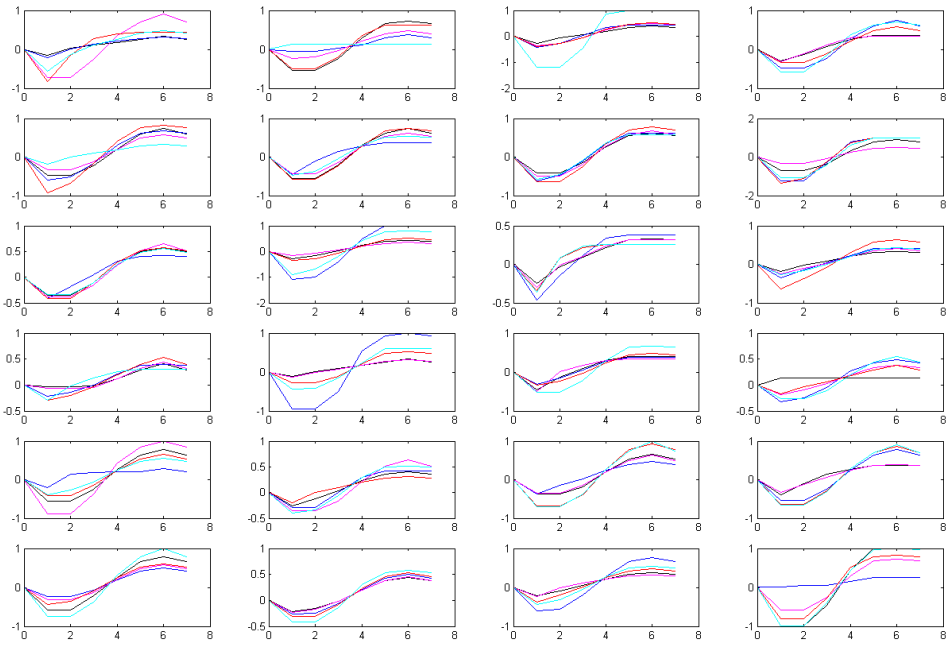

Figure 11: The plots of estimated HRFs for 24 control subjects with stimulus type = 2

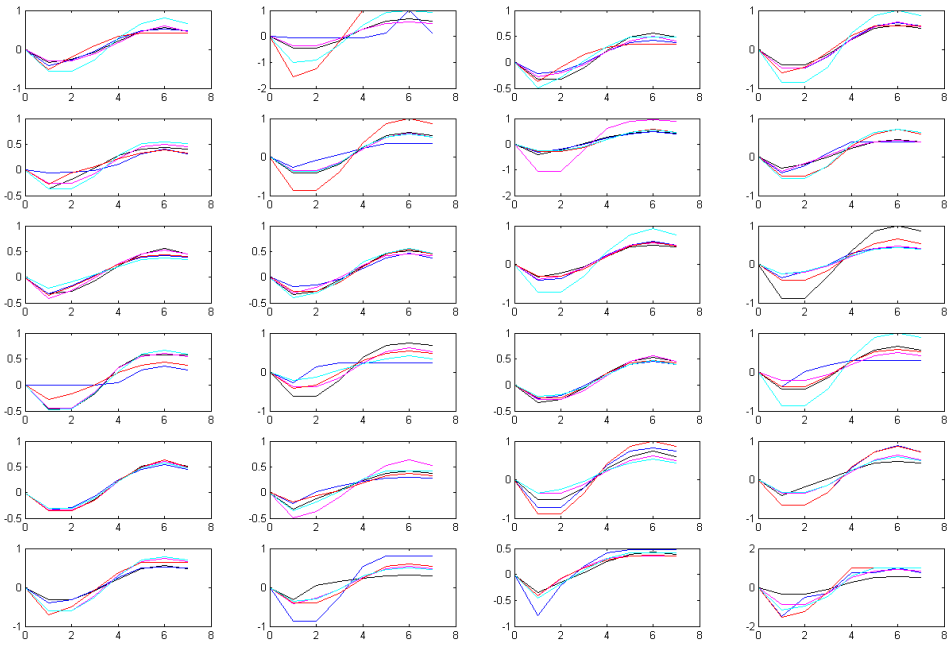

Figure 12: The plots of estimated HRFs for 24 control subjects with stimulus type = 4

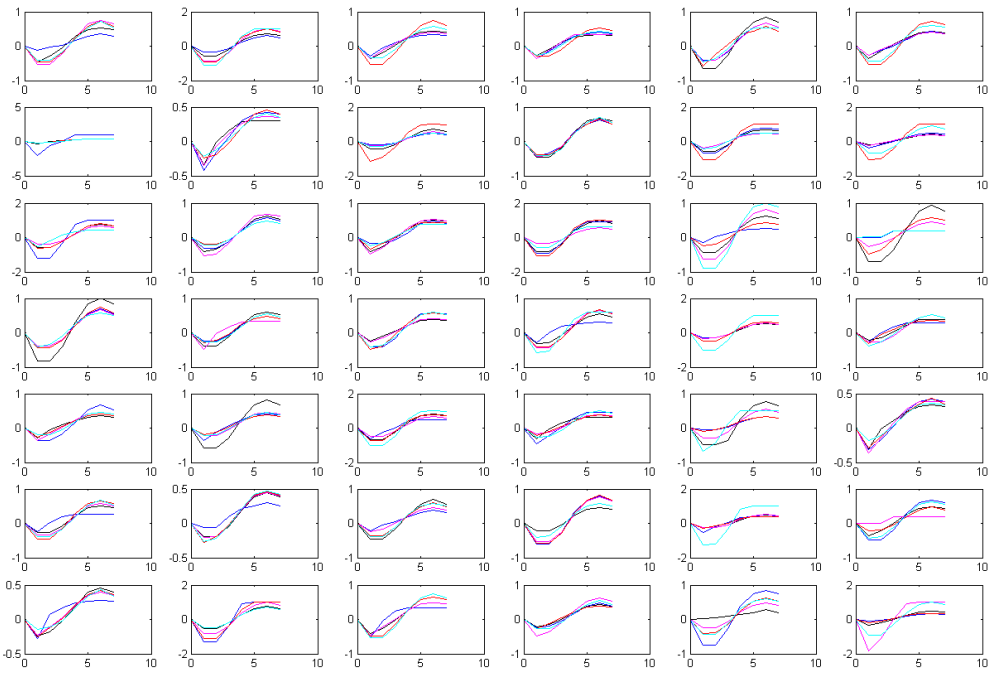

Figure 13: The plots of estimated HRFs for 42 case subjects with stimulus type = 1

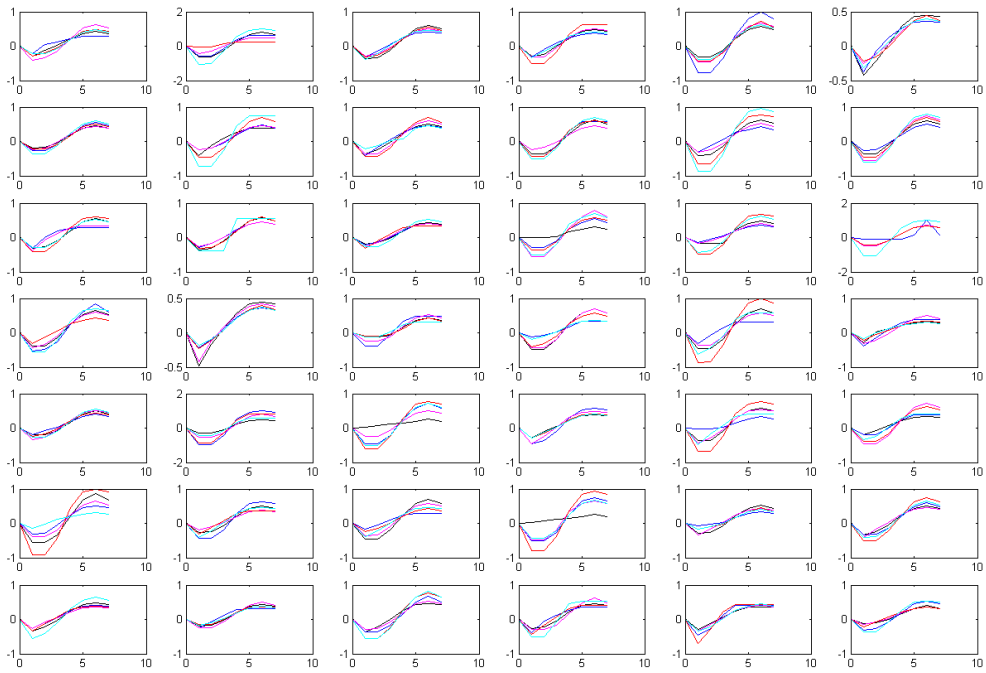

Figure 14: The plots of estimated HRFs for 42 case subjects with stimulus type = 2

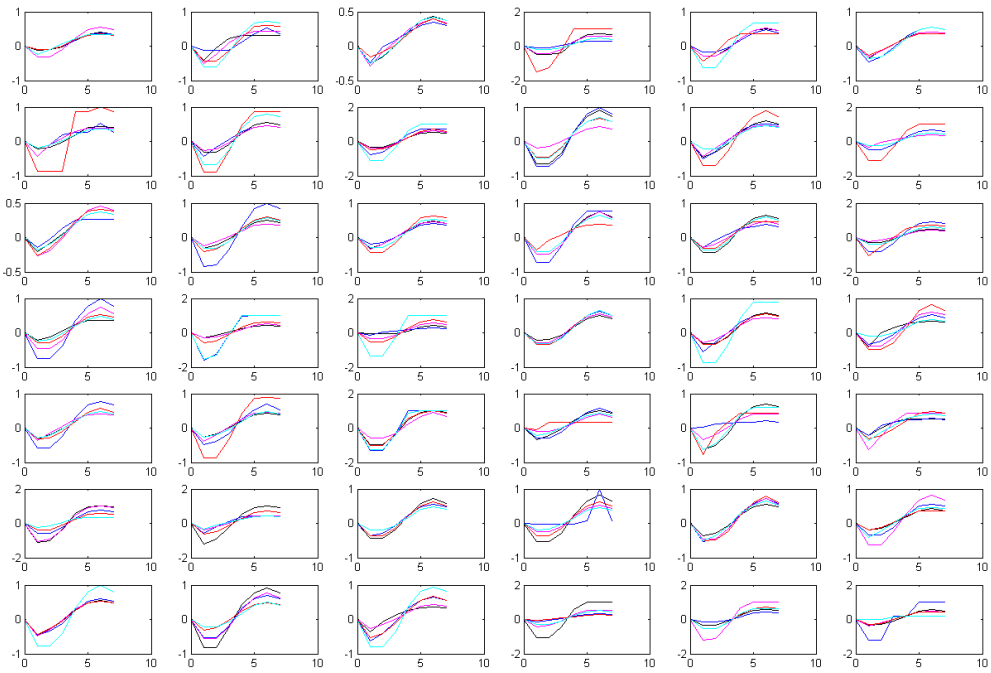

Figure 15: The plots of estimated HRFs for 42 case subjects with stimulus type = 4

APPENDIX C

ESTIMATED UNDERLYING NEURONAL SIGNAL

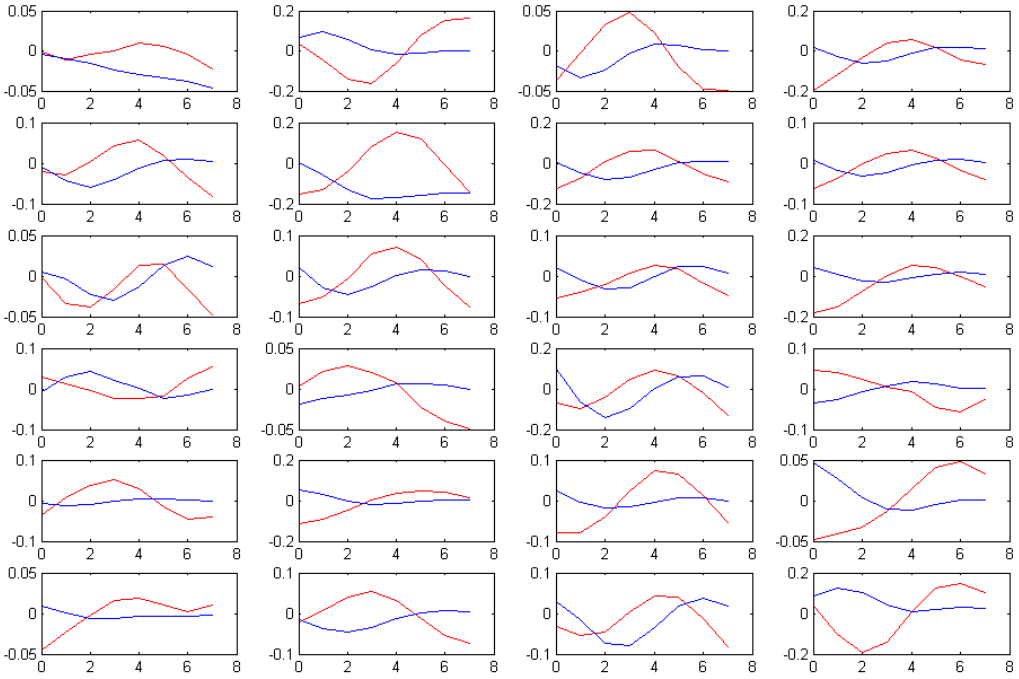

Figure 16: The plots of mean BOLD response vs mean estimated underlying neuronal signal of 24 control subjects for BA 24 with stimulus type = 1

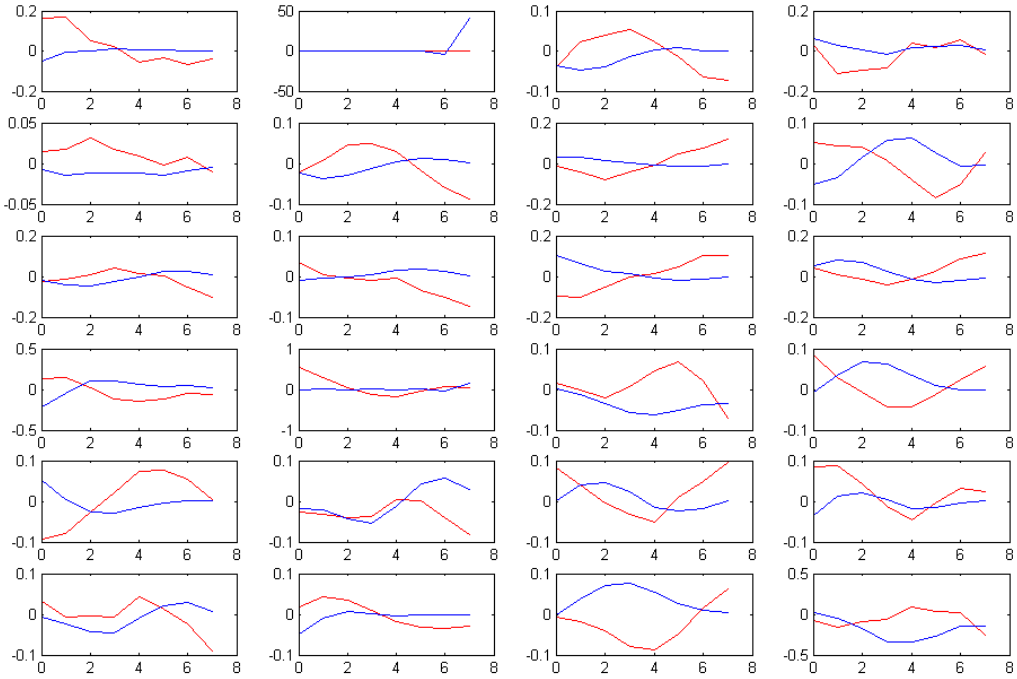

Figure 17: The plots of mean BOLD response vs mean estimated underlying neuronal signal of 24 control subjects for BA 25 with stimulus type = 1

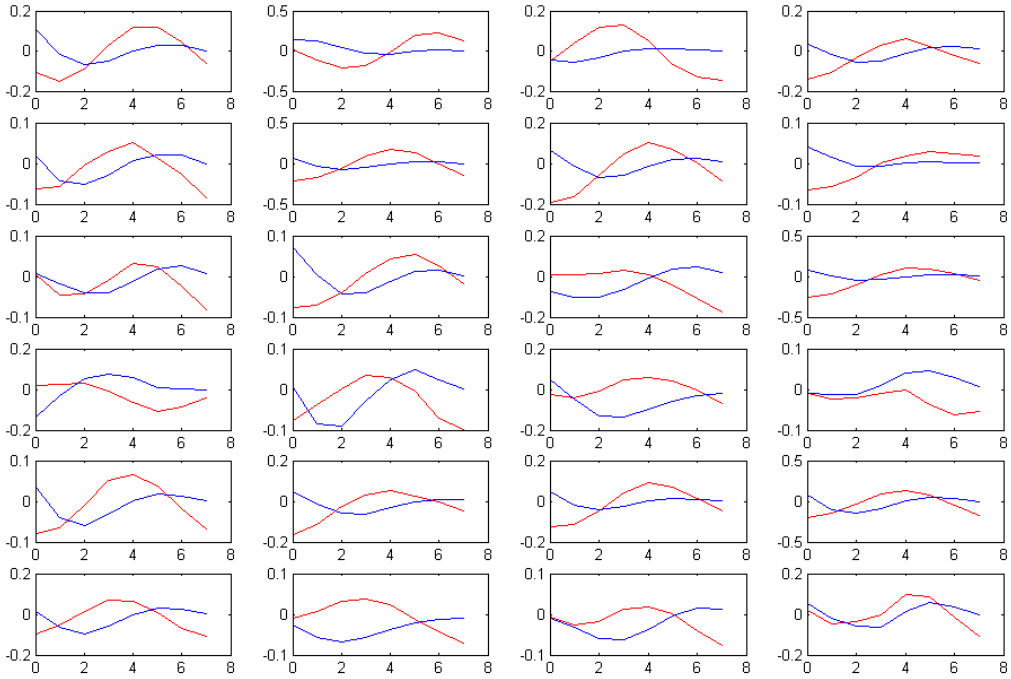

Figure 18: The plots of mean BOLD response vs mean estimated underlying neuronal signal of 24 control subjects for DLPFC with stimulus type = 1

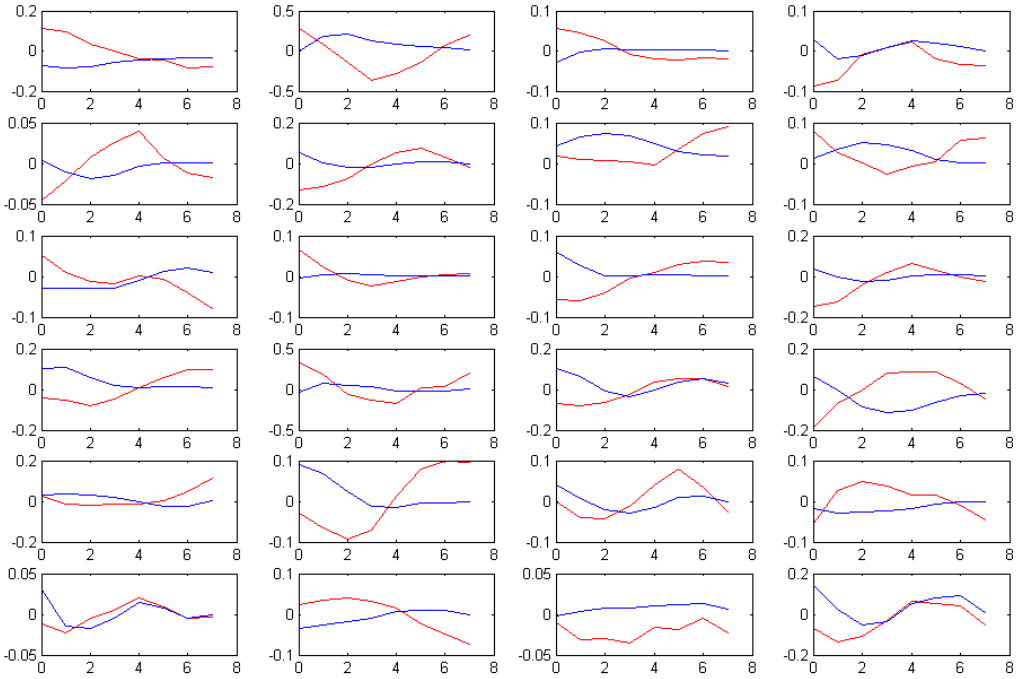

Figure 19: The plots of mean BOLD response vs mean estimated underlying neuronal signal of 24 control subjects for AMYG LEFT with stimulus type = 1

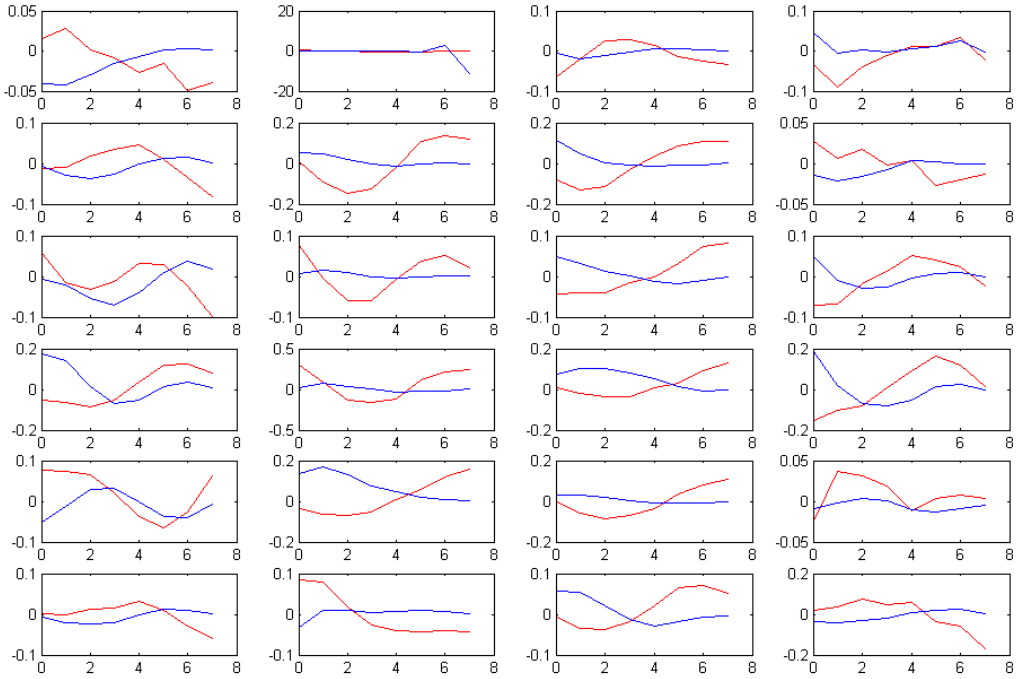

Figure 20: The plots of mean BOLD response vs mean estimated underlying neuronal signal of 24 control subjects for AMYG RIGHT with stimulus type = 1

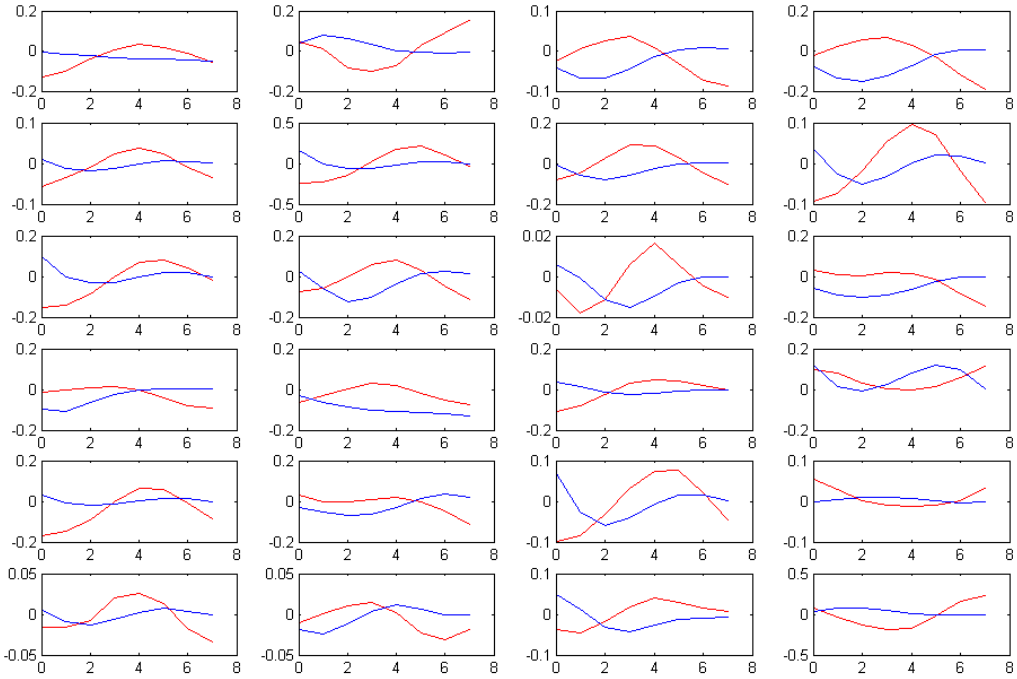

Figure 21: The plots of mean BOLD response vs mean estimated underlying neuronal signal of 24 control subjects for BA 24 with stimulus type = 2

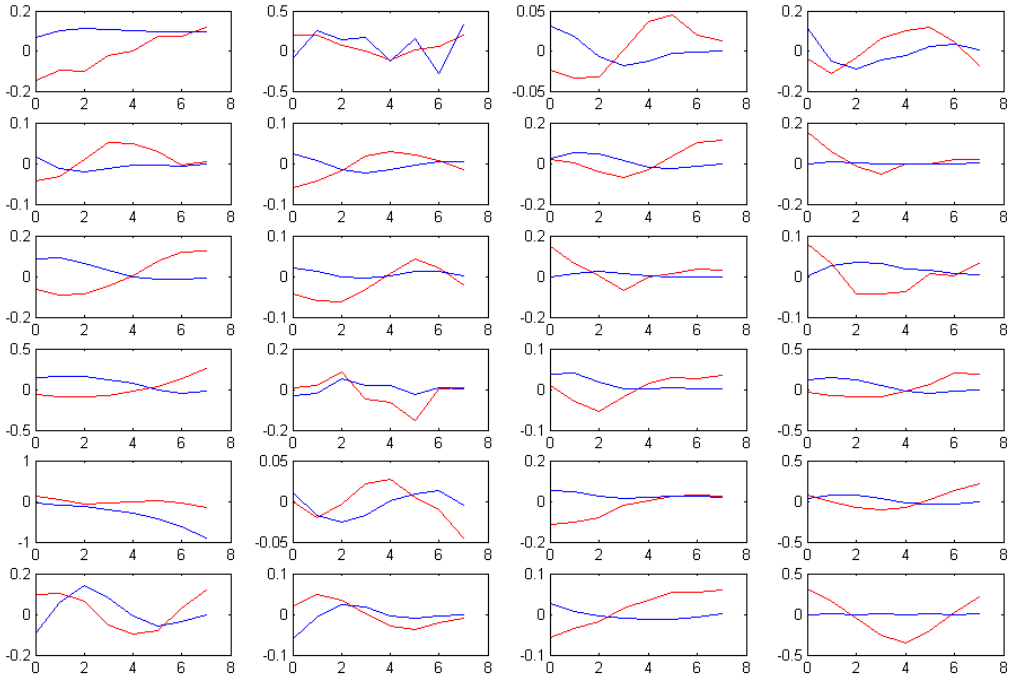

Figure 22: The plots of mean BOLD response vs mean estimated underlying neuronal signal of 24 control subjects for BA 25 with stimulus type = 2

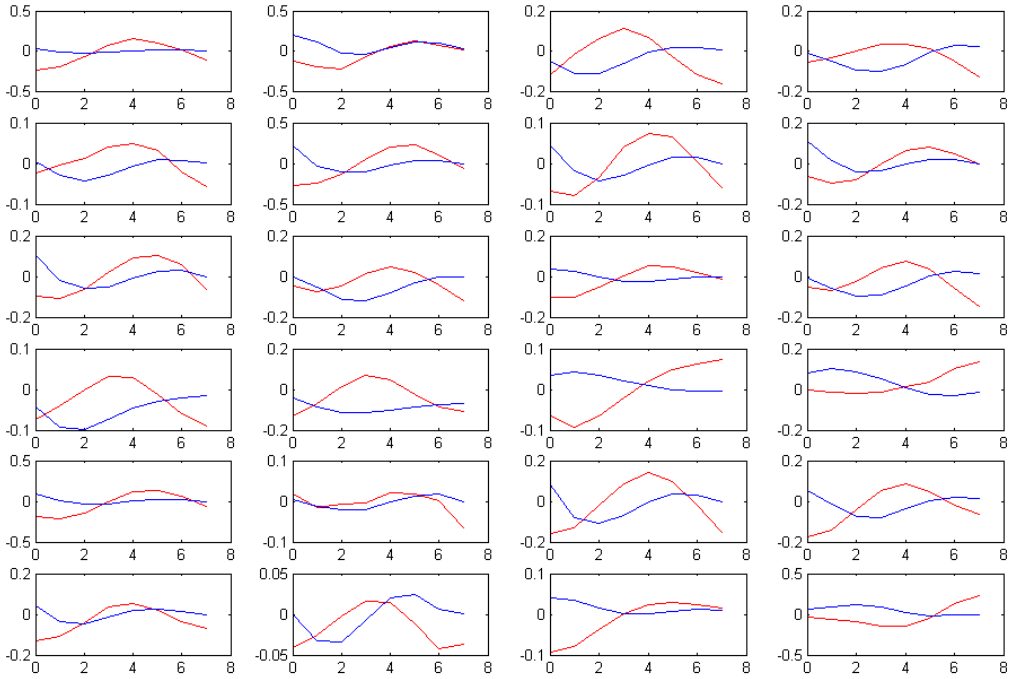

Figure 23: The plots of mean BOLD response vs mean estimated underlying neuronal signal of 24 control subjects for DLPFC with stimulus type = 2

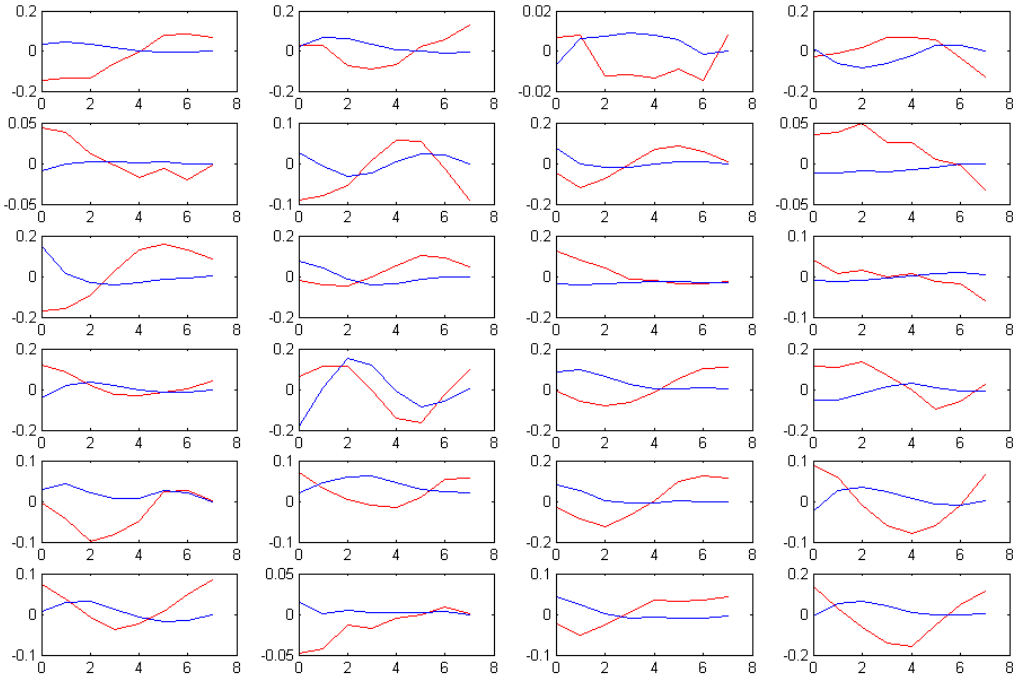

Figure 24: The plots of mean BOLD response vs mean estimated underlying neuronal signal of 24 control subjects for AMYG LEFT with stimulus type = 2

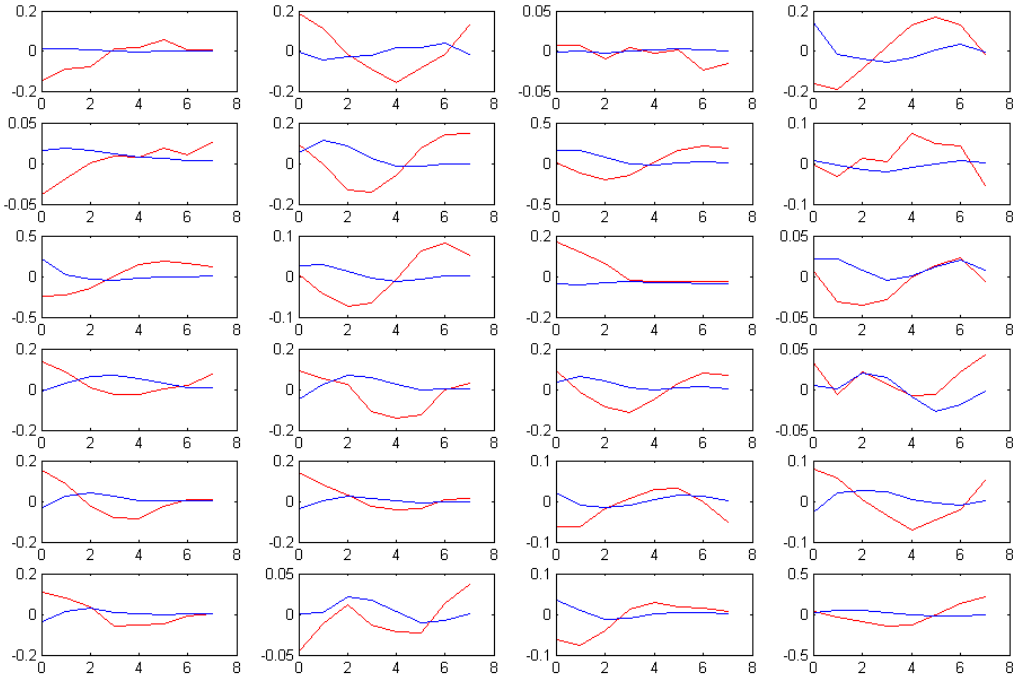

Figure 25: The plots of mean BOLD response vs mean estimated underlying neuronal signal of 24 control subjects for AMYG RIGHT with stimulus type = 2

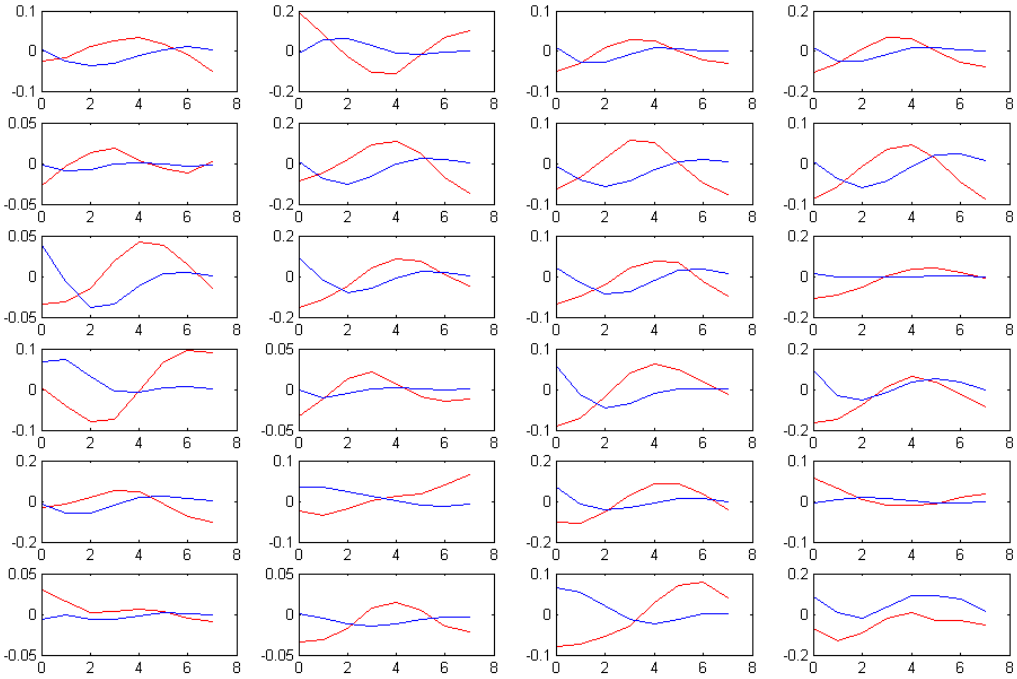

Figure 26: The plots of mean BOLD response vs mean estimated underlying neuronal signal of 24 control subjects for BA 24 with stimulus type = 4

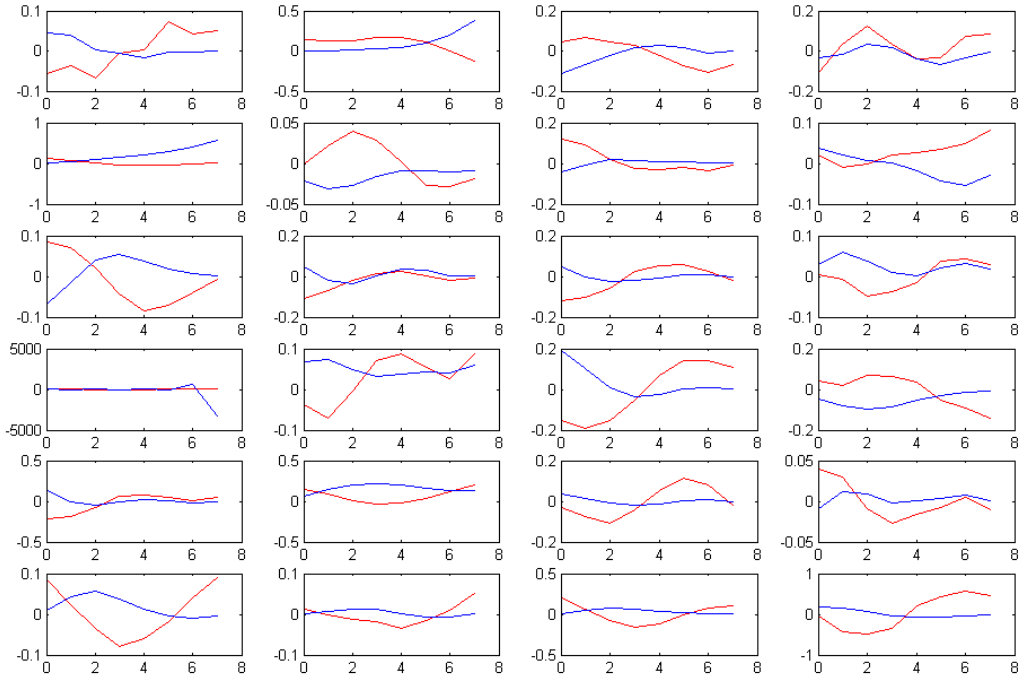

Figure 27: The plots of mean BOLD response vs mean estimated underlying neuronal signal of 24 control subjects for BA 25 with stimulus type = 4

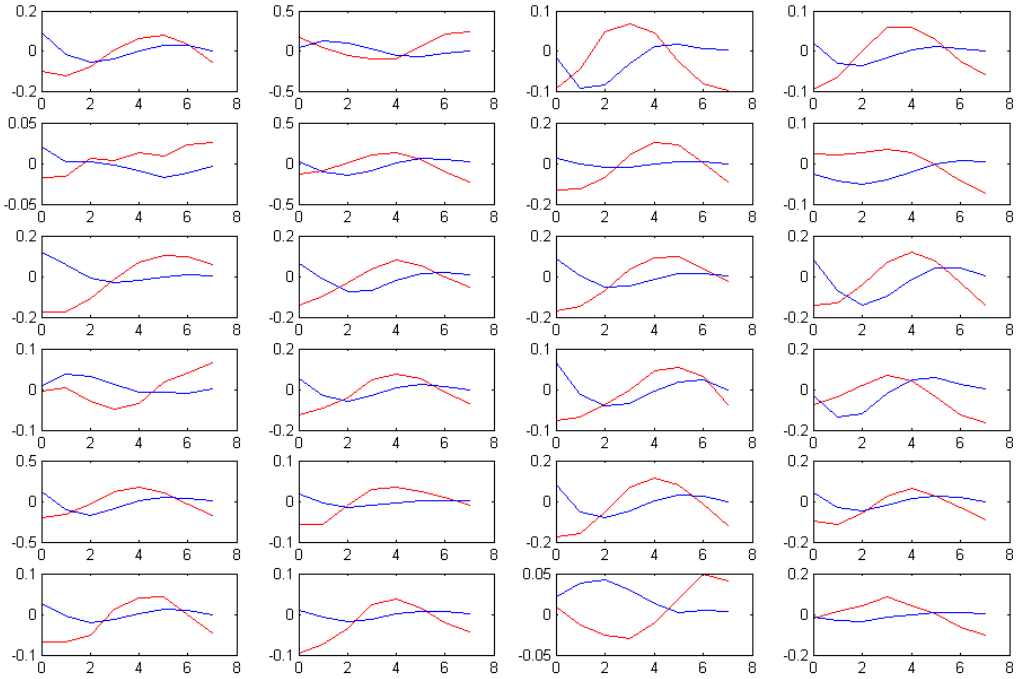

Figure 28: The plots of mean BOLD response vs mean estimated underlying neuronal signal of 24 control subjects for DLPFC with stimulus type = 4

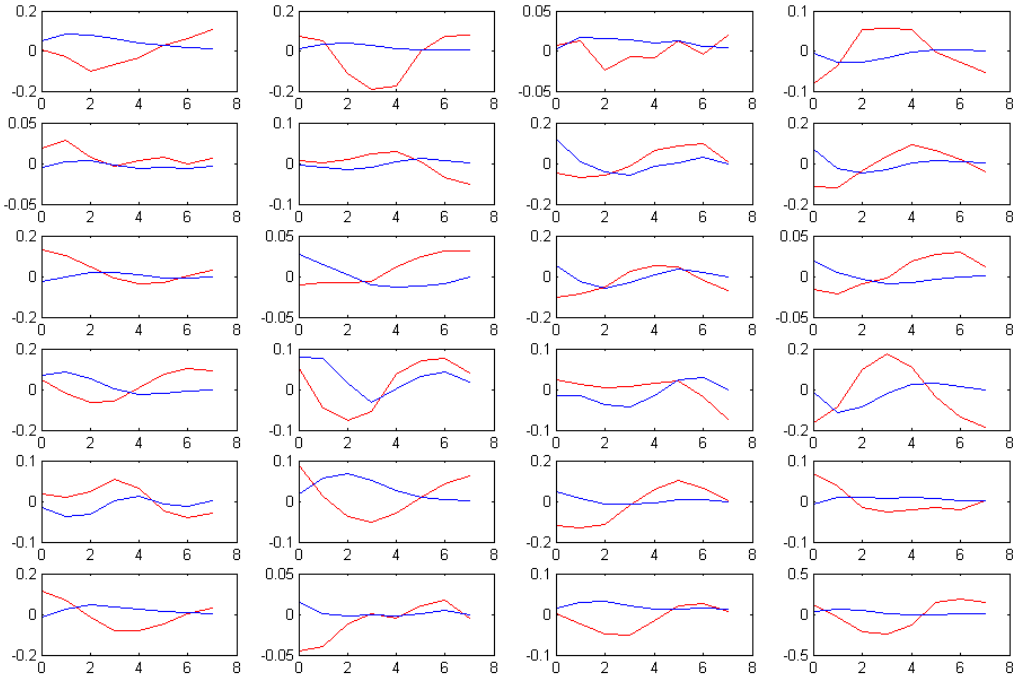

Figure 29: The plots of mean BOLD response vs mean estimated underlying neuronal signal of 24 control subjects for AMYG LEFT with stimulus type = 4

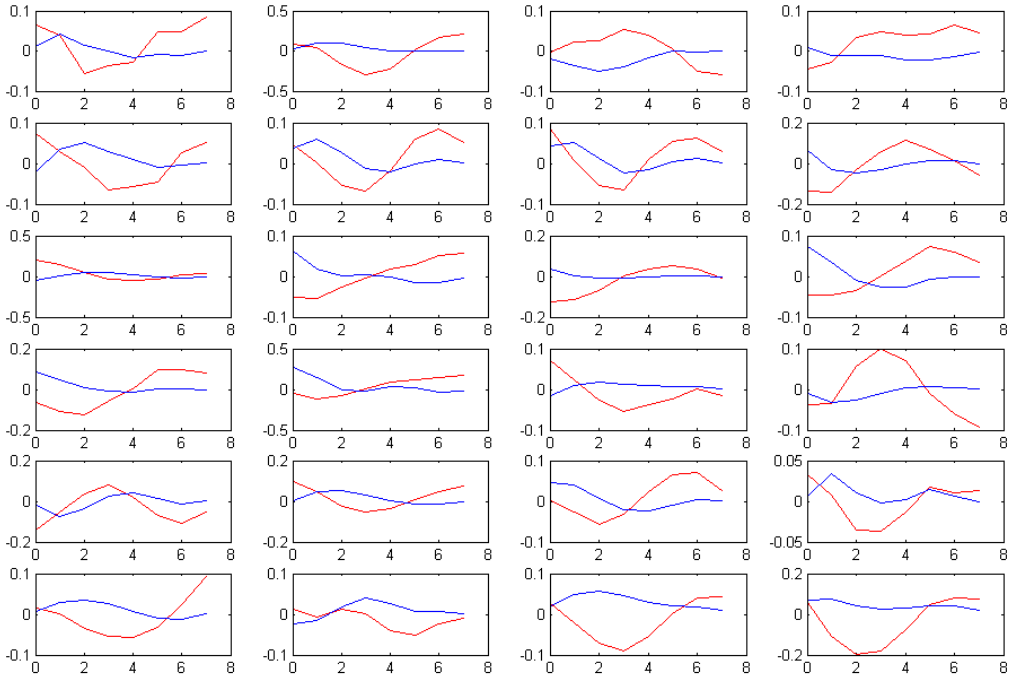

Figure 30: The plots of mean BOLD response vs mean estimated underlying neuronal signal of 24 control subjects for AMYG RIGHT with stimulus type = 4

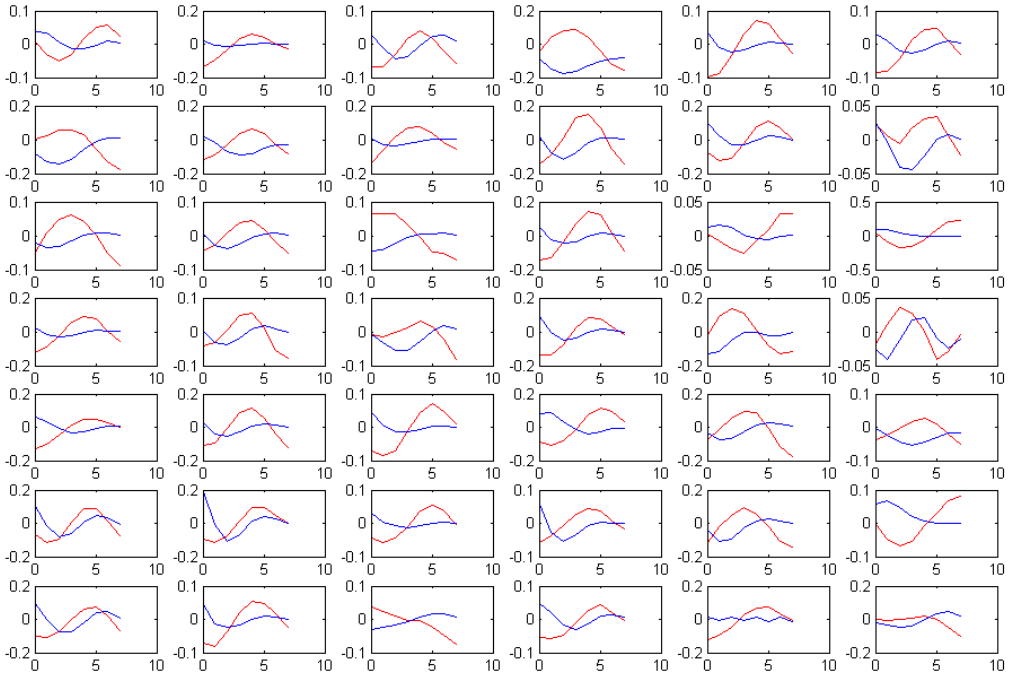

Figure 31: The plots of mean BOLD response vs mean estimated underlying neuronal signal of 42 case subjects for BA 24 with stimulus type = 1

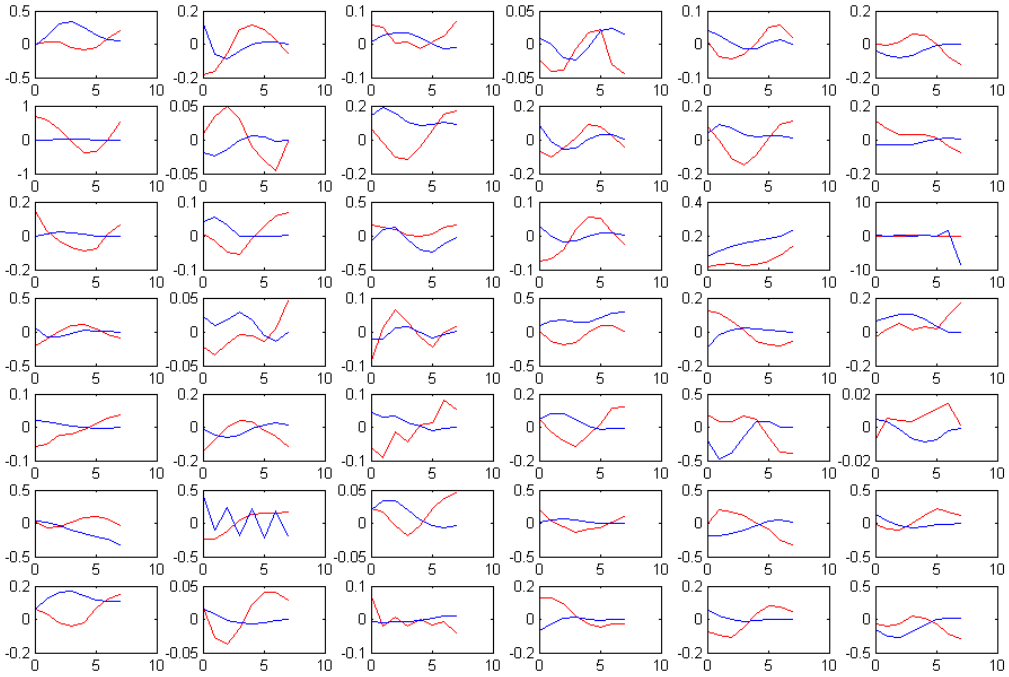

Figure 32: The plots of mean BOLD response vs mean estimated underlying neuronal signal of 42 case subjects for BA 25 with stimulus type = 1

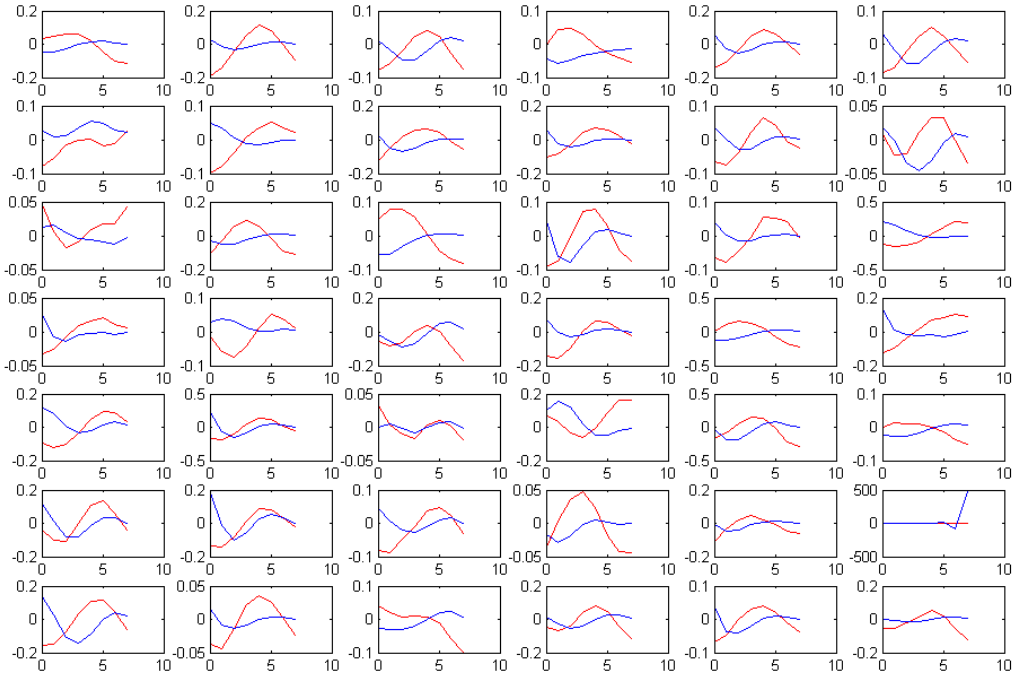

Figure 33: The plots of mean BOLD response vs mean estimated underlying neuronal signal of 42 case subjects for DLPFC with stimulus type = 1

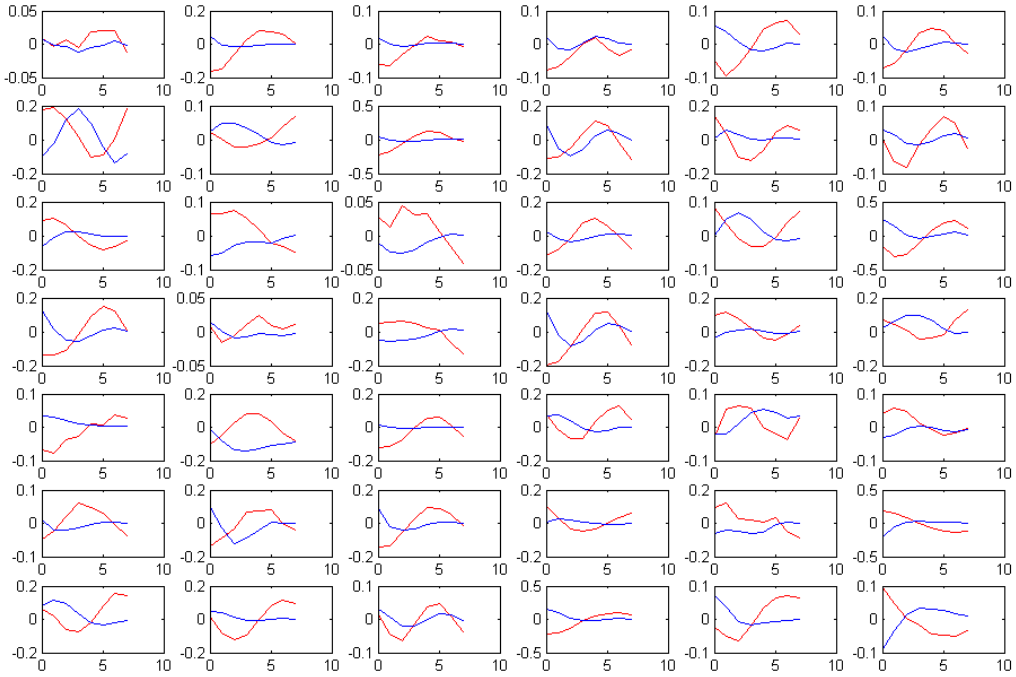

Figure 34: The plots of mean BOLD response vs mean estimated underlying neuronal signal of 42 case subjects for AMYG LEFT with stimulus type = 1

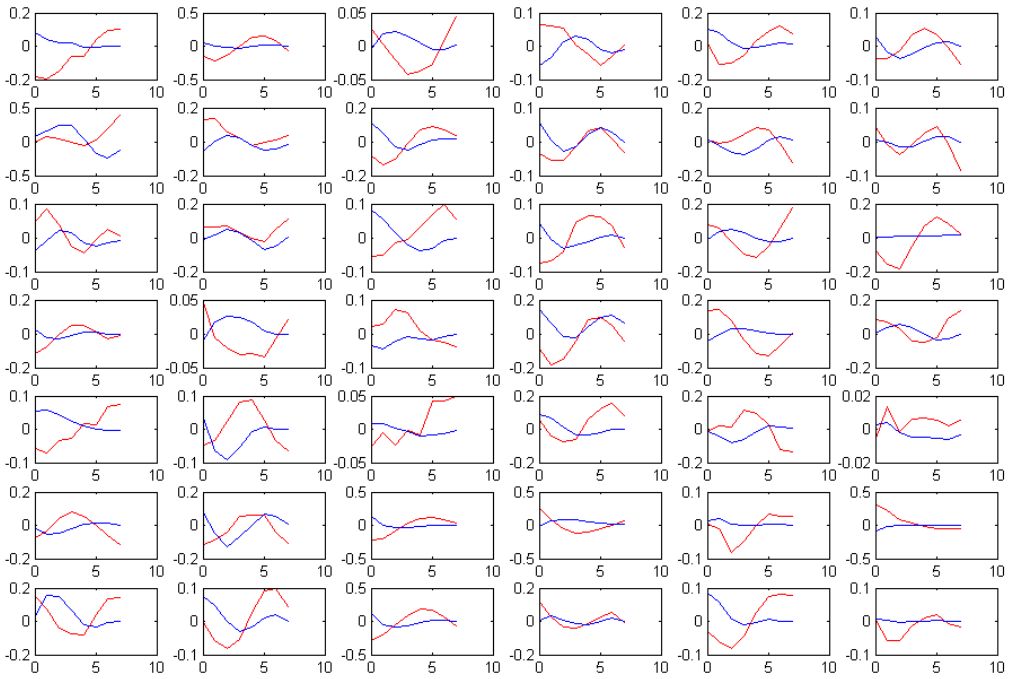

Figure 35: The plots of mean BOLD response vs mean estimated underlying neuronal signal of 42 case subjects for AMYG RIGHT with stimulus type = 1

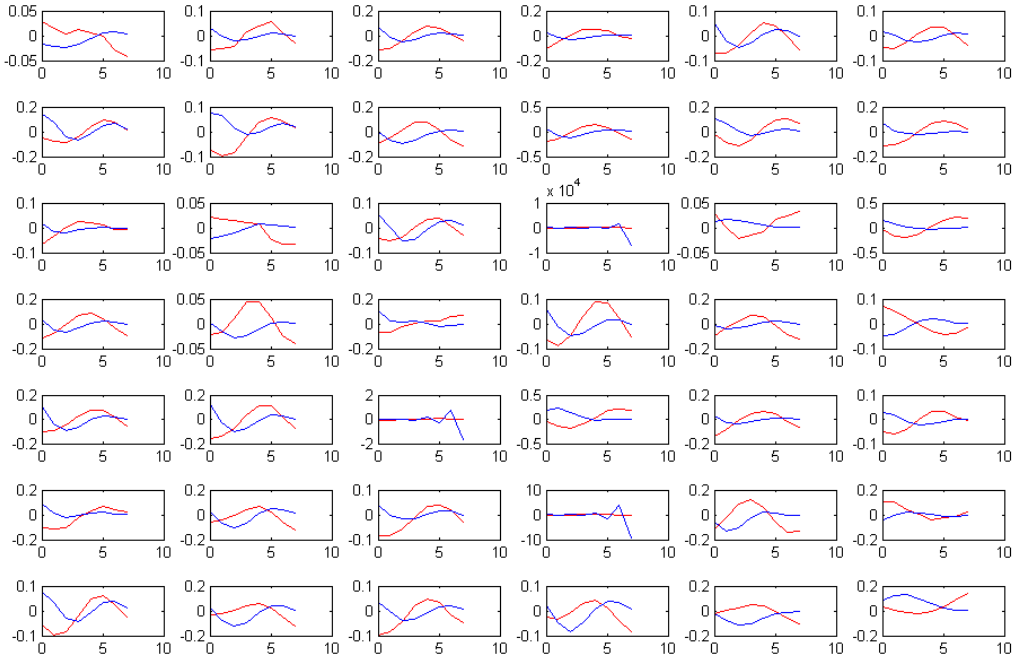

Figure 36: The plots of mean BOLD response vs mean estimated underlying neuronal signal of 42 case subjects for BA 24 with stimulus type = 2

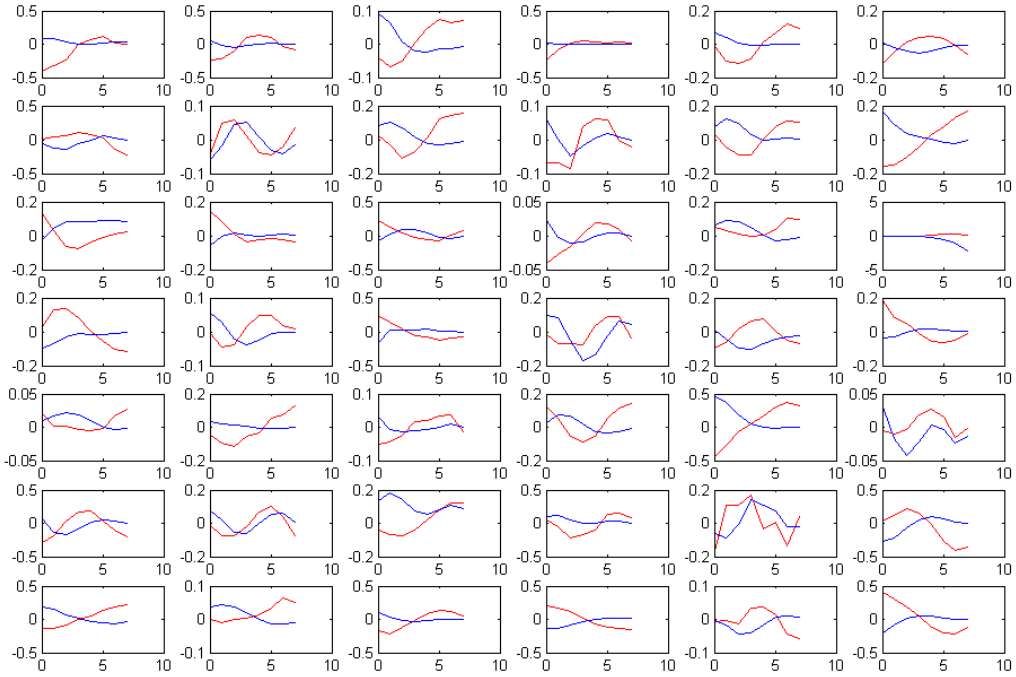

Figure 37: The plots of mean BOLD response vs mean estimated underlying neuronal signal of 42 case subjects for BA 25 with stimulus type = 2

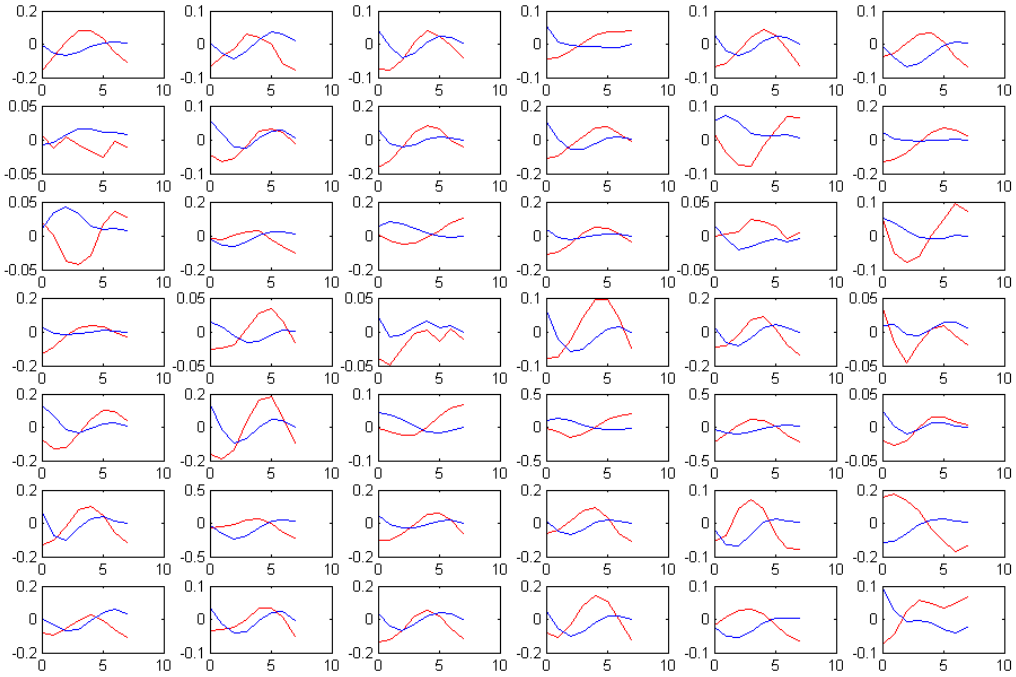

Figure 38: The plots of mean BOLD response vs mean estimated underlying neuronal signal of 42 case subjects for DLPFC with stimulus type = 2

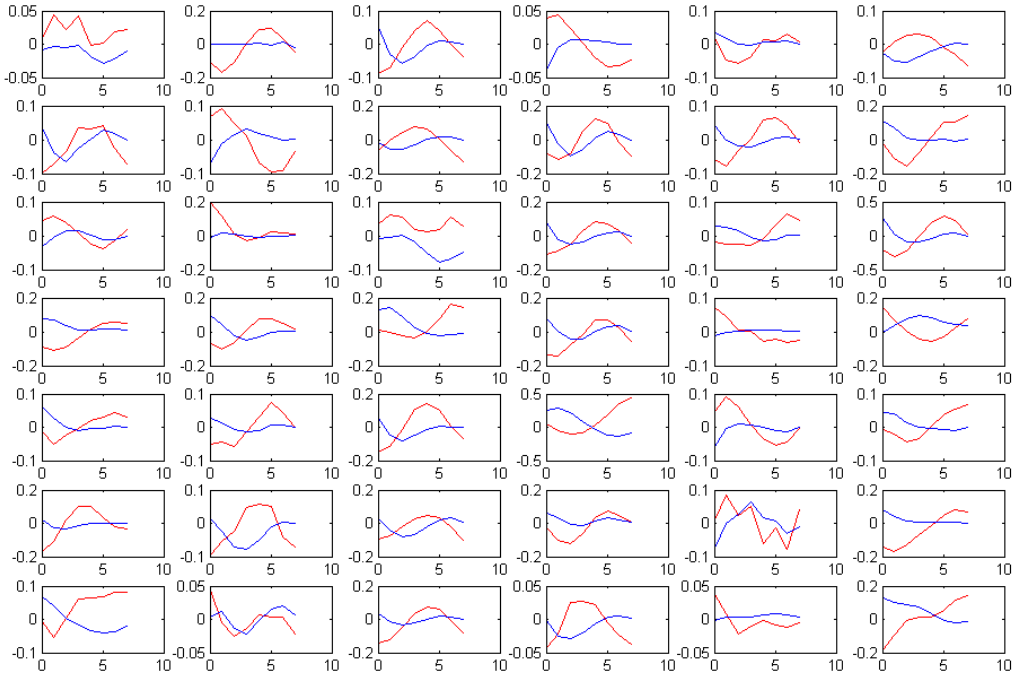

Figure 39: The plots of mean BOLD response vs mean estimated underlying neuronal signal of 42 case subjects for AMYG LEFT with stimulus type = 2

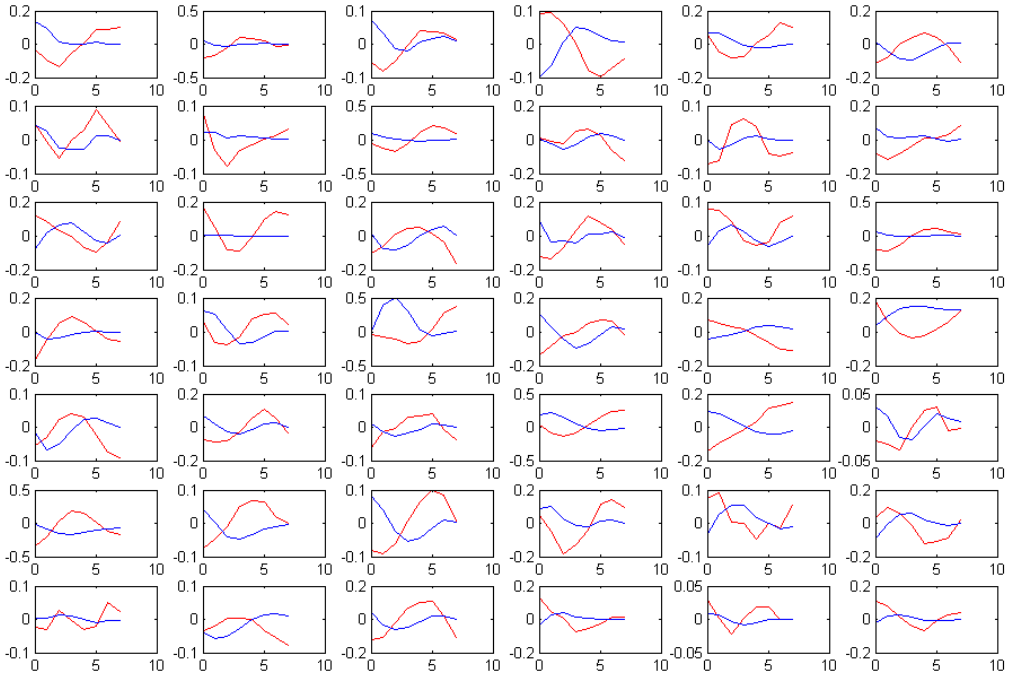

Figure 40: The plots of mean BOLD response vs mean estimated underlying neuronal signal of 42 case subjects for AMYG RIGHT with stimulus type = 2

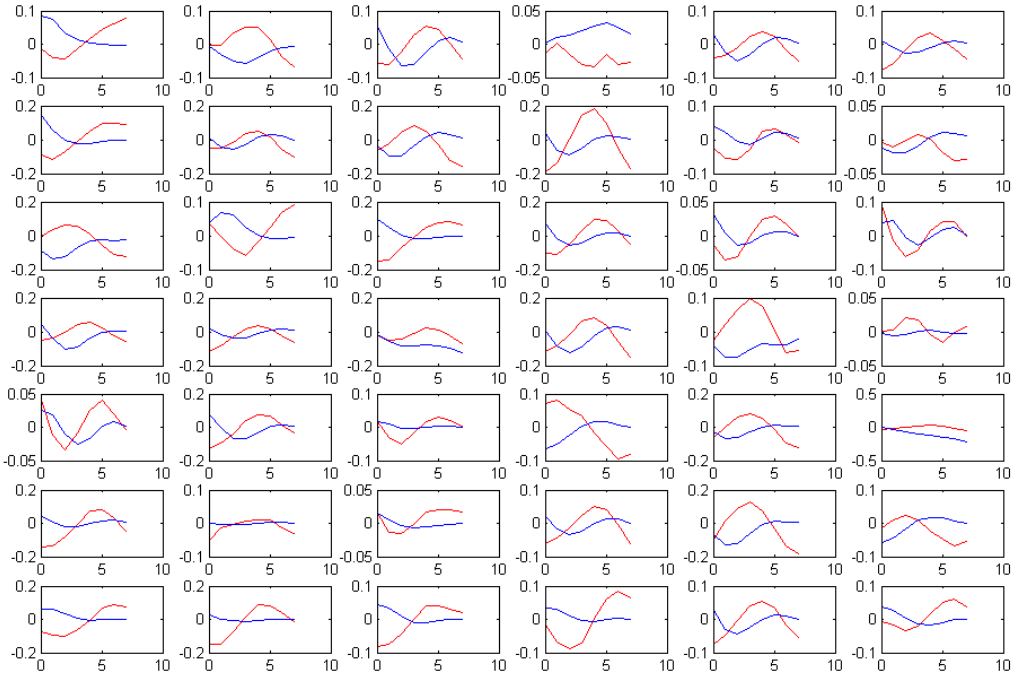

Figure 41: The plots of mean BOLD response vs mean estimated underlying neuronal signal of 42 case subjects for BA 24 with stimulus type = 4

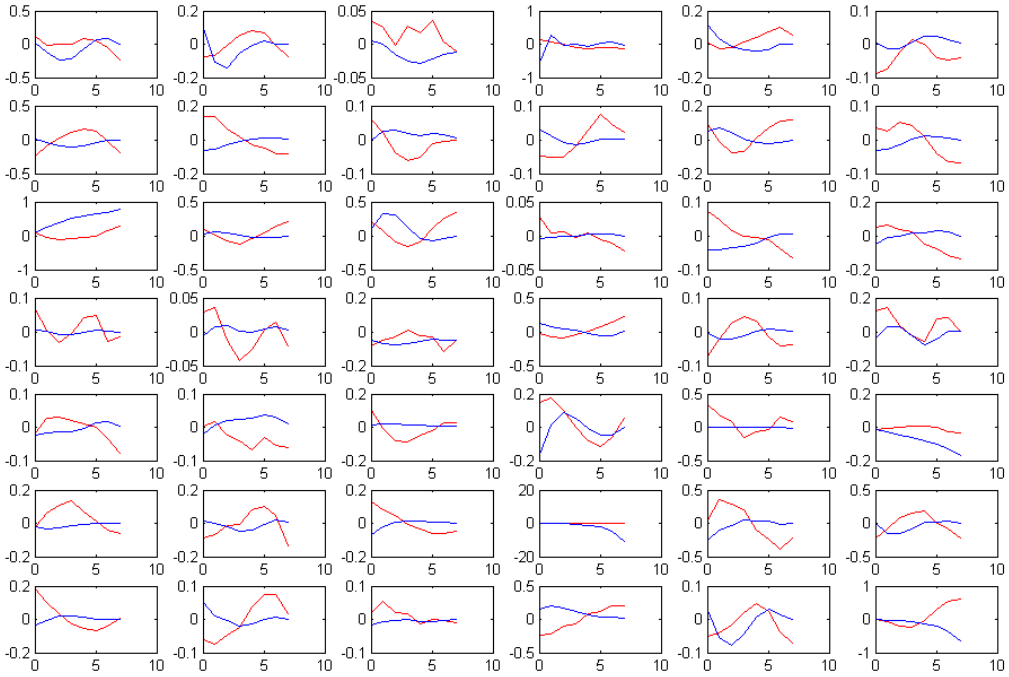

Figure 42: The plots of mean BOLD response vs mean estimated underlying neuronal signal of 42 case subjects for BA 25 with stimulus type = 4

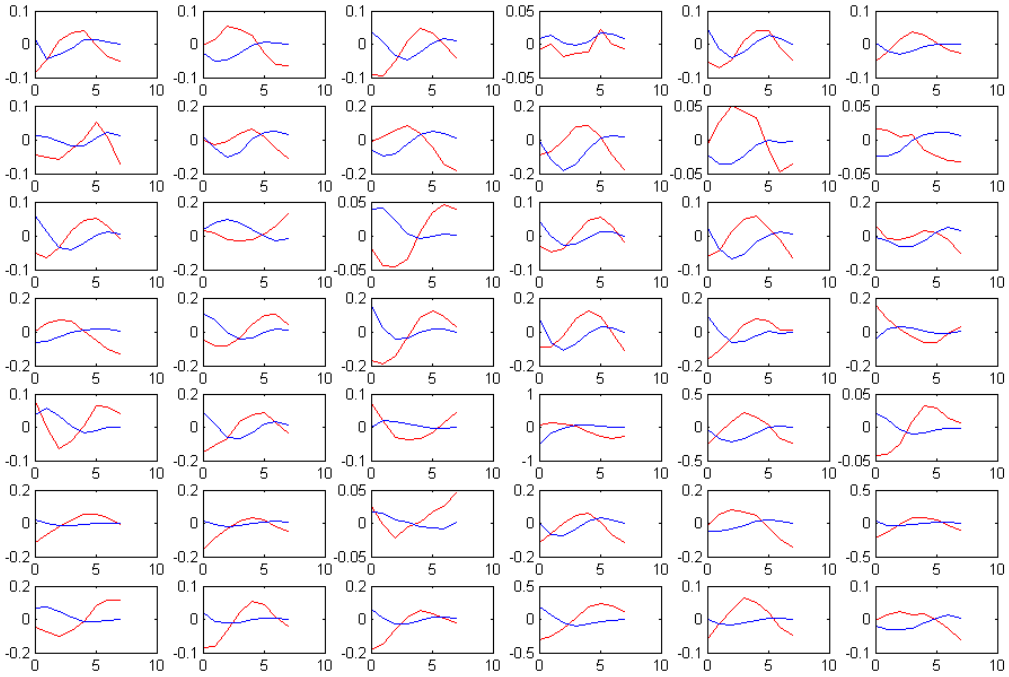

Figure 43: The plots of mean BOLD response vs mean estimated underlying neuronal signal of 42 case subjects for DLPFC with stimulus type = 4

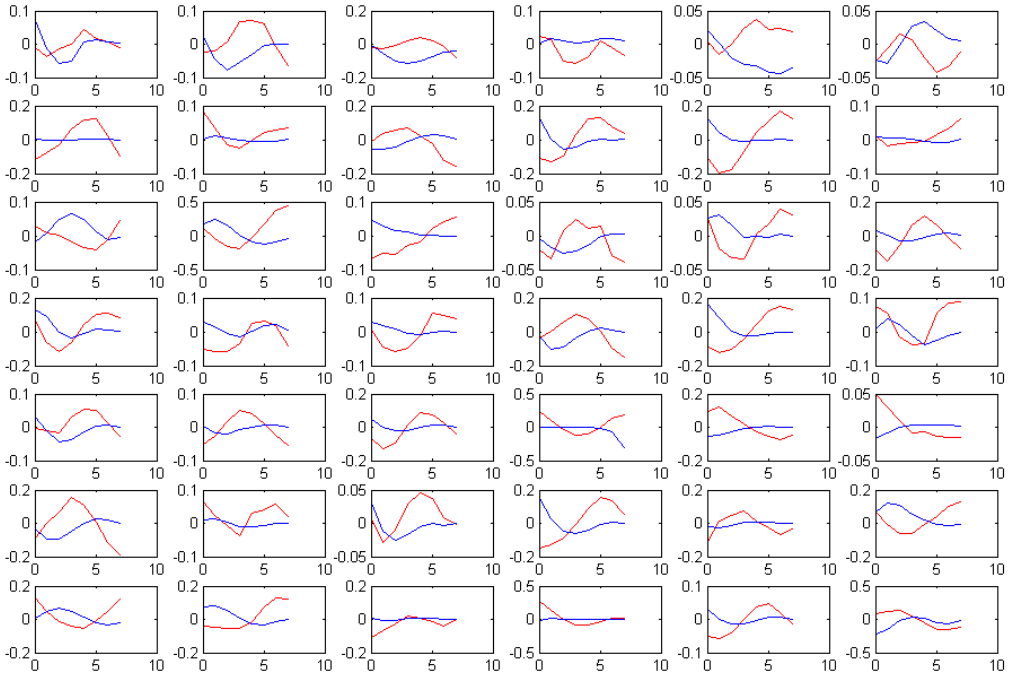

Figure 44: The plots of mean BOLD response vs mean estimated underlying neuronal signal of 42 case subjects for AMYG LEFT with stimulus type = 4

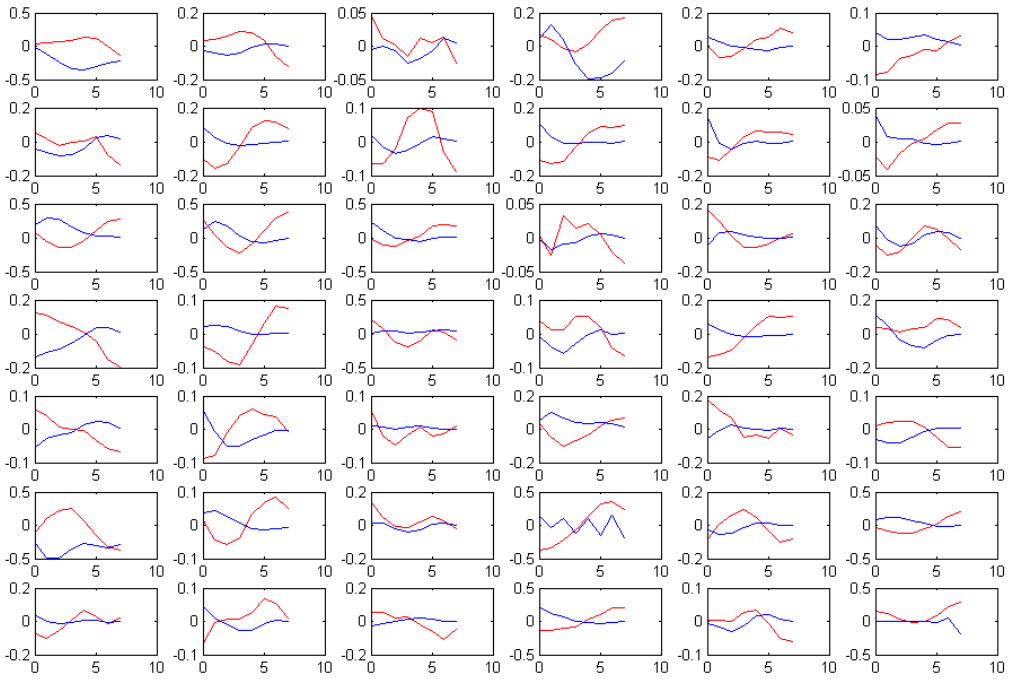

Figure 45: The plots of mean BOLD response vs mean estimated underlying neuronal signal of 42 case subjects for AMYG RIGHT with stimulus type = 4

BIBLIOGRAPHY

[1] A. Aertsen and H. Preissl. Dynamics of activity and connectivity in physiological neuronal networks. *Non Linear Dynamics and Neuronal Networks*, page 281?02, 1991.

[2] G. K. Aguirre, E. Zarahn, and M. D'Esposito. The variability of human, bold hemodynamic responses. *Neuroimage*, 8(4):360–369, 1998.

[3] H. Akaike. A new look at the statistical model identification. *Automatic Control, IEEE Transactions on*, 19(6):716–723, 1974.

[4] K. Amunts, O. Kedo, M. Kindler, P. Pieperhoff, H. Mohlberg, N. J. Shah, U. Habel, F. Schneider, and K. Zilles. Cytoarchitectonic mapping of the human amygdala, hippocampal region and entorhinal cortex: intersubject variability and probability maps. *Anatomy and Embryology*, 210(5):343–352, 2005.

[5] J. W. Belliveau, D. N. Kennedy, R. C. McKinstry, B. R. Buchbinder, R. M. Weisskoff, M. S. Cohen, J. M. Vevea, T. J. Brady, and B. R. Rosen. Functional mapping of the human visual cortex by magnetic resonance imaging. *Science*, 254(5032):716–719, 1991.

[6] J. W. Belliveau, B. R. Rosen, H. L. Kantor, R. R. Rzedzian, D. N. Kennedy, R. C. McKinstry, J. M. Vevea, M. S. Cohen, I. L. Pykett, and T. J. Brady. Functional cerebral imaging by susceptibility-contrast nmr. *MAGNETIC RESONANCE IN MEDICINE*, 14(3):538–546, 1990.

[7] S. Bhattacharya, M. H. Ringo Ho, and S. Purkayastha. A bayesian approach to modeling dynamic effective connectivity with fmri data. *Neuroimage*, 30(3):794–812, 2006.

[8] C. Buchel. Modulation of connectivity in visual pathways by attention: cortical interactions evaluated with structural equation modelling and fmri. *Cerebral Cortex*, 7(8):768–778, 1997.

[9] C. Buechel and K. J. Friston. Dynamic changes in effective connectivity characterized by variable parameter regression and kalman filtering. *Human Brain Mapping*, 6(5-6):403–408, 1998.

[10] G. Bush, P. Luu, and M. I. Posner. Cognitive and emotional influences in anterior cingulate cortex. *Trends in Cognitive Sciences*, 4(6):215–222, 2000.

[11] R. B. Buxton, E. C. Wong, and L. R. Frank. Dynamics of blood flow and oxygenation changes during brain activation: The balloon model. *MAGNETIC RESONANCE IN MEDICINE*, 39:855–864, 1998.

[12] M. Cannon. Blind deconvolution of spatially invariant image blurs with phase. *Acoustics, Speech, and Signal Processing [see also IEEE Transactions on Signal Processing], IEEE Transactions on*, 24(1):58–63, 1976.

[13] M. M. Chang, A. M. Tekalp, and A. T. Erdem. Blur identification using the bispectrum. *Signal Processing, IEEE Transactions on [see also Acoustics, Speech, and Signal Processing, IEEE Transactions on]*, 39(10):2323–2325, 1991.

[14] A. P. Dempster, N. M. Laird, and D. B. Rubin. Maximum likelihood from incomplete data via the em algorithm. *Journal of the Royal Statistical Society*, 39(1):1–38, 1977.

[15] M. Eichler. A graphical approach for evaluating effective connectivity in neural systems. *Philos Trans R Soc Lond B Biol Sci*, 360(1457):953–67, 2005.

[16] R. Fabian and D. Malah. Robust identification of motion and out-of-focus blur parameters from blurred and noisy images. *CVGIP: Graphical Models and Image Processing*, 53(5):403–412, 1991.

[17] J. Fan and R. Li. Variable selection via nonconcave penalized likelihood and its oracle properties. *Journal of the American Statistical Association*, 96(456):1348–1361, 2001.

[18] J. Fan and H. Peng. Nonconcave penalized likelihood with a diverging number of parameters. *Ann. Statist*, 32(3):928–961, 2004.

[19] P. T. Fox and M. E. Raichle. Stimulus rate determines regional brain blood flow in striate cortex. *Ann Neurol*, 17(3):303–5, 1985.

[20] K. J. Friston. Functional and effective connectivity in neuroimaging: A synthesis. *Human Brain Mapping*, 2(1-2):56–78, 1994.

[21] K. J. Friston. Bayesian estimation of dynamical systems: An application to fmri. *Neuroimage*, 16(2):513–530, 2002.

[22] K. J. Friston, C. D. Frith, and R. S. J. Frackowiak. Time-dependent changes in effective connectivity measured with pet. *Human Brain Mapping*, 1(1):69–79, 1993.

[23] K. J. Friston, C. D. Frith, P. F. Liddle, and R. S. Frackowiak. Functional connectivity: the principal-component analysis of large (pet) data sets. *J Cereb Blood Flow Metab*, 13(1):5–14, 1993.

[24] J. Geweke. Measurement of linear dependence and feedback between multiple time series. *J. AM. STAT. ASSOC.*, 77(378):304–313, 1982.

[25] D. R. Gitelman, W. D. Penny, J. Ashburner, and K. J. Friston. Modeling regional and psychophysiologic interactions in fmri: the importance of hemodynamic deconvolution. *Neuroimage*, 19(1):200–207, 2003.

[26] G. H. Glover. Deconvolution of impulse response in event-related bold fmri1. *Neuroimage*, 9(4):416–429, 1999.

[27] R. Goebel, A. Roebroeck, D. S. Kim, and E. Formisano. Investigating directed cortical interactions in time-resolved fmri data using vector autoregressive modeling and granger causality mapping. *Magnetic Resonance Imaging*, 21(10):1251–1261, 2003.

[28] C. W. J. Granger. Investigating causal relations by econometric models and cross-spectral methods. *Econometrica*, 37(3):424–438, 1969.

[29] C. W. J. Granger. Testing for causality. *Journal of Economic Dynamics and Control*, 2(4):329–352, 1980.

[30] J. A. Gray and N. McNaughton. The neuropsychology of anxiety: An enquiry into the functions of the septo-hippocampal system, vol. 1. *XVI. Oxford University Press, Oxford*, 2000.

[31] M. Hampson, B. S. Peterson, P. Skudlarski, J. C. Gatenby, and J. C. Gore. Detection of functional connectivity using temporal correlations in mr images. *Human Brain Mapping*, 15(4):247–262, 2002.

[32] L. Harrison, W. D. Penny, and K. Friston. Multivariate autoregressive modeling of fmri time series. *Neuroimage*, 19(4):1477–1491, 2003.

[33] S. C. Hinton, D. L. Harrington, J. R. Binder, S. Durgerian, and S. M. Rao. Neural systems supporting timing and chronometric counting: an fmri study. *Cognitive Brain Research*, 21(2):183–192, 2004.

[34] M. H. R. Ho, H. Ombao, and R. Shumway. A state-space approach to modelling brain dynamics. *Statistica Sinica*, 15:407–425, 2005.

[35] A. E. Hoerl and R. W. Kennard. Ridge regression: Biased estimation for nonorthogonal problems. *Technometrics*, 12(1):55–67, 1970.

[36] C. Hsiao. Autoregressive modelling and causal ordering of economic variables. *Journal of Economic Dynamics and Control*, 4(3):243–259, 1982.

[37] G. Jacovitti and A. Neri. A bayesian approach to 2d non minimum phase ar identification. pages 79–83, 1990. Spectrum Estimation and Modeling, 1990., Fifth ASSP Workshop on.

[38] R. E. Kalman. A new approach to linear filtering and prediction theory. *Trans. ASME J. Basic Eng*, 82:35–45, 1960.

[39] K. K. Kwong, J. W. Belliveau, D. A. Chesler, I. E. Goldberg, R. M. Weisskoff, B. P. Poncelet, D. N. Kennedy, B. E. Hoppel, M. S. Cohen, and R. Turner. Dynamic magnetic resonance imaging of human brain activity during primary sensory stimulation. *Proceedings of the National Academy of Sciences*, 89(12):5675–5679, 1992.

[40] R. L. Lagendijk, J. Biemond, and D. E. Boekee. Identification and restoration of noisy blurred images using theexpectation-maximization algorithm. *Acoustics, Speech, and Signal Processing [see also IEEE Transactions on Signal Processing], IEEE Transactions on*, 38(7):1180–1191, 1990.

[41] R. G. Lane and R. H. T. Bates. Automatic multidimensional deconvolution. *Journal of the Optical Society of America A: Optics, Image Science, and Vision*, 4(1):180–188, 1987.

[42] D. Malonek and A. Grinvald. Interactions between electrical activity and cortical microcirculation revealed by imaging spectroscopy: Implications for functional brain mapping. *Science*, 272(5261):551, 1996.

[43] H. S. Mayberg, A. M. Lozano, V. Voon, H. E. McNeely, D. Seminowicz, C. Hamani, J. M. Schwalb, and S. H. Kennedy. Deep brain stimulation for treatment-resistant depression. *Neuron*, 45(5):651–660, 2005.

[44] A. R. McIntosh and F. Gonzalez-Lima. Network analysis of functional auditory pathways mapped with fluorodeoxyglucose: associative effects of a tone conditioned as a pavlovian excitor or inhibitor. *Brain Res*, 627(1):129–40, 1993.

[45] A. R. McIntosh, C. L. Grady, L. G. Ungerleider, J. V. Haxby, S. I. Rapoport, and B. Horwitz. Network analysis of cortical visual pathways mapped with pet. *Journal of Neuroscience*, 14(2):655, 1994.

[46] A. R. McLntosh and F. Gonzalez-Lima. Structural equation modeling and its application to network analysis in functional brain imaging. *Human Brain Mapping*, 2(1-2):2–22, 1994.

[47] S. Ogawa, T. M. Lee, A. R. Kay, and D. W. Tank. Brain magnetic resonance imaging with contrast dependent on blood oxygenation. *Proceedings of the National Academy of Sciences*, 87(24):9868–9872, 1990.

[48] S. Ogawa, Tsom Lee, A. S. Nayak, and P. Glynn. Oxygenation-sensitive contrast in magnetic resonance image of rodent brain at high magnetic fields. *MAGNETIC RESONANCE IN MEDICINE*, 14(1):68–78, 1990.

[49] S. Ogawa, D. W. Tank, R. Menon, J. M. Ellermann, S. Kim, H. Merkle, and K. Ugurbil. Intrinsic signal changes accompanying sensory stimulation: Functional brain mapping with magnetic resonance imaging. *Proceedings of the National Academy of Sciences*, 89(13):5951–5955, 1992.

[50] A. V. Oppenheim, A. S. Willsky, and I. T. Young. Signals and systems. *Prentice-Hall Signal Processing Series, Englewood Cliffs: Prentice-Hall, 1983*, 1983.

[51] A. Papoulis. *Signal Analysis*. McGraw-Hill College, 1977.

[52] W. D. Penny and S. J. Roberts. Bayesian multivariate autoregressive models with structured priors. *Vision, Image and Signal Processing, IEE Proceedings-*, 149(1):33–41, 2002.

[53] R. A. Poldrack. Region of interest analysis for fmri. *Social Cognitive and Affective Neuroscience*, 2(1):67, 2007.

[54] E. Procyk and P. S. Goldman-Rakic. Modulation of dorsolateral prefrontal delay activity during self-organized behavior. *Journal of Neuroscience*, 26(44):11313, 2006.

[55] E. M. Robertson, J. M. Tormos, F. Maeda, and A. Pascual-Leone. The role of the dorsolateral prefrontal cortex during sequence learning is specific for spatial information. *Cerebral Cortex*, 11(7):628–635, 2001.

[56] A. Roebroeck, E. Formisano, and R. Goebel. Mapping directed influence over the brain using granger causality and fmri. *Neuroimage*, 25(1):230–242, 2005.

[57] D. L. Schacter, R. L. Buckner, W. Koutstaal, A. M. Dale, and B. R. Rosen. Late onset of anterior prefrontal activity during true and false recognition: An event-related fmri study. *Neuroimage*, 6(4):259–269, 1997.

[58] G. Schwarz. Estimating the dimension of a model. *Annals of Statistics*, 6(2):461–464, 1978.

[59] W. B. Scoville and B. Milner. Loss of recent memory after bilateral hippocampal lesions, 2000.

[60] R. H. Shumway and D. S. Stoffer. An approach to time series smoothing and forecasting using the em algorithm. *Journal of Time Series Analysis*, 3(4):253–264, 1982.

[61] R. H. Shumway and D. S. Stoffer. *Time Series Analysis and Its Applications*. Springer, 2000.

[62] G. J. Siegle, W. Thompson, C. S. Carter, S. R. Steinhauer, and M. E. Thase. Increased amygdala and decreased dorsolateral prefrontal bold responses in unipolar depression: Related and independent features. *Biological Psychiatry*, 61(2):198–209, 2007.

[63] D. W. Tank, S. Ogawa, and K. Ugurbil. Mapping the brain with mri. *Curr Biol*, 1992:525–8, 1910.

[64] R. Turner, D. Le Bihan, C. T. Moonen, D. Despres, and J. Frank. Echo-planar time course mri of cat brain oxygenation changes. *Magn Reson Med*, 22(1):159–66, 1991.

[65] P. A. Valdes-Sosa. Spatio-temporal autoregressive models defined over brain manifolds. *NeuroInformatics*, 2(2):239–250, 2004.

[66] P. A. Valdes-Sosa, J. M. Sanchez-Bornot, A. Lage-Castellanos, M. Vega-Hernandez, J. Bosch-Bayard, L. Melie-Garcia, and E. Canales-Rodriguez. Estimating brain functional connectivity with sparse multivariate autoregression. *Philos Trans R Soc Lond B Biol Sci*, 360(1457):969–81, 2005.

[67] B. A. Vogt, D. N. Pandya, and D. L. Rosene. Cingulate cortex of the rhesus monkey: I. cytoarchitecture and thalamic afferents. *J Comp Neurol*, 262(2):256–70, 1987.

[68] R. Wiggins. Minimum entropy deconvolution. *Computer-aided Seismic Analysis and Discrimination*, 1978.

[69] H. S. Wu. Minimum entropy deconvolution for restoration of blurred two-toneimages. *Electronics Letters*, 26(15):1183–1184, 1990.

[70] E. Zarahn. Testing for neural responses during temporal components of trials with bold fmri. *Neuroimage*, 11(6):783–796, 2000.